Title	Diffusion process in III-V compound semiconductors studied by in-situ transmission electron microscopy and optical spectroscopy
Author(s)	大野, 裕
Citation	大阪大学, 1998, 博士論文
Version Type	VoR
URL	https://doi.org/10.11501/3144298
rights	
Note	

Diffusion process in III-V compound semiconductors studied by *in-situ* transmission electron microscopy and optical spectroscopy

Y. Ohno

1997

Department of Physics, Graduate School of Science
Osaka University
Toyonaka, Osaka

Abstract

In order to understand the migration of interstitial atoms in III-V compound semiconductors at the temperature above 110 K, growth of dislocation loops of interstitial-type in the crystal has been systematically examined by *in-situ* transmission electron microscopy (TEM). Dislocation loops were formed by an annealing above 700 K following 200 keV electron irradiation in the temperature range from 110 to 700 K in GaP and from 110 to 400 K in InP. Dislocation loops were also introduced in GaAs by an annealing at 800 K following 300 keV electron irradiation at 300 K. In InP and GaAs, two types of dislocation loops, loops on {110} and {111} planes were introduced, while only ones on {111} were formed in GaP. Most of the loops were nucleated in the early stage of an annealing, and the number density of loops remained constant after the nucleation. The radius of each loop increased with annealing times, and then reached a certain final value. The number density of interstitials aggregated in loops, therefore, reached a final value when the growth of all loops stopped. The final density depended on not annealing temperature but irradiation conditions (electron dose and irradiation temperature), and it increased quadratically with increasing electron doses. These results were well explained by a new model that the loops were formed through the thermal migration of III_i-V_i interstitial-pairs that were introduced during an electron irradiation. From the analysis, the migration energies for Ga_i-P_i pairs in GaP and In_i-P_i pairs in InP were estimated as 0.9 and 1.5 eV, respectively. The onset temperatures for the migration of Ga_i-P_i pairs in GaP and In_i-P_i pairs in InP were estimated as about 530 and 550 K, respectively.

In order to investigate the migration of interstitial atoms in III-V compounds in the temperature range below 110 K, electron-irradiation-induced defects in GaP and GaInP have been investigated by utilizing an *in-situ* TEM-PL/CL observation apparatus, which enables

us to obtain simultaneously TEM images and PL (photoluminescence) / CL (cathodoluminescence) spectra. The results of *in-situ* PL/CL spectroscopy under electron-irradiation showed that the luminescence intensities in GaP, measured at the wavelength of 565, 725 and 850 nm, almost remained the same during an irradiation at 20 K. Since Frenkel-type defects are introduced even at the temperature, this result indicates that the effect of Frenkel-type defects on the optical properties in GaP is quite small. The intensities, however, decreased by an annealing at 90 K after an irradiation at 20 K. This fact indicates that Frenkel-type defects, introduced in GaP by an electron-irradiation at 20 K, are no longer frozen in the temperature range from 20 to 90 K and a thermal migration of interstitial atoms results in the formation of complexes associated with a non-radiative recombination center. Under an electron irradiation, the luminescence intensities measured at 90 K decreased with electron doses. Analyses of the decrease-rates suggest that the complexes, interstitial-vacancy pairs and interstitial-pairs, were formed through a second-order reaction. An introduction of defect complexes was not observed in GaInP with the CuPt-type ordered structure. In the crystal, Frenkel-type defects strongly affect on the optical properties. When an electron energy for an irradiation was above 140 keV, the peak energy of CL spectra shifts to a higher value with an electron irradiation, and the shift was well explained as the disordering of the CuPt-type ordered structure in GaInP through the migration of both Ga and In atoms.

Abrégé

Pour comprendre la migration des atomes interstitiels dans un III-V semiconducteur composé à la température au-dessus de 110 K, Je examinai de la crossance des anneaux dislocations du type interstitiel en microscopie électronique en transmission (TEM). Des anneaux dislocations furent formés dans un GaP et un InP de recuire à la température au-dessus de 700 K à la suite de l'irradiation electronique avec l'énergie electronique de 200 keV. Des anneaux dislocations aussi furent formés dans un GaAs de recuire à la température de 800 K à la suite de l'irradiation electronique avec l'énergie electronique de 300 keV. Dans un GaAs et un InP, des anneaux dislocations sur $\{110\}$ et $\{111\}$ furent formés, et des anneaux sur seul $\{111\}$ furent formés dans un GaP. La majeure partie de les anneaux furent formés dans le degré premier du recuit, et le nombre de l'anneaux conservierent après la formation. Le rayon de chaque anneau augmenta avec du temps recuit, et puis ce rayon atteint du prix definitif. Le nombre de atomes interstitiels dans les tout anneaux dislocations donc atteint du prix definitif quand la croissance de les tout anneaux arrêta. Le nombre definitif ne dépendit pas de température recuit mais ce nombre dépendit de la conditions pour de l'irradiation electronique. Le nombre augmenta quadratiquement avec de l'augmentation de dose electronique. Les résultants furent expliqués bien de un modèle nouveau que les anneaux furent formès de la migration des III_i-V_i paires interstitielles qui furent formès tout le temps que de l'irradiation. La énergies pour les migrations des Ga_i-P_i paires dans un GaP et des In_i-P_i paires dans un InP furent estimés 0.9 eV et 1.5 eV chacune. La températures commencementes pour les migrations des Ga_i-P_i paires et des In_i-P_i paires furent estimés 530 K et 550 K chacune.

Pour comprendre la migration des atomes interstitiels dans un III-V semiconducteur composé à la température au-dessous de 110 K, Je examinai des défauts qui furent formés à

l'irradiation electronique dans un GaP et un GaInP avec un dispositif qui obtient des TEM images et des spectres de la photoluminescence (PL) ou de la luminescence de rayons cathodiques (CL) simultanément. Les resultats des PL/CL spectroscopie dessous de l'irradiation electronique montrèrent que des intensités des luminescences dans un GaP, qui furent mesurés à les longeurs d'onde de 565, 725, et 850 nm, furent constantés àpproximativement à la température de 20 K. Comme les défauts de le Frank-type furent formés à la température de 20 K, les résultats attestèrent que les défauts de le Frank-type dans in GaP ne influent presque pas sur de la propriété d'optique. Les intensités décroîtrèrent de recuire à la température de 90 K à la suite de l'irradiation electronique à la température de 20 K. C'est ainsi que les défauts de le Frank-type se diffusent dans une température de 20 K à 90 K, et des défauts composée sont formés de la migration des atomes interstitiels. Des intensités des luminescences qui furent measurés à la température de 90 K decroîtrèrent avec le temps de l'irradiation elecrtonique. Des analyses de la raison de le décroissement attestèrent que les défauts composée, 1) de les paires de un atome interstitiel et un trou et 2) de les paires des deux atomes interstitiels, furent formés en une réaction quadratique. Des défauts composée ne furent formés pas dans un CuPt-type GaInP. Des défauts de le Frank-type influa fort sur de la propriété d'optique dans ces spécimen. Quand de l'énergie electronique pour de l'irradiation furent au-dessus de 140 keV, de l'énergie à la sommet dans un CL spectre se déplacé vers de l'énergie élevée avec de l'irradiation, et le déplacement furent expliqué une transformation de CuPt-type GaInP de la migration des atomes interstitiels.

Contents

1 Introduction

1-1 General introduction

It is well known that various types of lattice defects, such as interstitial atoms and vacancies, exist in III-V compound semiconductors and they form many localized energy levels between the conduction- and valence-band {1}. Since some of the levels implicitly affect on optical and electronic properties even when their concentration is small, they disturb development of high-functional devices. From a basic point of view, the behavior of point defects in III-V compounds is interesting in many aspects. One would expect defects in III-V compound semiconductors to be more stable than in elemental semiconductors on the basis of the obviously greater complexity in moving; for example, a Ga vacancy in GaP or GaAs compared with a vacancy in Si. A nearest-neighbor jump is sufficient in Si, whereas in III-V compounds a jump must be made to a second-nearest-neighbor position. Similarly, very rapid motion of a split-interstitial configuration is possible in Si due to the <110> chains of atoms {2}; such motion is impossible in a compound semiconductor. It is well known that the onset temperatures for the migration of point defects in GaP and GaAs are rather higher than ones in Si {1}, indicating the high stability of lattice defects in III-V compounds.

For studying the defects, electron irradiation is commonly used, since pairs of isolated interstitials and vacancies can be introduced intentionally in a crystal. Studies of radiation effects in III-V compounds have received considerable recent interest since they were reviewed by Aukerman {3} and Eisen {4}. So far, GaAs and GaP have been widely used for a variety of optoelectronic devices such as light-emitting diodes (LEDs). InP has also been used for devices such as hf-transistors. These materials have extensively been investigated with several experimental techniques, and the structural and dynamical properties of the primary defects in them have been well described. It is well known that various kinds of defect complexes, such as interstitial clusters, are introduced by an annealing after an electron irradiation through a migration of point defects. Nevertheless, the kinetics of the defects has not yet been fully examined. The present knowledge of point defects is briefly summarized in the following sections.

1-2 Point-like defects in GaP

1-2-1 Isolated vacancy and their complexes in GaP

In the present section, I summarize briefly the structural and electronic properties of point-like defects in GaP. Isolated Ga-vacancy, V_{Ga}, was first observed by electron spin resonance (ESR) {5, 6}. The atomic and electronic structures of the defect are clarified; the ESR signal, NRL-1, is concluded to derive from a spin-3/2 defect with T_d symmetry {7} and the model agrees well with the ordering of energy levels given by the theoretical calculations for V_{Ga} {8}. Since the ESR signal disappears by an annealing above 600~700 K, it is believed that Ga-vacancies are mobile thermally at the temperature above 700 K {9}. The V_{Ga} was also observed by deep level transient spectroscopy (DLTS): two hole traps were found in electron-irradiated GaP, and one of these, I_2, had the same annealing temperature and a similar introduction rate to that of NRL-1 {10}; the charge states as measured by both ESR and DLTS were consistent {10}. In the temperature range from 550 to 700 K, that is the same value as the annealing temperature of V_{Ga}, an annealing of a defect lifetime was observed in electron-irradiated GaP by positron annihiration spectroscopy (PAS) {11-13}. The annealing stage is believed to arise from the annealing of V_{Ga} {13}, since trends of the lifetime are similar to ones of V_{Ga} for GaAs {14}.

The isolated P-vacancy, V_P, was also studied by PAS {15-17} and theoretical {18, 19} approaches; the charge state of P-vacancy shifts from V_P^0 to V_P^- at the temperature about 400 K due to the shift of Fermi level {16, 19} and V_P can migrate thermally above 900-1100 K {15, 17}. The E-center observed by DLTS {20, 21} is proposed to associates with V_P: these levels are considered to be associated with different charge states of the V_P perturbed by the presence of P-interstitials located at different distances from V_P {21}, and the annealing of the defect is characterized by first-order process with the activation energies of 1.35±0.05 eV. It is claimed that the annealing are due to the migration of isolated P-interstitials (P_i), even though the annealing temperature of the defect, about 450 K, is extremely higher than the onset temperature for the migration of P-interstitials estimated by infrared (IR) absorption spectroscopy (Sec. 1-2-3).

1-2-2 Isolated interstitial atom and their complexes in GaP

The structural properties of interstitial-related defects were also described. The isolated Ga-interstitial, Ga_i, was directly observed by optically detected magnetic resonance (ODMR) in oxygen- [22] or copper- [23] doped GaP. The ODMR signal, KL1, is due to Ga_i at a T_d-interstitial lattice site that has a spin triplet in its electronic excited state. The assignment of the Ga_i is identified unambiguously by the central-hyperfine structure resolved in experiments [23] and theoretical calculations [24]. These experimental results demonstrate the tendency of pairing of Ga_i with other defects to form complexes, even though the kinetics of the defect is not yet fully investigated.

The isolated P-interstitial (P_i) is not yet observed directly, but it is considered that P_i in p-type GaP can migrate easily and form the P_{Ga} anti-site defect (P-atom on a Ga-site). The defects, named P-P4 center, were studied by ESR [25, 26] and ODMR [27, 28]; P_{Ga} behaved as a deep double donor with its second donor state at E_C-1.1 eV [27, 28], and it annealed at the temperature about 700 K [29]. The annealing temperature is almost the same as one of V_{Ga} observed by ESR and DLTS [6, 9].

It is generally believed that Ga_i and P_i can migrate thermally even at low temperature. Defects of a boron [30] and a carbon [31] atom on Ga-site with P-interstitial, B(1) and C(1)-center, were observed by IR spectroscopy in the electron-irradiated GaP. Since the concentration of B(1)-defect introduced by an electron-irradiation at 100 K does not increased significantly by an annealing, P_i is considered to be mobile under an electron irradiation even at 100 K [32]. A Ga-atom on P-site, Ga_P (Ga(1)-center) was also found [33]; the formation of the Ga(1) defects is explained that a Ga_i exchanges sites with a substitutional impurity atom on P-sites [34]. Therefore, the experimental results that the defects are introduced by an electron irradiation even at 100 K, indicating that the onset temperature for the migration of Ga_i is about 100 K [32].

3

1-2-3 Annealing properties of point-like defects in GaP

Annealing properties of lattice defects in GaP are summarized in Table 1-1. The annealing of NRL-1 center observed by ESR (~650 K) is explained as the disappearance of V_{Ga} due to its thermal migration {9}. From the experimental results of PAS, the onset temperature for the migration of V_p is estimated to be about 950 K {15-17}. Above the onset temperatures, some defects associated with vacancies were found; B(2)-center observed by IR spectroscopy was formed above 670 K {27}, and a CL emission was detected in GaP that is electron-irradiated and subsequently annealed at 925 K {8}. The structure of these defects is still unknown.

From the results of IR spectroscopy, the onset temperatures of Ga_i and P_i are estimated as about 100 K {32}. In the temperature range between the onset temperature for the migration of isolated interstitials and ones for isolated vacancies, two annealing stages of electrical conductivity (EC) were observed in electron irradiated GaP. The annealing temperatures of the stages are 430 (Stage I) and 530~570 K (Stage II), and they are characterized by two first-order processes with the activation energies of about 1.5 and 2.0 eV {35, 36}. These annealing stages were also observed by thermally stimulated conductivity (TSC) measurement; the defects annealed at 430 K, named D-center, behaves as a deep donor at $E_C-1.24$ eV and ones annealed at 550 K, M-center, acted as an acceptor at $E_V+1.43$ eV {37}. The former defects were also investigated by DLTS: the E2 and E3 levels observed by DLTS annealed at 450 K {20}. At the temperature of two annealing stages, similar defect-annealing were observed by IR spectroscopy. It is known that the C(1)-centers anneal at about 400 K {31}. The B(1) centers anneal out on heating sample to around 530 K, and the annealing temperature is the same temperature region as for the annealing of the Ga(1) centers {31}.

The V_{Ga} and V_p are believed to migrate thermally above 700 {6, 9, 11-13} and 1000 K {15-17}, respectively. The annealing stages at 400 and 550 K are, therefore, independent of the migration of vacancies. It is thus concluded that these annealing are due to several kinds of complexes associated with interstitial atoms, even though the structure and annealing mechanism of the complexes are still debatable.

4

Table 1-1 Annealing properties of lattice defects in GaP

Defect	Defect name	Experiments	Onset temperature for defect-formation [K]	Annealing temperature [K]	References
V_{Ga}	NRL-1	ESR	-	600~700	{9}
	I_2	DLTS	-	600~700	{10}
		PAS	-	550~750	{11-13}
V_P		PAS	-	900~1000	{15-17}
V_P-X	E2	DLTS	-	450	{20, 21}
	Stage I	EC	-	430	{35, 36}
	D	TSC	-	430	{37}
Ga_i	KL1	ODMR	< 4	-	{22}
Ga_i-Y		ODMR	-	-	{23}
Ga_P	Ga(1)	IR	~100	~530	{32, 34}
P_{Ga}	P-P4	ESR	-	700	{25, 26}
	P-P4	ODMR	-	~700	{27, 28}
B_{Ga}-P_i	B(1)	IR	~100	~530	{30, 32}
C_{Ga}-P_i	C(1)	IR	~100	~400	{31}
?	Stage II	EC	-	530~570	{35, 36}
	M	TSC	-	550	{37}
??	B(2)	IR	670	» 800	{27}
???		CL	925	-	{8}

X, Y, ?, ??, ??? : Unknown defects

1-3 Point-like defects in InP

1-3-1 Isolated vacancy and their complexes in InP

Isolated P-vacancy, V_P, was first observed by ESR {38}. The atomic and electronic structures of the defect are clarified; the ESR signal, with a g-value of 2.05, is concluded to derive from a nuclear spin-9/2 defect with T_d symmetry. The V_P was also observed by photoluminescence (PL) spectroscopy {39}. The band B and C luminescence, peaking at the energy of 1.06 and 1.20 eV, are believed to arise from an impurity-V_P complex and single V_P, respectively. The intensity of the band C luminescence decreases by an annealing at the temperature above 1023 K. Since the decrease is considered to be due to the formation of new impurity-V_P complexes through the migration of V_P, this temperature might be the onset temperature for the migration of V_P. The E5 center observed by DLTS, with the activation energy of 0.42 eV {40}, is believed to arise from a V_P included defect.

The isolated In-vacancy, V_{In} was observed by means of magnetic circular dichroism (MCD-) ODMR method {41}. The atomic and electronic structure of the defect is, however, still uncertain, since it was observed as the broadening of an ODMR signal {41}. The V_{In} is extensively investigated by PAS {42} and theoretical approaches {44}; it is confirmed that the positron lifetime of 297 ps in 2 MeV electron irradiated InP is due to V_{In}. The lifetime anneals at the temperature above 200-250 K due to the migration of isolated In-interstitials {42}. Combined study of PAS and hall effect measurements, it is concluded that positrons are trapped at negatively charged V_{In} with an ionization level at E_c-0.33 eV {43}. Above room temperature, the defect has two annealing stages; 423 and 573 K {43}. The former annealing is, believed to be, due to the formation of vacancy clusters with the activation energy of 0.16 eV through the migration of V_{In}, and the latter is explained as a breaking up of vacancy clusters, such as V_{In}-V_P vacancy-pairs {43}. The V_{In} was recently observed by PL spectroscopy; the band A luminescence, peaking at the energy of 1.13 eV, is supposed to be arise from an impurity-V_{In} complexes {39}.

1-3-2 Isolated interstitial atom and their complexes in InP

The H and E centers observed by DLTS are proposed to be related with isolated In and P interstitials, In_i and P_i; these levels are, respectively, introduced due to the pairs of V_{In} and In_i, and V_P and P_i, as similar as in GaAs [45]. The electron traps named E4 and E5 and hole trap H6 anneal at the temperature above 100 K [46, 47], and the annealing is due to the recombination of isolated interstitials and vacancies; the onset temperatures for the migration of both the In_i and P_i are, therefore, about 100 K.

The P atom on an In-site, P_{In} was first observed in electron irradiated [48] and as-grown [49] InP by means of ESR. The ESR signal with a g-value of 1.992 is due to P_{In}, and the introduction rate of the defect is in the order of 10^{-2} cm^{-1}. Combined use of the MCD-ODMR [50, 51] and theoretical [52] results, it is concluded that P_{In} forms $P_{In}^{+/2+}$ and $P_{In}^{0/+}$ levels at $E_v+1.1$ and $E_v+1.39$ eV, respectively. The defect was introduced by electron irradiation at room temperature, and this indicates that isolated In interstitials can migrate even at 300 K [48]. The P_{In} was also observed by the magnetic circular dichroism of the optical absorption (MCDA); P_{In} has two annealing stages in the temperature range from 300 to 400 K and 550 to 650 K [53]. The H4 center observed by DLTS is believed to arise from a P_{In}-included defects [54].

The In atom on a P-site, In_P was first observed in electron irradiated InP by PL spectroscopy [55 - 58]. From the experimental [56] and theoretical [58] results, it is concluded that the emission bands peaking at the energy of 1.305 and 1.392 eV arise from the electron transition between the conduction band and $In_P^{-1/-2}$ ($E_v+0.115$ eV) and $In_P^{0/-1}$ ($E_v+0.030$ eV) levels, respectively. Since the defect is introduced by an electron irradiation at room temperature, In_i could also migrate even at 300 K [55, 57]. The In_P anneals at the temperature above 573 K [57], and the onset temperature is almost the same as one of P_{In} [53]. The e_1 defect observed by TSC, with the trap depth of 0.18 eV, is considered to be due to the complexes including In_P [59]. Recently, it was proposed that the band D luminescence observed by PL spectroscopy, peaking at the energy of 0.97 eV, is due to the In_P [39].

1-3-3 Annealing properties of point-like defects in InP

Annealing properties of lattice defects in InP are summarized in Table 1-2. Annealing at the temperature of 423K observed by PAS is explained as the clustering of V_{In} due to its thermal migration {43}. The annealing stage was also observed by HDS {60} and EC measurements {61}; the stage III is confirmed to be due to the migration of vacancies, even though the kind of the vacancy is not identified in the papers. From the experimental results of PL {39}, the onset temperature for the migration of V_P is estimated to be about 1023 K.

From the results of DLTS, Frenkel pairs of V_{In}-In_i, and V_P-P_i anneal at the temperature above 100 K; the onset temperatures of both In_i and P_i are about 100 K {46, 47}. The similar result has reported by HDS {60} and EC measurements {61}; the stage I is in the same temperature range, and it is explained as the recombination annihiration of the close Frenkel pairs in InP. The thermal migration of isolated interstitials is also confirmed by ESR {48} and PL {57}. The formation of P_{In} and In_P are considered to be due to the migration of P_i and In_i, respectively.

In the temperature range between the onset temperature for the migration of isolated interstitials and ones for isolated vacancies, an annealing stage (330 ~ 420 K) was observed By HDS {60}. In the temperature range, an annealing of P_{In} was reported {53, 54}. The same stage was also observed by EC measurement (270 ~ 400 K) {61} and DLTS (323 K~) {46, 47}. The most E and H centers observed by DLTS are several kinds of complexes of irradiation-induced defects (vacancies, interstitials, anti-site, etc.) and dopant impurities. This annealing might be explained as the change of the charge state of the defects due to the shift of Fermi level {53}, as observed in GaP {16, 19}.

Another annealing stage was observed in the temperature range above 573 K by PAS {43, 62}; a breaking up of vacancy clusters such as V_{In}-V_P results in the annealing. The same temperature range, both P_{In} {53} and In_P {57} also anneal out. The annealing mechanism of these defects is still debatable. In neutron irradiated InP, annealing stage of 723~973 K is reported by PAS {62}.

Table 1-2   Annealing properties of lattice defects in InP

Defect	Defect name	Experiments	Onset temperature for defect-formation [K]	Annealing temperature [K]	References
V_P	Band C	PL	-	~1023	{39}
V_P-X	Band B	PL	-	» 1023	{39}
V_{In}		PAS	< 77	200~250	{42}
				423~550	{43}
V_{In}-Y	Band A	PL	-	« 873	{39}
P_i-V_P	E4, E5	DLTS	< 77	100~	{46, 47}
P_{In}		ESR	~100	-	{48}
		MCDA	< 300	300~400	{53}
				550~650	{53}
	H4	DLTS	< 300	273~	{54}
In_i-V_{In}	H6	DLTS	< 77	100~	{46, 47}
In_P		PL	~100	530~	{57}
?	stage I	HDS	-	100~250	{60}
??	stage II	HDS	-	330~420	{60}
???	stage III	HDS	-	420~650	{60}
!	stage I	EC	-	100~150	{61}
!!	stage I'	EC	-	180~230	{61}
!!!	stage II	EC	-	270~400	{61}
!!!!	stage III	EC	-	480~540	{61}
#		PAS	-	573~	{43, 62}
##		PAS	-	723~973	{62}
$	other E, H	DLTS	< 77	323~	{46, 47}

X, Y, ??, !!!, $: Unknown defects
?, !, !! : vacancy-interstitial pairs
???, !!!! : vacancy-related defects
#, ## : vacancy clusters

9

1-4 Point-like defects in GaAs

1-4-1 Isolated vacancy and their complexes in GaAs

Isolated As-vacancy, V_{As}, was well investigated by PAS; it forms two donor levels at E_c-0.03 and E_c-0.14 eV {63}. Compared use of experiments and theoretical results {64}, these levels are identified as of $V_{As}^{-/0}$ and $V_{As}^{0/+}$, respectively {65}, and V_{As}^{+} is positron inactive {66}. V_{As} was also observed with ESR {67}; only a fraction of V_{As} annealed at 500 K, and a larger fraction disappeared at around 723 K. The former annealing stage is concluded as the recombination of V_{As}-As_i pairs through the migration of As_i, and the latter is due to the migration of V_{As} {67}.

Some kinds of defect complexes including V_{As} were also observed. Close Frenkel pairs of As site, pairs of V_{As} and As_i, were observed by HDS; the distance between V_{As} and As_i was about 10 Å, and they annealed at the temperature about 500 K {68}. The electron traps named E centers and hole traps named H3-H5 centers observed by DLTS are proposed to associates with the pairs of V_{As} and As_i {69-71}, and all levels anneal at 500 K. V_{As}-As_{Ga} was observed with ESR; the ESR signal, with a g-factor of 1.97, is concluded to derive from a spin 1/2 defect {72, 73}.

Isolated Ga-vacancy, V_{Ga}, was well investigated by means of PAS. It is believed that V_{Ga}^{3-} forms acceptor level below midgap {74, 75}. The level anneals in the temperature range from 77 to 500 K {75}, mainly anneals at the temperature about 300 K {76}. V_{Ga}^{0} was observed with MCDA {77} and V_{Ga}^{2-} was investigated by ESR {78}.

Some complexes including V_{Ga} were also found. Close Frenkel pairs of Ga site, pairs of V_{Ga} and Ga_i, were observed by HDS; the distance between V_{Ga} and Ga_i was about 10 Å, and they annealed at the temperature about 300 K {68}. MCDA spectrum at 0.8 eV is concluded to be related to V_{Ga} {79, 80}, and proposed to be due to V_{Ga}-Ga_i {81}. P2 center peaking at 0.8 eV in PL spectra is also concluded to be related to V_{Ga} {82}. Since it anneals at 600 K, it is believed that V_{Ga} can migrate at above 600 K {82}. This annealing was also observed in ESR spectra {83, 84}.

1-4-2 Isolated interstitial atom and their complexes in GaAs

The H and E centers observed by DLTS are proposed to be related to isolated As interstitials, As_i; these levels are associated with the pairs of V_{As} and As_i, {69-71}. These traps anneal at the temperature above 500 K {71}, and the annealing is believed to be due to the recombination of isolated interstitials and vacancies through the migration of As_i; the onset temperature for the migration of As_i is about 500 K. The migration energy of As_i is estimated as 0.51 eV {85}. The annealing stage was also observed by HDS {6}. A boron {86} and a carbon {87, 88} atom on Ga-site with As-interstitial, B(1) and C(1)-center, were observed by IR spectroscopy in the electron-irradiated GaAs. B(1) center anneals at 500 K with the activation energy of 1.65 eV {89}, while C(1) center anneals at around 425 K {90}.

The pairs of V_{Ga} and Ga_i were observed by HDS; the annealing stage at the temperature about 300 K is believed to be due to the recombination of isolated Ga interstitials and vacancies through the migration of Ga_i; the onset temperature for the migration of Ga_i is about 300 K {68}.

The As atom on a Ga-site, As_{Ga} was first observed by ESR {91} with a theoretical result {92}. Combined use of the results and IR data, it is concluded that As_{Ga} are not introduced by recombination of V_{Ga} and As_i through the migration of As_i {93}. As_{Ga} related complexes, that are proposed as As_{Ga}-V_{As} and As_{Ga}-Ga_{As}, were observed by ESR {72, 73} and ODENDOR {94}, respectively. EL2 defect, that are the most extensively investigated in GaAs, is also including As_{Ga}, and the properties are summarized in the next section.

The Ga atom on an As-site, Ga_{As} was preciously investigated by PAS. Ga_{As}^{2-} forms acceptor levels below midgap {74, 75}, and they anneal at around 520 K {76}. Ga_{As} was also observed by PL; it forms two acceptor levels at E_V+0.077 and E_V+0.203 eV {95}, and has T_d symmetry {96}. MCDA spectrum at 1.45 eV is also considered to be due to Ga_{As} {97}. Ga_{As} related complex, that is proposed to be Ga_{As}-As_{Ga}, was observed by ODENDOR {94}

1-4-3 EL2 defect in GaAs

EL2 defect was first observed by DLTS {98}. Since the defect compensates the residual acceptor impurities and pins the Fermi level to the midgap position, it has extensively investigated experimentally and theoretically. DLTS result indicates that EL2 forms the energy level at $E_c-0.82$ eV {98-100}. The level was also observed by optical absorption measurement {101} and MCDA {102, 103}. It is believed that the luminescence in the wavelength range 0.62-0.65 eV observed by PL {104, 105} and CL {106} is due to EL2 defect.

At a temperature below 100 K, EL2 changes to a metastable state by illumination with 1.1-1.3 eV light {83, 107}. It recovers by an annealing at the temperature above 120 K with the activation energy of 0.3 eV or by illumination with 0.7 or 1.5 eV light {83, 107}. Since the metastability is the same as one of As_{Ga}, EL2 is believed to include As_{Ga} {99, 108, 109}.

A structure model of EL2 was proposed with ESR and ODENDOR results. As_{Ga} related defect was observed by ESR {109-111}; it forms two acceptor levels at $E_V+0.52$ and $E_V+0.75$ eV, and these levels are identified as of $As_{Ga}^{+/2+}$ and $As_{Ga}^{0/+}$, respectively {112}. The defect was identified as As_{Ga}-As_i defects by ODENDOR {113}; the defect has C_{3v} symmetry and As_i is located at the second tetrahedral interstitial site (T_{d2}) at 4.88 Å from As_{Ga} {113}. Since the photo-quenching properties of this defect are similar as one of EL2, the defect is concluded to be the origin of EL2 defect {114}.

Another model was proposed with PAS results. The introduction of metastable gallium vacancies, V_{Ga}^*, was observed when an as-grown si-GaAs is illuminated with 1.1-1.3 eV light at 25 K, and they annealed at 120 K {115}. Similar defects were also introduced in electron-irradiated si-GaAs, and the introduction rate of the defect was 0.3 cm^{-1} {116}; this value is very close to one for As_{Ga} {116}. From the results and MCDA data {117}, it was concluded that V_{Ga}^* belongs to the metastable state of As_{Ga} {118}. It is thus proposed that EL2 defect is single As_{Ga} defect; when the defect transforms to the metastable state, the As anti-site atom moves from the substitutional lattice site towards the interstitial position (As_{Ga} -> $V_{Ga}^*+As_i$) {115, 116, 118}. The result is consistent with the theoretical result {119}.

12

1-4-4 Annealing properties of point-like defects in GaAs

Annealing properties of lattice defects in GaAs are summarized in Table 1-3. The thermal migration of V_{Ga} is confirmed by PAS [76]; the annealing stage of V_{Ga} at the temperature range from 200 to 300 K is due to the migration of Ga_i. This annealing stage was also observed by HDS [68], EC [120], and PL measurements [123]. The annealing of MCDA spectra peaking at 0.8 eV was observed in the same temperature range, and it is due to the recombination of V_{Ga}-Ga_i pairs through the migration of Ga_i [81].

From DLTS results, Frenkel pairs of V_{As} and As_i anneal at the temperature above 493 K; the onset temperature of As_i is about 493 K [71]. This annealing stage was observed by ESR [67]; the annealing stage at around 493 K is due to the recombination of V_{As}-As_i pairs through the migration of As_i. The similar result was reported by HDS [68], EC [120, 124, 125], and PL measurements [123]; the stage III was in the same temperature range and was explained as the recombination annihilation of the close Frenkel pairs in GaAs, even though the kind of the vacancy was not identified in the paper. The annealing of B(1) [89] and C(1) centers [90] observed by IR is also believed to be due to the migration of As_i, even though the annealing temperature for C(1) center is slightly lower than 500 K [90].

It is believed that V_{Ga} can migrate at the temperature above 600 K, since the PL spectra due to a defect complex including V_{Ga} disappear at around 600 K [82]. Reverse-annealing at the temperature range from 520 to 620 K [121] and at 573 K [122] observed by PAS was explained as the clustering of vacancies due to its thermal migration, and it is considered as the formation of V_{Ga} clusters through the migration of V_{Ga}. The annealing stage in the similar temperature range (600 - 800 K) was also observed by HDS [68].

From ESR results, the onset temperature for the migration of V_{As} is concluded as 723 K [67]. In the same temperature range, similar annealing stages ware observed by HDS (stage IV) [68] and EC measurements [124, 125].

From MCDA results [81], Ga_{As} and As_{Ga} are considered to migrate at the temperature range from 600 to 850 and 500 to 600 K, respectively.

Table 1-3   Annealing properties of lattice defects in GaAs

Defect	Defect name	Experiments	Onset temperature for defect-formation [K]	Annealing temperature [K]	References
V_{As}		ESR	-	493	{67}
			-	723	{67}
V_{Ga}		PAS	-	200~300	{76}
V_{Ga}-X	P1, P2	PL	-	600	{82}
As_i-V_{As}	E, H3-H5	DLTS	-	493	{71}
As_i-B_{Ga}	B(1)	IR	-	500	{89}
As_i-C_{As}	C(1)	IR	-	423	{90}
As_{Ga}-Y	EL2	MCDA	-	600~850	{81}
Ga_i-V_{Ga}		MCDA	-	300	{81}
Ga_{As}-As_{Ga}		MCDA	-	500~600	{81}
?	stage (I, II)	HDS	-	250~350	{68}
??	stage III	HDS	-	500~550	{68}
???	stage IV	HDS	-	600~800	{68}
!	stage I	EC	-	235	{120}
!!	stage II	EC	-	280	{120}
!!!	stage III	EC	-	520	{120}
#		PAS	-	520~620	{121}
##		PAS	-	~573	{122}
$		PL	-	~300	{123}
$$		PL	-	~473	{123}
%		EC	-	373~573	{124, 125}
%%		EC	-	673~	{124, 125}

X, %, %% : Unknown defects

?, ??, !, !!, !!!, $, $$: vacancy-interstitial pairs

???, #, ## : vacancy clusters

14

1-5 Formation of extended defects

In order to study the kinetics of point defects in III-V compound semiconductors, *in-situ* high-voltage electron microscopy was performed. Under strong electron irradiation of 1.4×10^{20} cm^{-2}s^{-1}, small dislocation loops of interstitial type were observed in GaP, GaAs, and InP above 117 K {126 - 129}. These loops were proposed to be perfect loops {128}, and recently it is confirmed that they are perfect dislocation loops on {110} in InP {130} and GaAs {131}. These loops were nucleated near the electron entrance surface of each specimen having two defect free zones along both surfaces which become thicker with raising an irradiation temperature. The formation of the loops strongly depends on electron diffraction condition; the maximum formation rate of the loops is realized when [220] type reflection is strongly excited {126 - 129}.

These loops are formed by the thermal migration of interstitial atoms which are introduced by an electron irradiation. The formation process of the loops is considered as follows; impurity atoms on the electron entrance surface may be injected into the specimen by incident electrons of 2 MeV under the condition of thermal diffusion and/or radiation enhanced diffusion, and some kinds of the shot-in impurity atoms may play an important role as nuclei for the formation of the loops. The number density of loops was observed as a constant value up to the irradiation temperature of about 500 K, and then it decreased with raising the irradiation temperature. In the higher temperature range above 500 K, the nucleation of the interstitial-type dislocation loops is considered to be performed during the repeated process of trapping and release of isolated interstitials by impurities; the sum of their binding energy and the energy for the migration of isolated interstitials can be derived as the twice of the energy shown by the slope of the logarithms of the number density against the reciprocal of the irradiation temperature {126}. From the analysis, the migration energies of isolated interstitials in GaP and InP are roughly estimated as 0.9 eV, even though the energy may be affected by impurity atoms {126}.

1-6 Purpose of this thesis

As I summarize in the previous sections, kinetics of point defects in III-V compounds is still uncertain; especially, there is no reliable information on the kinetics of point defects in the temperature range from the onset temperature for the migration of isolated interstitials (about 100 K) to one of vacancies (about 700 K). In the temperature range, several kinds of defects anneal at almost the same temperature, and the annealing temperature does not depend on impurity atoms contained in the specimen. It is considered that the defect-annealing is closely connected with the migration of interstitial atoms, even though the annealing mechanism of the defects is still uncertain.

In this study, I found that dislocation loops of interstitial-type are formed uniformly in GaP, InP, and GaAs due to the thermal migration of interstitial-related defects introduced by electron irradiation. The formation of the loops is independent of the presence of impurity atoms. In order to understand the migration of the defects in III-V compounds at the temperature above 110 K, I have systematically examined the growth of the loops by *in-situ* transmission electron microscopy.

The loops are formed by an annealing at the temperature above 700 K following an electron irradiation, and thus the kinetics of defects at low temperature is hardly studied by TEM. In the temperature range below 110 K, I found that luminescence spectra in GaP and GaInP change with an electron irradiation due to the formation of electron-irradiation-induced defects; the defects are closely related to interstitial atoms introduced by an irradiation. For investigation of the migration of interstitial-related defects directly in the temperature range from 20 to 110 K, I have investigated the electron-irradiation-induced defects in III-V compounds by utilizing an *in-situ* TEM-PL/CL observation apparatus, which enables us to obtain simultaneously TEM images and photoluminescence (PL) / cathodoluminescence (CL) spectra.

2 Diffusion process of interstitial atoms at high temperature

2-1 Introduction

As shown in the previous section, the atomic and electronic structures of a single vacancy on III and V atomic sites in III-V compound semiconductors, V_{III} and V_V, have been clarified by ESR, DLTS and PAS with theoretical approaches. From the investigation of annealing properties of these defects, the onset temperatures for the migration of the defects have been estimated. The electrical and annealing properties of a single interstitial of III and V atoms, III_i and V_i, and two types of anti-site defects on III and V atomic sites, V_{III} and III_V, have been also clarified. Above an onset temperature of a defect, the defects become unstable and then diffuse through semiconductors until they become trapped another defects, impurities, or surfaces. Such behavior is well investigated in Si {32, 133}. On the other hand, very few defect diffusions in III-V compound semiconductors have been conclusively identified. In the temperature range between the onset temperature for the interstitial-migration and one for the vacancy-migration, annealing stages of defects have been observed in III-V compounds. These results indicate the existence of several kinds of complexes associated with interstitial atoms. It is proposed that these annealing stages are concerned with the migration of the complexes or isolated interstitials, even though the diffusion processes of the defects are still uncertain.

In the present study, I found the formation of small dislocation loops of interstitial-type by an annealing above 700 (GaP and InP) and 800 (GaAs) K following 200 (GaP and InP) and 300 (GaAs) keV electron irradiation. I found that the loops are formed through the thermal migration of interstitial-related complexes introduced during electron irradiation and the migration of the complexes is closely related to the annealing stage around 500 K. In order to understand the diffusion process of point defects in III-V compounds, I examined the growth of the loops by in-$situ$ weak-beam TEM method under several annealing and irradiation conditions, and I concluded that the loops are formed by the thermal migration of III_i-V_i interstitial-pairs which are introduced during an electron irradiation.

2-2 Preparation of specimens

2-2-1 properties of specimens

Specimens were undoped GaP, InP and GaAs single crystals grown by Czochralski method. Even though the specimens were nominally undoped, small amount of impurities was introduced during crystal growth. From the measurements of the selected ion mass spectroscopy (SIMS), the concentrations of impurities were estimated as shown in Table 2-1.

Table 2-1 Concentration of impurity atoms (cm^{-3})

	Oxygen	Sulfur	Silicon	Carbon
GaAs	$<1\times10^{16}$	$>1\times10^{15}$	$<1\times10^{15}$	$>1\times10^{15}$
InP	4.6×10^{17}	$>1\times10^{15}$	$<4\times10^{15}$	$<1\times10^{15}$
GaP	1.2×10^{18}	1.4×10^{16}	1.5×10^{15}	2.9×10^{15}

2-2-2 TEM specimens

Specimens for TEM observation were prepared as follows. Disks with {110} or {100} surfaces, 3 mm in diameter and 0.4 mm in thickness, were cut from a crystal using an ultrasonic cutter. The central part of a surface on each disk was dug about 0.32 mm deep and 1 mm in diameter by an ultrasonic drill. Finally, each disk was polished chemically in a mixture of HNO_3 and HCl until a small opening was formed. The crystal around the opening was wedge-shaped and suitable for TEM observation.

For introducing Frenkel-type defects intentionally, specimens were irradiated with the electron beam exactly parallel to the <110> or <100> direction in a transmission electron microscope (JEOL JEM 2000 EX or Hitachi H-300). The acceleration voltages of electrons were 200 kV for GaP and InP, and 300 kV for GaAs specimens, respectively. Irradiation temperature, T_{ir}, was kept at 300 K, otherwise it is noted in the text. The irradiation area on a specimen surface was about 2 μm in diameter.

After an electron irradiation, the specimens were annealed at a temperature, T_{an}

(700~1000 K) for a period, τ_{an} (0~25200 s). For GaP specimens, annealing were performed in a microscope. Due to the thermal drift of a TEM specimen at an elevated temperature, I started to take TEM photographs about 2400 s after the annealing commenced. For GaAs and InP, specimens were annealed in a flowing argon atmosphere in a furnace, since they rapidly deteriorated when they annealed in vacuum at a temperature above 700 K. In my experiments, it took about 600 s to stabilize a furnace temperature, so I used only $\tau_{an} \geq 600$ s. Because of the deterioration of specimen surfaces even in an argon atmosphere, I could not anneal InP and GaAs samples at the temperature above 825 K.

Dislocation loops of interstitial-type, created by an annealing following an electron irradiation, were observed by the weak-beam TEM technique using a 220- or 113-type diffraction spot. Weak-beam TEM images were taken with the beam of an off-axial incident direction in order to avoid irradiation-effects during observation (see Sec. 2-4-1).

I measured the radii of dislocation loops as follows. I fond two kinds of dislocation loops; on {110} and {111} internal atomic planes. Both kinds of the loops showed the obvious double-arc lobe contrast in a weak-beam condition. I measured the radii of the contrasts as ones of the loops. For a dislocation inclined to the plane of the foil at an angle φ, the displacement of the image from the center of the dislocation is on the order of $\cos\varphi/2\pi s$, in which s represents the deviation parameter {133}. Since s is in the order of 1.0 nm^{-1}, the error in the measurement of the loop radius is roughly estimated as about 1 nm. For the {111} defects, I also measured the radii of the contrast due to staking faults as ones of the loops, and confirmed that the value is almost the same as one estimated with double-arc lobe contrasts within the experimental error of 1 nm.

2-3   Theoretical basis for study of electron-irradiation-induced defects

2-3-1   Introduction of lattice defects by electron irradiation

High energy electrons passing through a material produce displacements of atoms; an atom is pushed into the lattice to form an interstitial atom, leaving a vacancy behind.   Figure 2-3-1 shows a collision between an electron of mass m_0 and energy E with an atom of mass M.   The scattering angle is θ.   The energy transferred to the atom is given by

$$E_p = \frac{2E}{Mc^2}\left(E + 2m_0c^2\right)\sin^2\frac{\theta}{2}, \qquad (2\text{-}3\text{-}1)$$

in which c represents the light velocity.   The maximum energy $E_{p,max}$ is transferred when $\theta = \theta_{max} = \pi$, and thus

$$E_{p,max} = \frac{2E}{Mc^2}\left(E + 2m_0c^2\right). \qquad (2\text{-}3\text{-}2)$$

A displacement damage occurs when the energy transferred to an atom is larger than the displacement threshold energy.
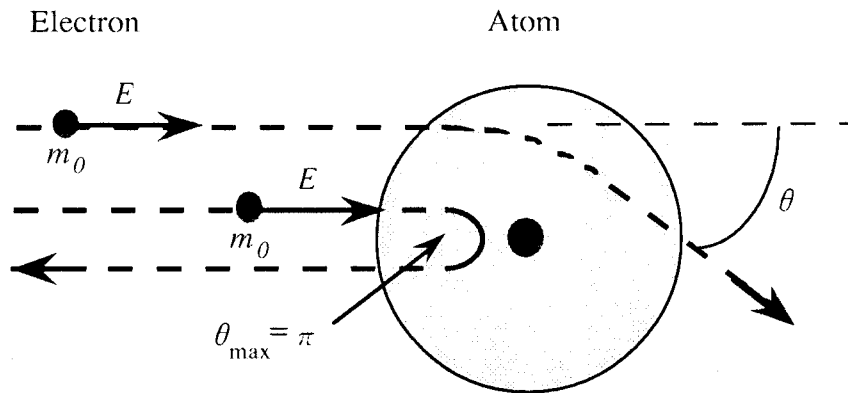
Fig. 2-3-1   A collision between an electron of mass m_0 and an atom of mass M

Electrons accelerated by a high voltage in the order of keV are relativistic and the scattering of an electron by a nucleus of an atom necessitates a quantum treatment. The exact calculation of the displacement cross section σ, derived by Mott {134, 135}, can be approximated by McKinley-Feshbach's formula {136} for the case of atoms whose atomic number is not too larger. The formula is written as

$$\sigma = \pi \left[\frac{Ze^2\gamma}{m_0c^2(\gamma^2-1)} \right]^2 \left[\left(\frac{E_{p,max}}{E_d} - 1 \right) - \frac{\gamma^2-1}{\gamma^2} \ln \frac{E_{p,max}}{E_d} \right.$$
$$\left. + \alpha\pi Z \sqrt{\frac{\gamma^2-1}{\gamma^2}} \left(2\sqrt{\frac{E_{p,max}}{E_d}} - 2 - \mathrm{Ln}\frac{E_{p,max}}{E_d} \right) \right] \qquad (2\text{-}3\text{-}3)$$

where Z is atomic number of the atom, α ($= 1/137$) is the fine structure constant, and

$$\gamma = \sqrt{1 - \frac{v^2}{c^2}}, \qquad (2\text{-}3\text{-}4)$$

in which v is the velocity of the incident electron. E_d is the displacement threshold energy and it is rewritten as

$$E_d = \frac{2eV_{th}}{Mc^2} \left(eV_{th} + 2m_0c^2 \right), \qquad (2\text{-}3\text{-}5)$$

in which V_{th} represents the threshold acceleration voltage for displacement. Figure 2-3-2 shows the cross section σ for the displacement of (a) Ga and P atoms in GaP, (b) In and P atoms in InP, and (c) Ga and As atoms in GaAs calculated with Eq. (2-3-3), respectively. In the calculation, I used the displacement threshold energy for the displacement of As atoms in GaAs of 10 eV ($V_{th} \sim 270$ kV) {137, 138}. The energy for Ga atoms in GaAs was directly estimated to be 25 eV by DLTS {139}. However, this value was pointed out to be due to secondary displacement of Ga atoms and thus I use 10 eV for Ga atoms, that is believed the "real" displacement threshold energy {140}. The displacement threshold energies for the

displacement of In and P atoms in InP are 4 (V_{th} ~ 120 kV) and 8 eV (V_{th} ~ 100 kV), respectively {141}. For GaP, I used E_d for P atoms of 8 eV (V_{th} ~ 100 kV), that is estimated for P atom in InP {142}. E_d(Ga) is roughly estimated as 6 eV with the experimental result of V_{th} = 125~150 kV {143}. Since σ for each specimen is extremely small, I can expect that displacements of atoms in a sample occur uniformly in the case of specimens for an electron microscopy.
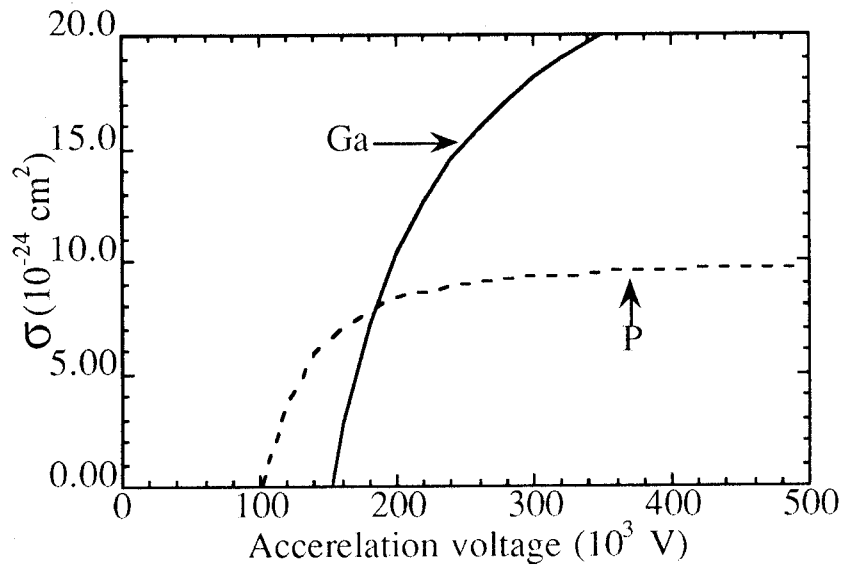

Fig. 2-3-2(a) Estimated cross section σ for the displacement of Ga and P atoms in GaP
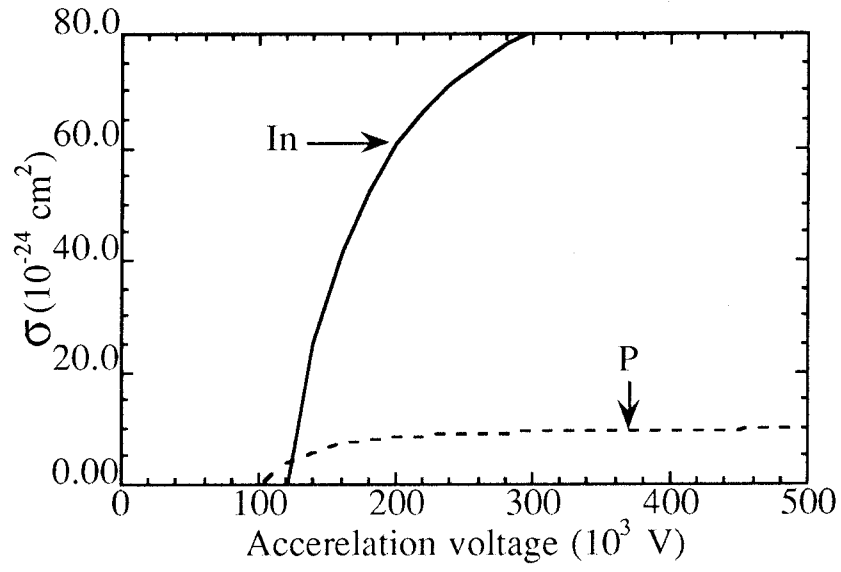
Fig. 2-3-2(b) Estimated cross section σ for the displacement of In and P atoms in InP
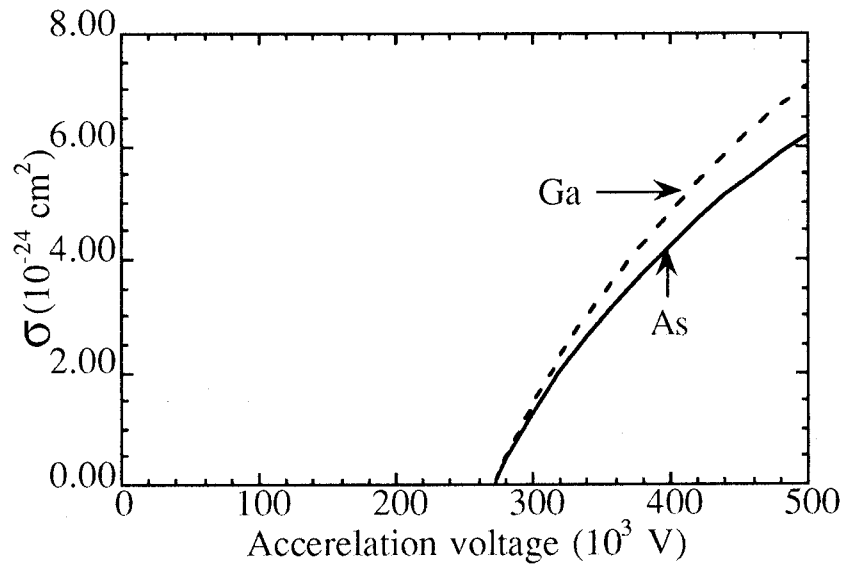
Fig. 2-3-2(c) Estimated cross section σ for the displacement of Ga and As atoms in GaAs

The average energy of the primary knock-on atoms, $\overline{E}_p$ can be obtained as

$$\overline{E}_p = \frac{\int E_p d\sigma_p\left(E, E_p\right)}{\int d\sigma_p}$$

$$= E_{p,max}\frac{\ln\chi - \beta^2(1 - 1/\chi) + \pi\alpha\beta\left[2(1 - 1/\chi) - (1 - 1/\chi)\right]}{(\chi - 1) - \beta^2\ln\chi + \pi\alpha\beta\left[2\left(\sqrt{\chi} - 1\right) - \ln\chi\right]},$$

(2-3-6)

where $\chi = E_{p,max}/E_d$. Figure 2-3-3 shows the average energy of (a) the primary knock-on Ga and P atoms in GaP, (b) In and P atoms in InP, and (c) Ga and As atoms in GaAs calculated with Eq. (2-3-6). Since the average energies are of the order of E_d s, most of the displacements are single displacements which result in the formation of a pair of single interstitial and vacancy.
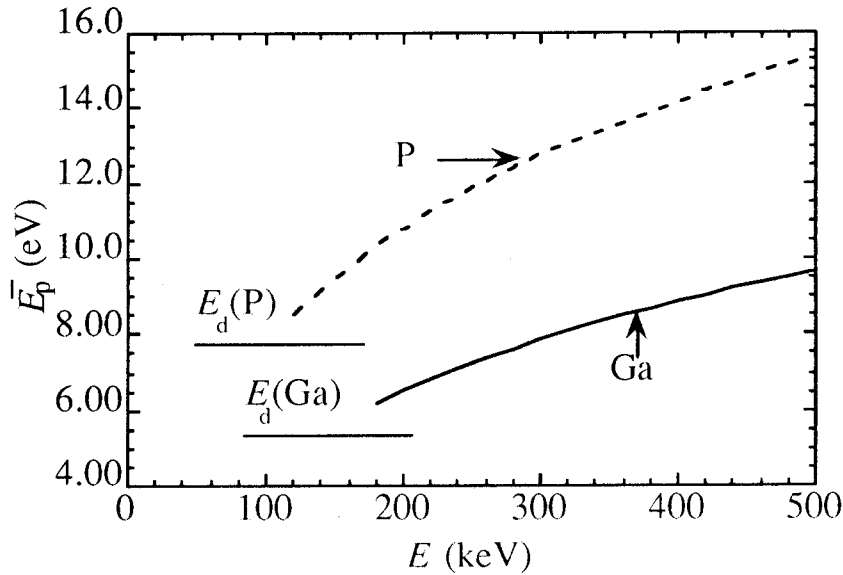
Fig. 2-3-3(a) Estimated average energy of the primary knock-on Ga and P atoms in GaP
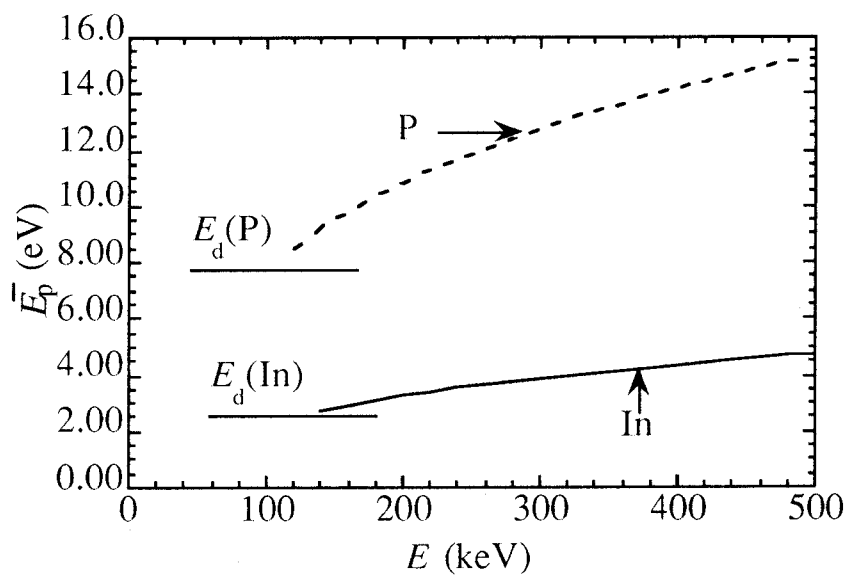
Fig. 2-3-3(b) Estimated average energy of the primary knock-on In and P atoms in InP
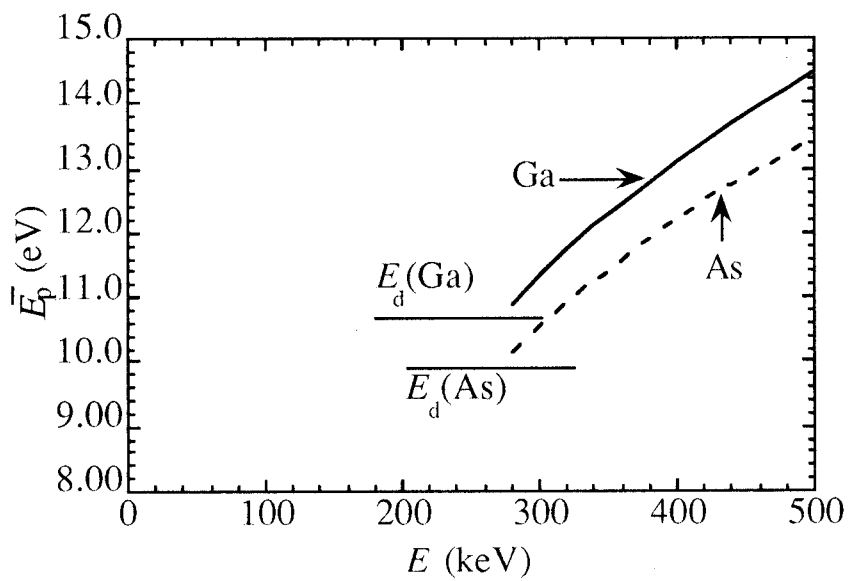

Fig. 2-3-3(c) Estimated average energy of the primary knock-on Ga and As atoms in GaAs

25

The damage rate P is given by the following formula,

$$P = \sigma\phi(1 - f),$$
(2-3-7)

where ϕ is the electron flux and f the correlated recombination factor; i.e. the probability that a displaced atom returns to the vacant site from which it originates {144}. In the present study, the irradiation was carried out with an electron microscope operated at 200 or 300 kV and the typical electron flux ϕ is 10^{18} electrons cm^{-2} s^{-1}. The value of f under electron irradiation is roughly estimated to be about 0.8 with the experimental result for Ga and In atoms in GaInP {145}. The production rate P is, therefore, estimated as about 10^{-6} displacement per atom per second. That is to say, after irradiation for about 10^6 s, every atoms in the specimen will be displaced from its lattice site one time.

2-3-2 Analysis of a defects reaction with rate equations

In general, above the onset temperature for the migration of a lattice defect, the defects migrate thermally and/or react with another kinds of defects. In order to understand the rate of the reaction quantitatively, rate equations have been commonly used. The rate of the bimolecular reaction $A + B \rightarrow AB$ is determined by two factors; 1) the probability that an A and a B will encounter one another in their random motions, and 2) the probability that an A and a B will react upon encounter. It is well known that the reaction rates of gases phases are second order with specific reaction rates of the form:

$$\frac{dC_A}{dt} = Z_{AB}(r_{AB}{}^*, C_A, C_B)\, p \exp\left(-\frac{\Delta E^*}{kT}\right),$$
(2-3-8)

where $Z_{AB}(r_{AB}{}^*, C_A, C_B)$ is the A-B collision frequency for particles of collision diameter $r_{AB}{}^*$ and concentration C_A and C_B; p and ΔE^* are the steric and activation energy factors characteristic of the reacting particles {146}. A quantitative expression for the rate of the bimolecular reaction $A + B \rightarrow AB$ in condensed phases in terms of $r_{AB}{}^*$, p, ΔE^* and the

diffusion parameters of the reacting species were discussed by Waite {146, 147}. In the theory, it is necessary to make three major assumptions in addition to those already implied in Eq. (2-3-8). First, it is necessary to assume that every motion of a reactive particle is independent of its previous history. This is equivalent to the assumption that after each jump or free flight the particle comes immediately to thermal equilibrium with its surroundings. This permits the use of stochastic theory for the calculation of the average motions of each particle. Second, any discreteness in the positions available to a particle, as might be imposed by the lattice of a solid, is approximated by a continuum of positions so that the random walk or diffusion of the particles may be described by differential equations. Third, at one point it is assumed that, although the distribution of each A is correlated to the distribution of each B, no correlation between the distribution of two A's (or two B's) exists either by virtue of their direct interactions or their mutual interaction with the B's. With these assumptions, the rate equation is expressed as

$$\frac{dC_A}{dt} = \frac{dC_B}{dt} = -Z(M_A + M_B)C_A C_B \qquad (2\text{-}3\text{-}9)$$

in which Z represents the number of reaction sites around a ξ-particle and M_ξ the mobility for ξ-particle (ξ=A, B). It is believed that Z is of the order of 10^2 in case of the recombination of an interstitial atom and a vacancy in metals and alloys {148}; i.e. in this case, A means interstitial atoms and B means vacancies.

2-3-3 Weak beam TEM method

Transmission electron microscopy (TEM) has extensively applied to the analysis of lattice defects {149, 150}. A schematic TEM is shown in Fig. 2-3-4. Electrons from an electron gun accelerate at high voltages (200~300 kV) and focused on a specimen by condenser lenses. The diameter of the electron beam is about a few μm. The sample must thin enough (0 ~ 500 nm) for electrons to be transmitted through it. The transmitted and forward scattered electrons from a diffracting planes in a specimen are focused on the back focal plane (Ewald sphere), and either the image or the diffraction pattern is projected onto a screen for viewing or for photographic recording with additional lenses. Images formed using only transmitted electrons are known as bright-field images and ones formed using a specific diffracted beam are called dark-field images, as illustrated in Fig. 2-3-4.
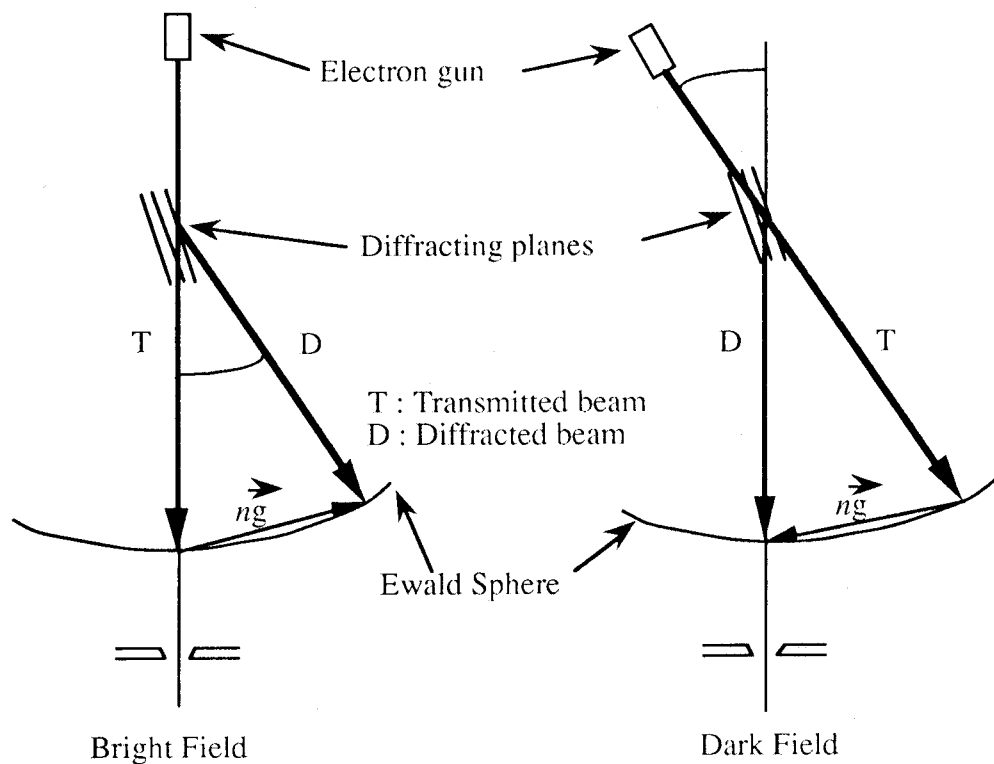
Fig. 2-3-4   Schematic representation of transmission electron microscopy

When some defects exist in a specimen, the contrast arises from local changes in diffracting conditions caused by the defect strain field. This is the most common mechanism used in defects studies {149}. A weak-beam dark-field image is formed in a "weak" reflection with large deviation parameter $|s_g|$ (Fig. 2-3-5). The contrast in this case arises from regions of large lattice strain close to the cores of defects. Far away from defects the foil is tilted well away from the Bragg condition and so the image intensity is very low. However, in regions close to defects, the local strain-field may bend the reflecting planes back towards the Bragg condition, resulting in a local image peak of high relative (but low absolute) intensity.
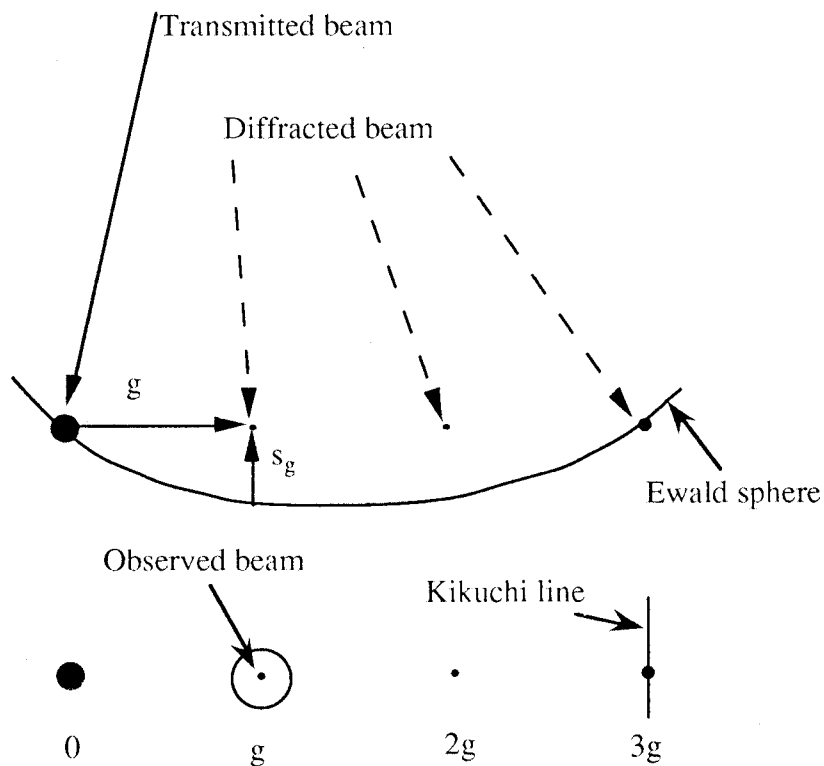
Fig. 2-3-5 Schematic representation of the weak-beam diffraction condition

It is usually considered that true weak beam conditions are obtained when the value of the deviation parameter $|s_g|$ is in the order of 10^{-1} nm^{-1} {149}. The appropriate diffraction condition can be set up by reference to Kikuchi lines in a diffraction pattern. Suppose the foil is tilted such that the Ewald sphere cuts the line of systematic reflections at the point ng. The value of "n" is immediately apparent from the kikuchi pattern. If n is integral then the bright excess Kikuchi line corresponding to the reflection ng will pass directly through the diffraction spot ng. Figure 2-3-5 represents the case of $n = 3$. $|s_g|$ can be calculated from the formula

$$s_g = \frac{(n-1)g^2}{2k},$$
(2-3-9)

where $g = 1/d_{hkl}$ is the magnitude of the reciprocal lattice vector corresponding to the planes (hkl) with interplanar spacing d_{hkl}; $k = 1/\lambda$ is the radius of the Ewald sphere, where λ is the electron wavelength; and the "reflection" ng is satisfied in the sense explained above. I observed weak-beam TEM images using a 220- or 113-type diffraction spot with 200 keV electrons ($n = 3$ or 5, $\lambda = 2.51 \times 10^{-3}$ nm). The estimated $|s_g|$, n, and the lattice constant a for each specimen are summarized in Table 2-2.

Table 2-2 Deviation parameter for III-V compounds

	a (10^{-1} nm)	n	$|s_{220}|$ (10^{-2} nm^{-1})	$|s_{113}|$ (10^{-2} nm^{-1})
GaAs	5.65	3	6.3	8.6
		5	12.6	17.3
GaP	5.45	3	6.8	9.3
		5	13.5	18.6
InP	5.87	3	5.8	8.0
		5	11.7	16.2

2-4 Results of in-situ TEM observation {151-154}

2-4-1 Formation of dislocation loops of interstitial-type

2-4-1-1 Nature of dislocation loops

Fig. 2-4-1(a) shows a weak-beam TEM image of GaP after an electron irradiation (an electron flux, ϕ_{ir} = 5.5x10^{18} cm^{-2} s^{-1} and an irradiation period, τ_{ir} = 7200 s). There is no distinct contrast of lattice defects in the irradiated area (indicated by the circle in Fig. 2-4-1(a)). Fig. 2-4-1(b) shows the result after a subsequent annealing (T_{an} = 1000 K, τ_{an} = 1800 s). A number of defects exist in the irradiated area; the defects were formed after a subsequent annealing at the temperature range $T_{an} \geq 700$ K. From the observation of the defects with several reflections and incident-beam directions, I concluded that they are dislocation loops on {111} planes; the {111} loops were located homogeneously on four equivalent {111} planes. The defects were identified as the Frank-type dislocation loops of interstitial-type by means of the inside-outside method. The nature of the loops was confirmed by high-resolution TEM (Fig. 2-4-2); an oblique view of the image along the horizontal direction indicates that the extra {111} plane is inserted.

Similar defects were also introduced in InP with the same procedure; they were formed by a subsequent annealing at the temperature range $T_{an} \geq 700$ K after an electron irradiation. Figure 2-4-3 shows a result; ϕ_{ir} = 4.7x10^{18} cm^{-2} s^{-1}, τ_{ir} = 3600 s, T_{an} = 800 K, and τ_{an} = 1800 s. The defects introduced in the irradiated area (the upper side of the thick line in Fig. 2-4-3) were identified to be dislocation loops on {111} and {110} planes; the {111} and {110} loops were located homogeneously on four equivalent {111} planes and on six equivalent {110} planes, respectively. In Fig. 2-4-3, the {111} defects show a strong white-dot contrast due to stacking faults with a weak double-arc lobe contrast (Frank-type loops), while the {110} defects show no contrast in a double-arc lobe contrast (they should be perfect loops). Two kinds of the defects were identified as loops of interstitial-type by means of the inside-outside method. The nature of the {111} loops was confirmed by high-resolution TEM (See Fig. 2-4-4).
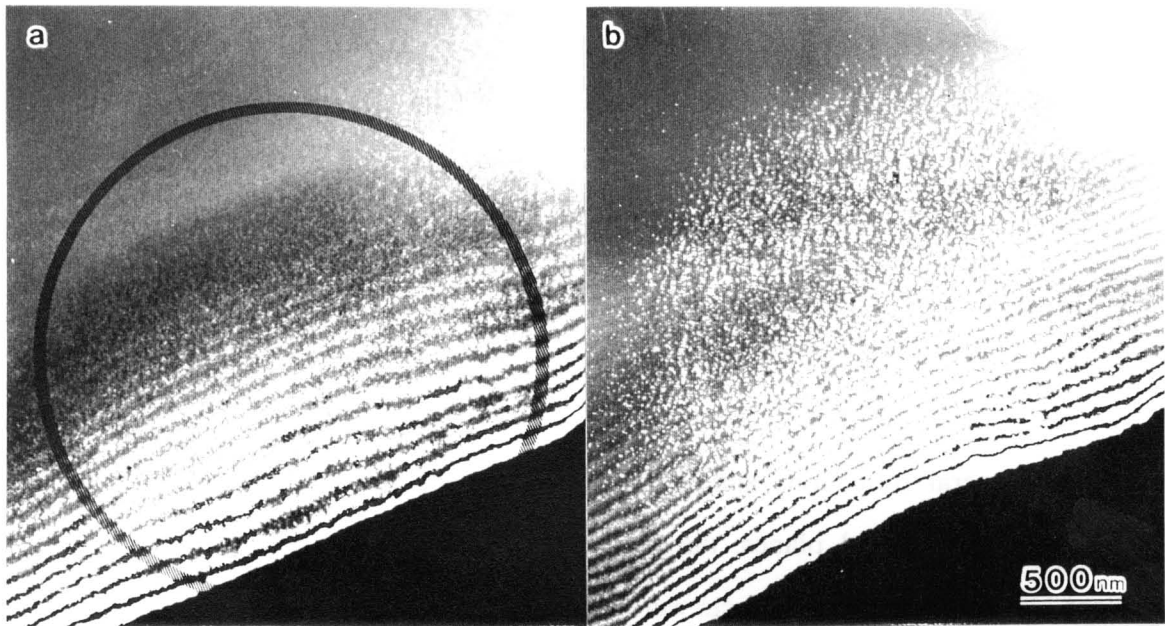
Fig. 2-4-1 Weak-beam TEM images of an electron irradiated GaP (a) before and (b) after an annealing at 1000 K. The irradiated area is about 2 μm in diameter.
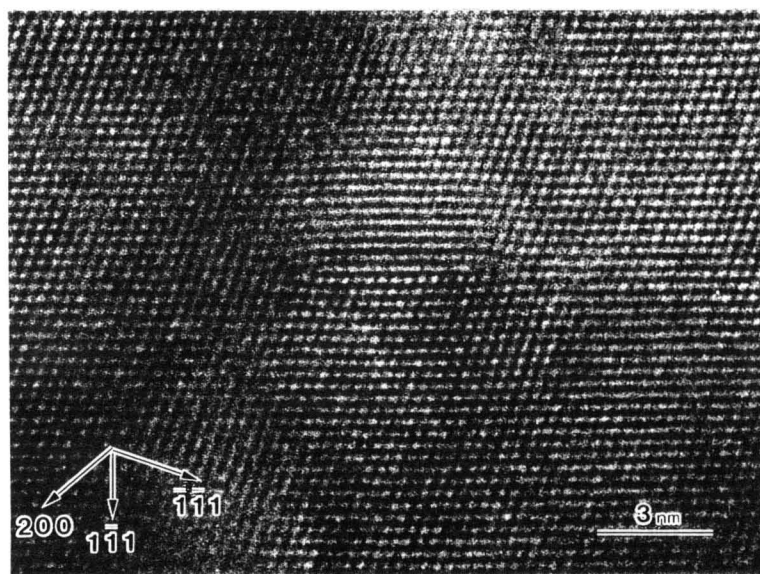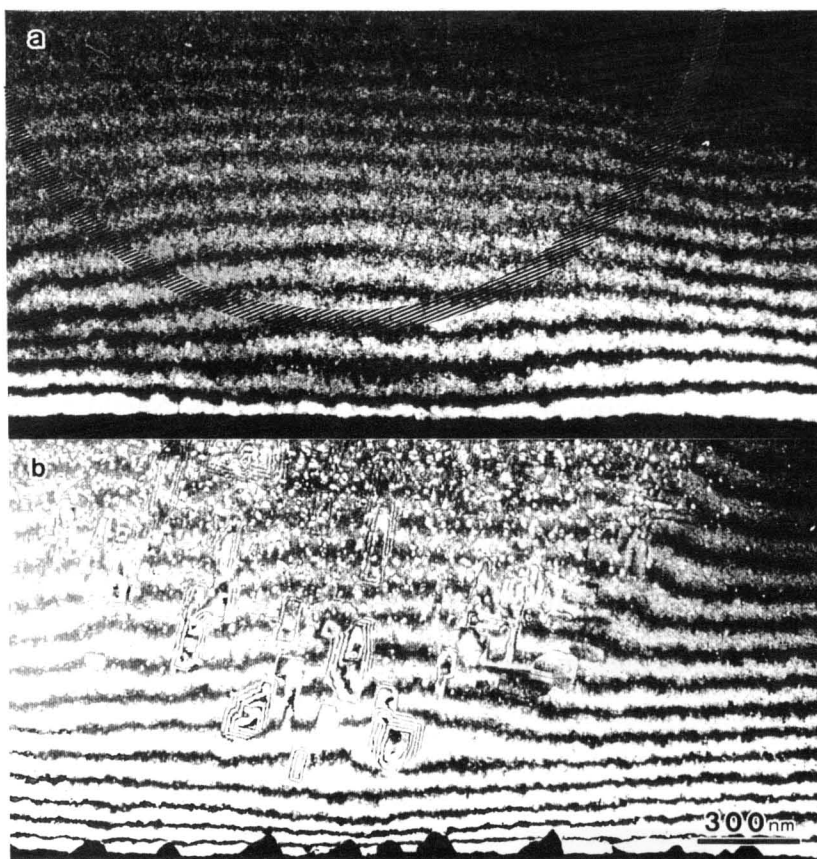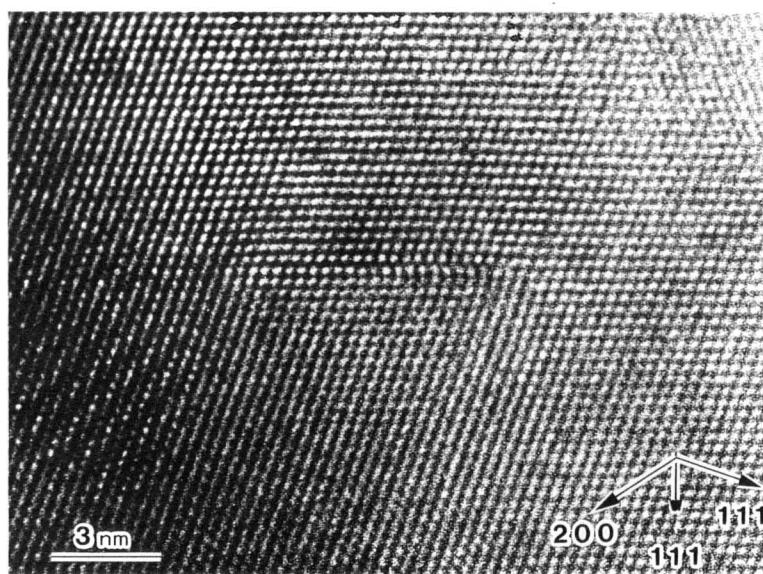

Fig. 2-4-2 High-resolution TEM image of a Frank-loop of interstitial-type in GaP taken with the <110> incidence.

32

Fig. 2-4-3 Weak-beam TEM images of an electron irradiated InP (a) before and (b) after an annealing at 800 K. The irradiated area is about 2 μm in diameter.

Fig. 2-4-4 High-resolution TEM image of a Frank-loop of interstitial-type in InP taken with the <110> incidence.

33

The similar defects were also introduced in GaAs by the same procedure; the onset temperature for the formation of loops was about 800 K, and it is slightly higher than that in GaP and InP. Figure 2-4-5(a) shows a result for GaAs; $\phi_{ir} = 8.9 \times 10^{18}$ cm^{-2} s^{-1}, $\tau_{ir} = 3600$ s, $T_{an} = 800$ K, and $\tau_{an} = 1800$ s. Since the defects introduced were very small, I could not identify the nature of the defects. The introduction of defect clusters by following annealing above 773 K after 2 MeV electron irradiation were reported by Neethling et al {150, Fig. 2-4-5(b) and (c)}. They claimed that the defects were dislocation loops of interstitial-type on {111} and {110} planes. Therefore, even though the electron energy is rather different, the defects that I observed must be the same nature as Neethling's; i.e., the same types and nature of dislocation loops as ones in InP.
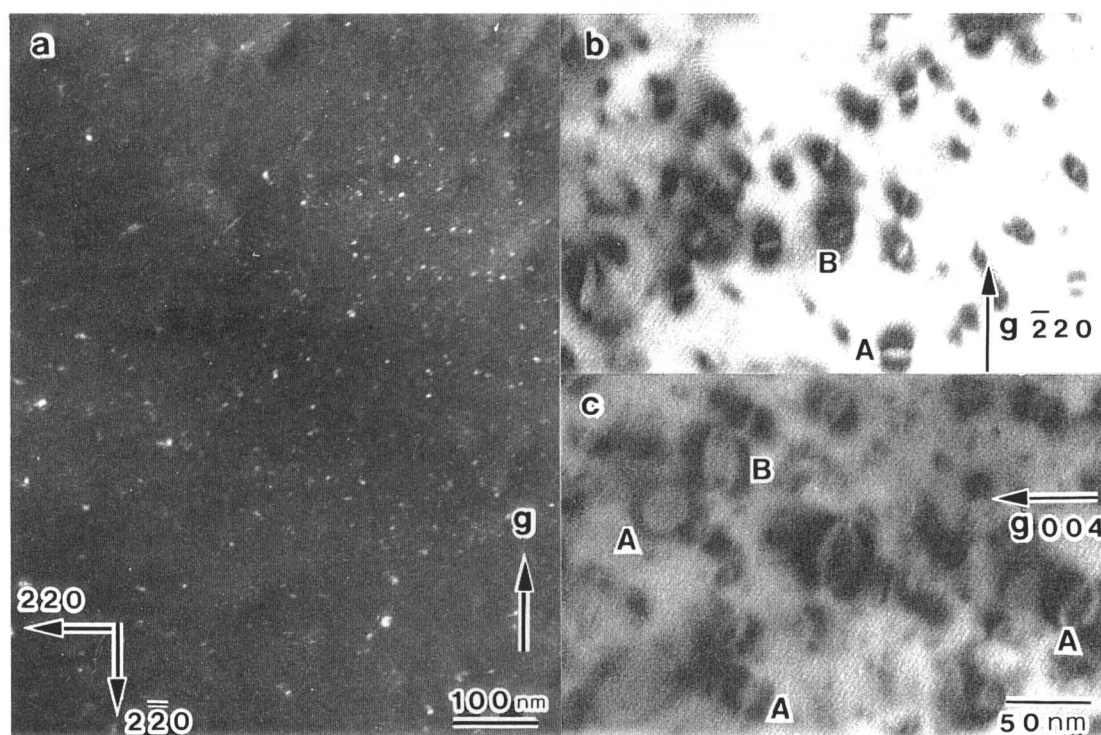

Fig. 2-4-5 Weak-beam TEM images of electron irradiated GaAs with an electron energy of (a) 300 keV and (b, c) 2 MeV, respectively. (a, b) A 220- and (c) 400-type diffraction spots are used for the imaging. ((b) and (c); from ref. 150)

2-4-1-2 Distribution of the dislocation loops

Fig.2-4-6(a) shows a stereo view of the irradiated (ϕ_{ir} = 5.5x10^{18} cm^{-2} s^{-1}, τ_{ir} = 3600 s, T_{ir} = 500 K) and annealed (T_{an} = 1000 K, τ_{an} = 1800 s) GaP, indicating that the loops were generated deep inside the specimen. Fig. 2-4-6(b) shows the planar density of the loops in Fig. 2-4-6(a) as a function of specimen thickness. As shown in Fig. 2-4-6(b), the density can be fitted with the single straight line that penetrates the origin. This indicates that the volume number density of loops, C_L, is independent of the specimen thickness and there is virtually no inhomogeneous distribution of loops near surfaces. Therefore, 1) specimen surfaces do not act as a sink of interstitials and 2) the loops do not originate from contaminant impurity atoms injected under the electron entrance surface.

Similar distributions were observed in InP and GaAs. Fig. 2-4-7(a) shows a stereo view of the irradiated (ϕ_{ir} = 4.7x10^{18} cm^{-2} s^{-1}, τ_{ir} = 3600 s) and annealed (T_{an} = 825 K, τ_{an} = 1800 s) InP. Fig. 2-4-7(b) shows the planar densities of two kinds of dislocation loops in Fig. 2-4-7(a) vs. the specimen thickness. The densities can be fitted with straight lines, even though the lines do not penetrate the origin. This obviously indicates that the loops do not originate from contaminant impurity atoms injected under the electron entrance surface. In InP, there exists a "denuded zone" near surfaces; specimen surfaces can act as a sink of interstitials. Thus I estimated C_L as the value of the slope of the planar densities vs. the specimen thickness.

I also confirmed that the concentration of interstitials introduced (in the order of 10^{19} cm^{-3}) was much larger than that of native impurity atoms in the specimens (less than 10^{18} cm^{-3}). Hence, I concluded that the formation of the dislocation loops was an intrinsic bulk phenomenon.
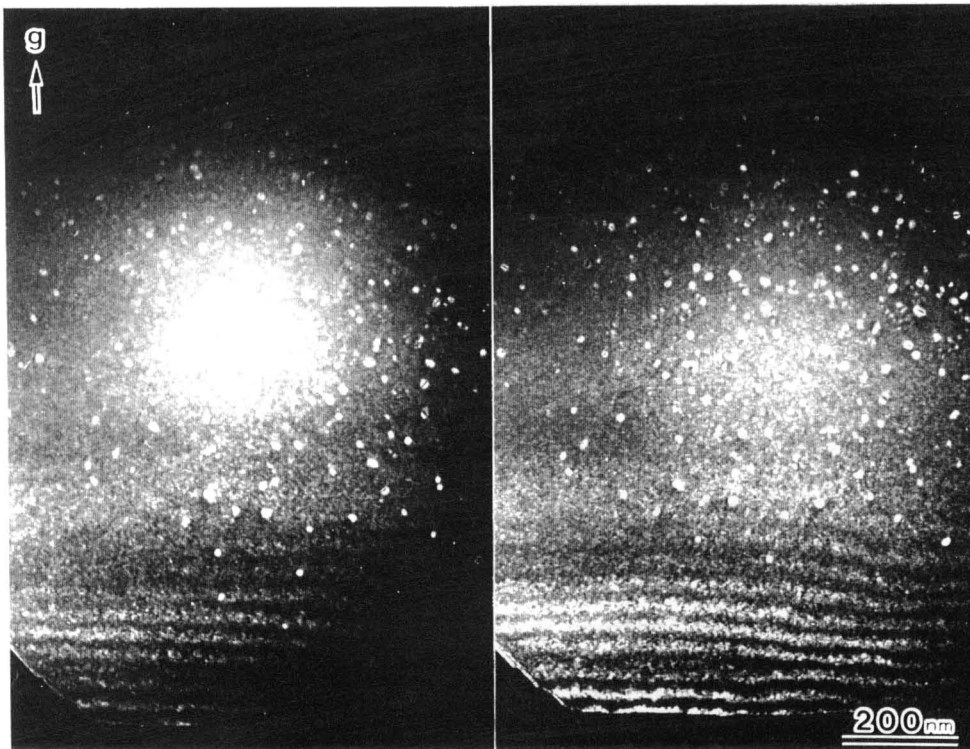
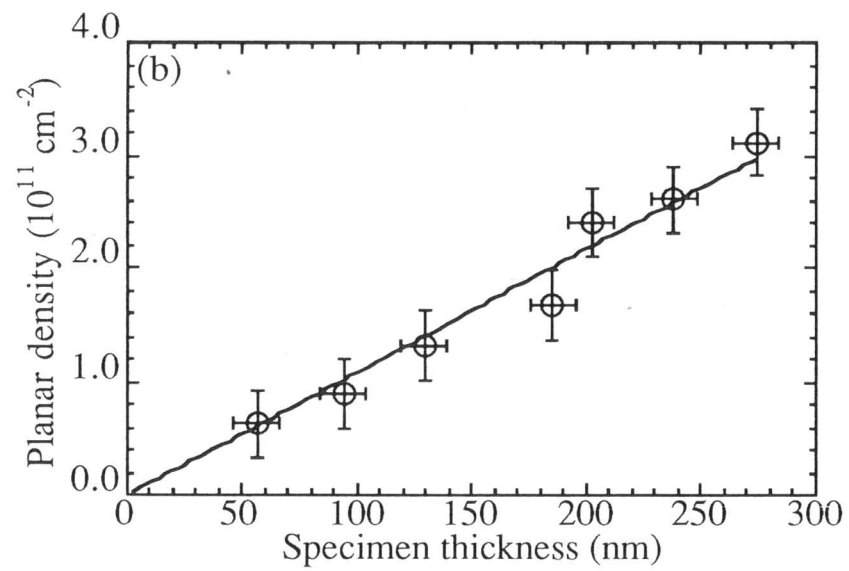Fig. 2-4-6   Stereo view of an irradiated and subsequently annealed GaP

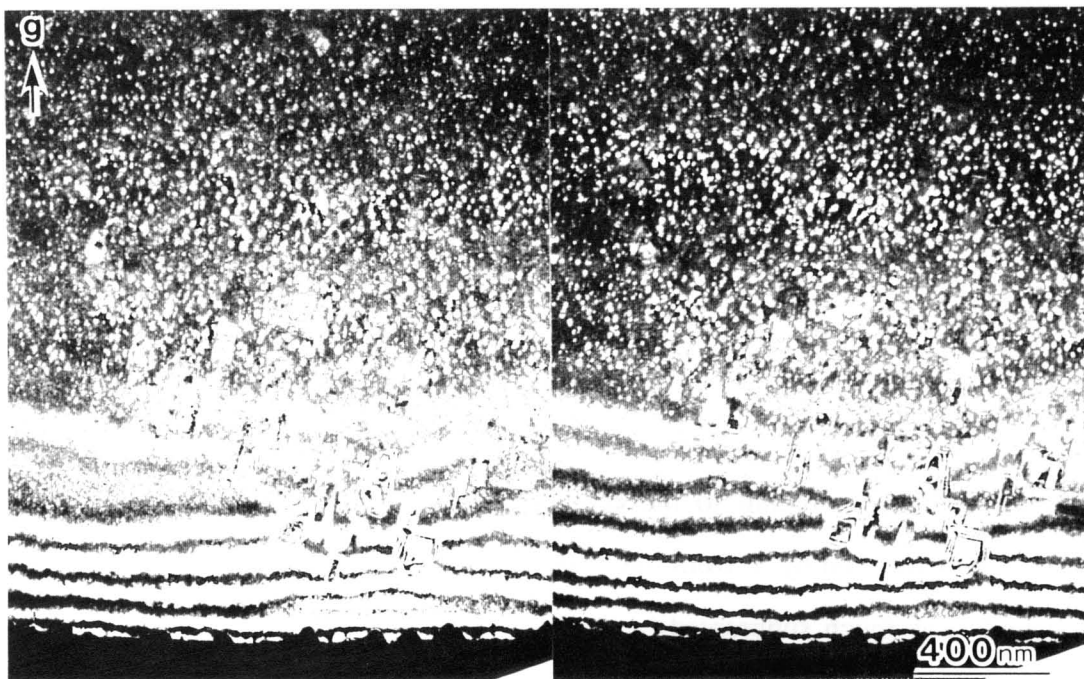Fig. 2-4-7   Planar density of loops vs. specimen thickness.

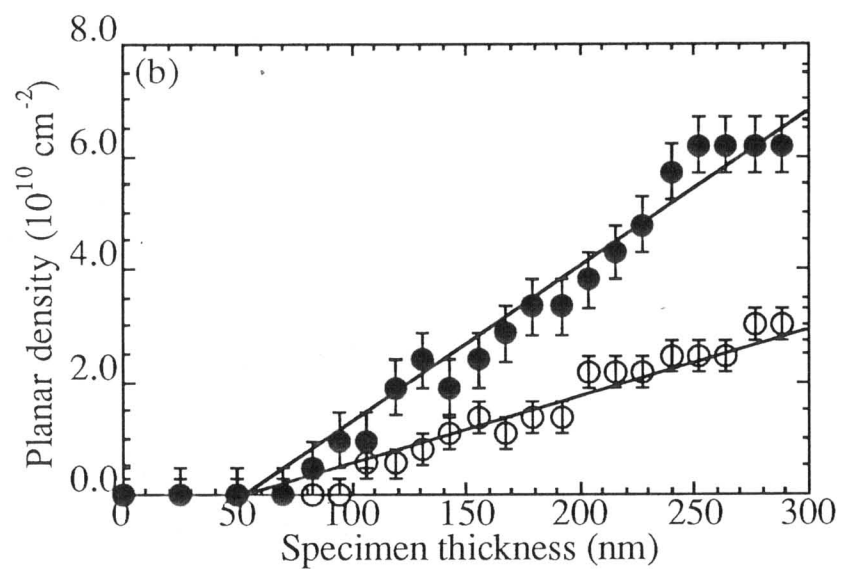Fig. 2-4-6   Stereo view of an irradiated and subsequently annealed InP

Fig. 2-4-7   Planar density of loops vs. specimen thickness.   Open and closed circles represent the loops on {111} and {110} planes, respectively.

37

2-4-1-3 Irradiation effects on the formation of dislocation loops

No defects were observed in GaP, InP, and GaAs annealed at 800 K after 100 keV electron irradiation, since the electron energy is lower than E_d in each specimen (see Fig. 2-3-2). Since $\bar{E}_p/E_d$ are in the order of unity in the electron energy range below 500 keV (see Fig. 2-3-3), the electron energy used in this experiment introduces only pairs of an interstitial and a vacancy, i.e. Frenkel-type defects, at both III- and V-sublattices in specimens. Therefore, the dislocation loops of interstitial type were formed by the thermal migration of both III- and V-interstitials which are introduced by an electron irradiation at 300 K.

The nucleation of the dislocation loops strongly depended on the irradiation direction of an electron-beam with regard to the crystal axis. No loops were formed when the electron-beam was inclined by 5° from the <100> or <110> direction, since the introduction of point defects was much suppressed by the electron-diffraction-channeling effect {155}. Weak-beam TEM images were taken with the beam of an off-axial incident direction. The total electron dose during an observation was much less than 10^{21} electrons cm^{-2}, and it is smaller than that of an irradiation (about 10^{22} electrons cm^{-2}). Therefore, I could safely neglect the introduction of point defects during TEM observation.

I also neglected an electron-irradiation-enhanced migration of point defects during TEM observation, since I confirmed that the growth speed of loops with intermittent observation was the same as that with continuous observation in GaP.

2-4-2 Annealing and irradiation effects on the growth of dislocation loops

In this section, I show the growth of dislocation loops in GaP and InP. Since the sizes of dislocation loops were very small, I could not investigate quantitatively the annealing and/or irradiation effects on the loops in GaAs. However, since the nature, irradiation conditions for the introduction, and the distribution in a specimen of the loops were very similar as ones in GaP and InP (see previous section), I convince that the formation mechanism of the loops in GaAs is the same as one in GaP and InP.

2-4-2-1 Nucleation and growth of dislocation loops by annealing

Growth of the dislocation loops in GaP during annealing was pursued by TEM. Figure 2-4-8 shows *in-situ* TEM images taken at 800 K (ϕ_{ir} = 5.5x10^{18} cm^{-2}s^{-1}, τ_{ir} = 1800 s). Most of loops were nucleated within τ_{an} ≤ 2400 s, and the number density remained constant after the nucleation. The radii, $r_{(GaP)}$, of the loops named a, b, c and d in Fig. 2-4-8 were measured at several τ_{an} (Fig. 2-4-9(a)). I found that $r_{(GaP)}$ of the loops are well expressed by a function,

$$r_{(GaP)} = r_{0(GaP)} \cdot \tanh(A \cdot \tau_{an}), \qquad (2\text{-}4\text{-}1)$$

where $r_{0(GaP)}$ and A represent the final loop-radii and the growth rates, respectively. The values of $r_{0(GaP)}$, A, and $r_{0(GaP)} \cdot A$ for the best fitted curves indicated in Fig. 2-4-9(a) are summarized in Table 2-3. The products $r_{0(GaP)} \cdot A$ of the loops are a common value, though $r_{0(GaP)}$ and A of each loop are slightly different.

The growth of loops was observed *in-situ* at various T_{an}. The variation of $r_{(GaP)}$ measured at T_{an} = 775, 750, 725, 700 K are depicted in Fig. 2-4-9(b), (c), (d), and (e), respectively. These figures obviously indicate that $r_{(GaP)}$ are well described by Eq. (2-4-1), though the growing-rate of the loops are different depending on T_{an}. The values of $r_{0(GaP)}$, A and $r_{0(GaP)} \cdot A$ for the best fitted curves in Fig. 2-4-9 are summarized in Table 2-3. As shown in the table, the product $r_{0(GaP)} \cdot A$ depended only on T_{an}, and it increased with rising T_{an}. I could not estimate the value of A in the temperature range T_{an} > 800 K, since the growth of loops stopped within a short period less than 2400 s.

I could not pursue quantitatively the growth of the dislocation loops in InP with τ_{an} since the growth was so fast; the growth stopped within an annealing time less than 600 s even at 700 K.
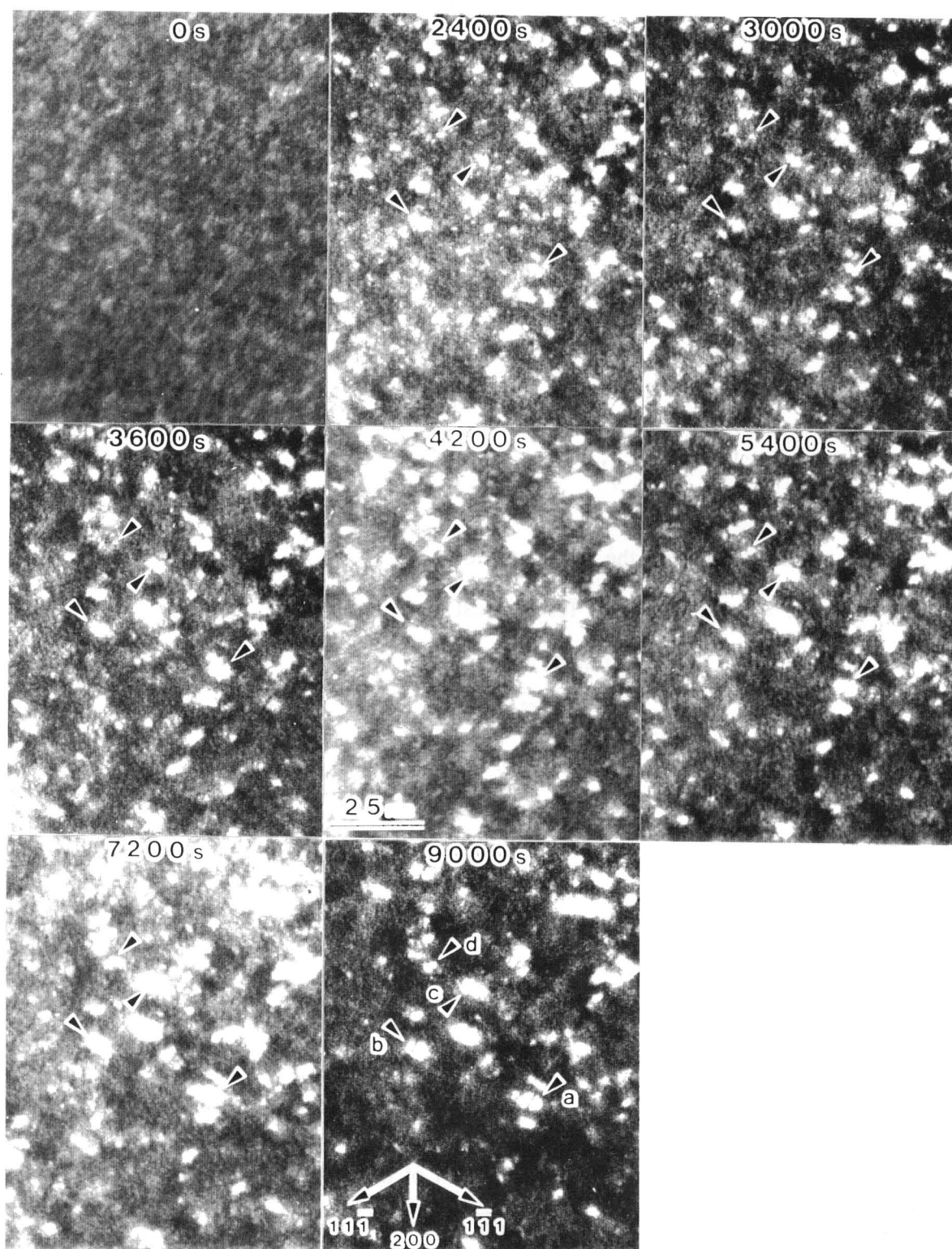
Fig. 2-4-8   Growth of the dislocation loops in GaP observed *in-situ* by TEM at the annealing temperature, $T_{an} = 800$ K.
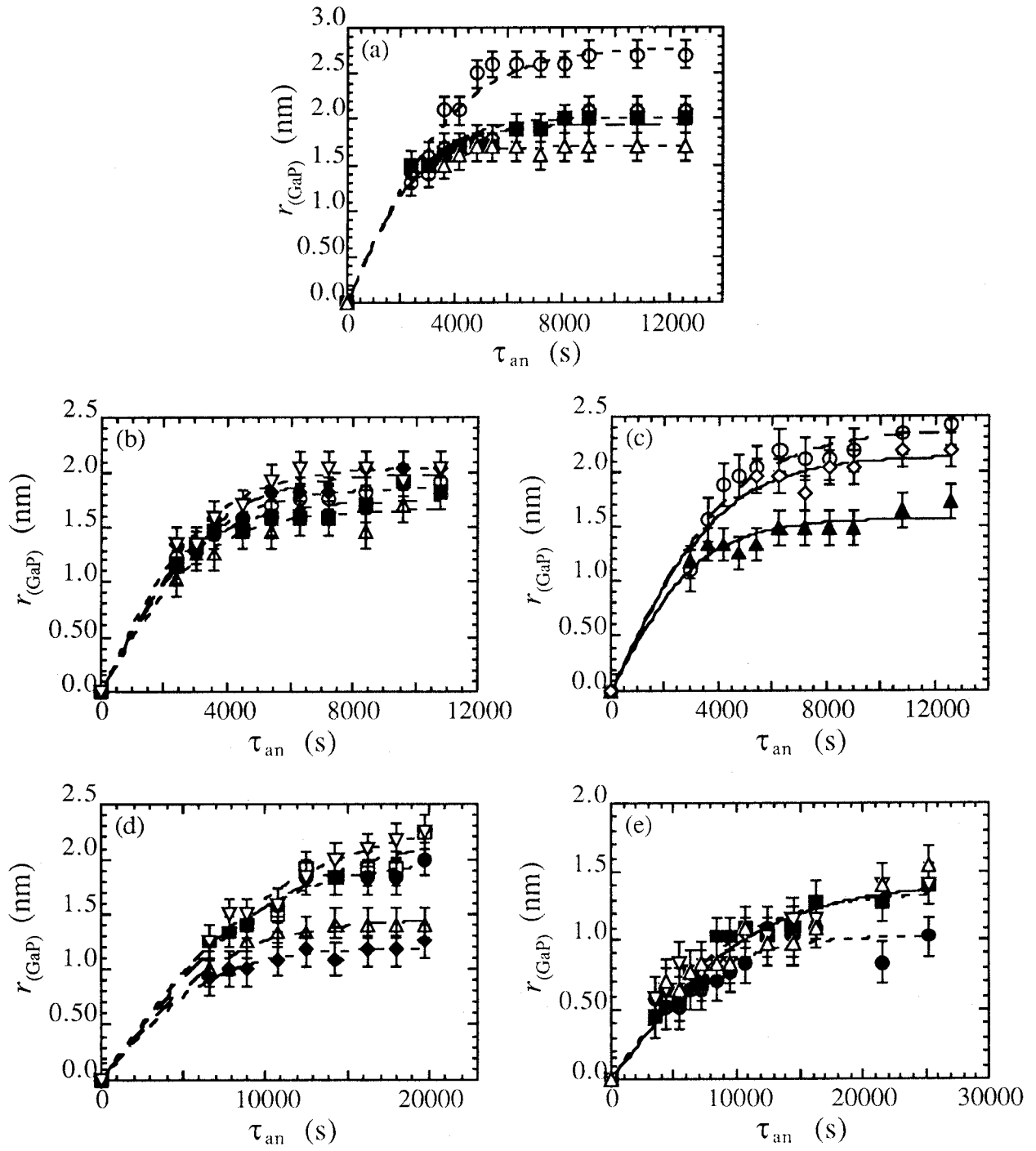
Fig. 2-4-9 Variation of loop-radii in GaP $r_{(GaP)}$ measured at (a) 800, (b) 775, (c) 750, (d) 725, and (e) 700 K as a function of annealing time, τ_{an}.

41

Table 2-3 Fitting parameters for the best fitted curves indicated in Fig. 2-4-9.

T_{an} (K)	No.	$r_{(GaP)}$ (nm)	A (10^{-4} s^{-1})	$r_{(GaP)} \cdot A$ (10^{-4} nm s^{-1})
800	1	2.79	4.80	13.39
	2	2.02	6.58	13.29
	3	1.95	6.87	13.40
	4	1.70	8.37	14.23
775	1	1.86	5.96	11.09
	2	1.99	5.59	11.12
	3	1.74	6.34	11.03
	4	1.66	6.02	9.99
	5	2.04	5.92	12.08
750	1	2.37	4.37	10.36
	2	1.57	5.83	9.15
	3	2.13	4.79	10.20
725	1	2.00	2.10	4.20
	2	2.23	1.73	3.86
	3	1.19	2.98	3.55
	4	1.46	2.50	3.65
	5	2.37	1.70	4.03
700	1	1.02	2.38	2.43
	2	1.36	1.92	2.61
	3	1.35	1.92	2.59
	4	1.65	1.65	2.34

2-4-2-2 Number density of dislocation loops

Figure 2-4-10 shows the logalithms of the volume number density of loops in GaP, $C_{L(GaP)}$ as a function of the reciprocal of the annealing temperature, $1/kT_{an}$. $C_{L(GaP)}$ was measured after all loops were nucleated. $\phi_{ir} = 5.5\times10^{18}$ cm^{-2} s^{-1}, and $\tau_{ir} = 3000$ s (open and closed circles) and 1500 s (squares). As shown in Fig. 2-4-10, $C_{L(GaP)}$ increased exponentially with increasing $1/kT_{an}$. The slopes of the straight lines in Fig. 2-4-10 provided the energies of 0.47 eV (open circles) and 0.45 eV (squares); these values were almost the same. The closed circles in Fig. 2-4-10 were measured in a specimen which was annealed stepwise at 700, 900, and 1000 K. In the step-annealing process, some loops occasionally shrunk and released interstitial atoms, which then took part in another loops. The estimated energy in Fig. 2-4-10 (0.53 eV) differed from those in the constant temperature annealing.

Figure 2-4-11 shows the volume number densities of the dislocation loops on {111} (open circles) and {110} (closed circles) planes in InP, $C_{L(InP)(111)}$ and $C_{L(InP)(110)}$ vs. T_{an}, measured after all loops were nucleated. $\phi_{ir} = 4.7\times10^{18}$ cm^{-2} s^{-1}, and $\tau_{ir} = 3600$ s. As shown in the figure, both the densities increased exponentially with increasing $1/kT_{an}$, as similar as in case of GaP. Both the slopes of $\ln(C_{L(InP)(111)})$ and $\ln(C_{L(InP)(110)})$ vs. $1/kT_{an}$ provided the same energy of 0.76 eV, even though the value of $C_{L(InP)(110)}$ was about twice larger than $C_{L(InP)(111)}$.
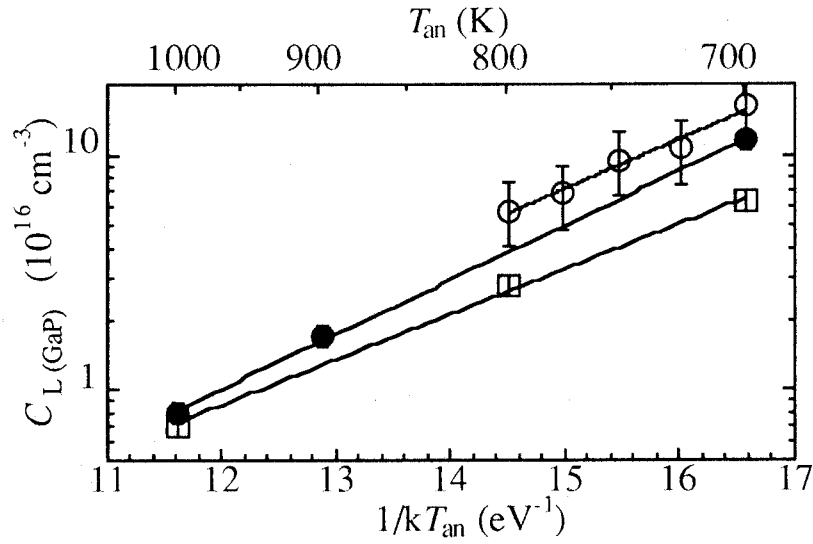
Fig. 2-4-10 The logarithms of the number densities of loops $C_{L(GaP)}$ against the reciprocal of annealing temperature $1/kT_{an}$. Irradiation period $\tau_{ir} = 3000$ s (open and closed circles) and 1500 s (open squares), respectively. The closed circles represent the results of a specimen that underwent the step annealing.
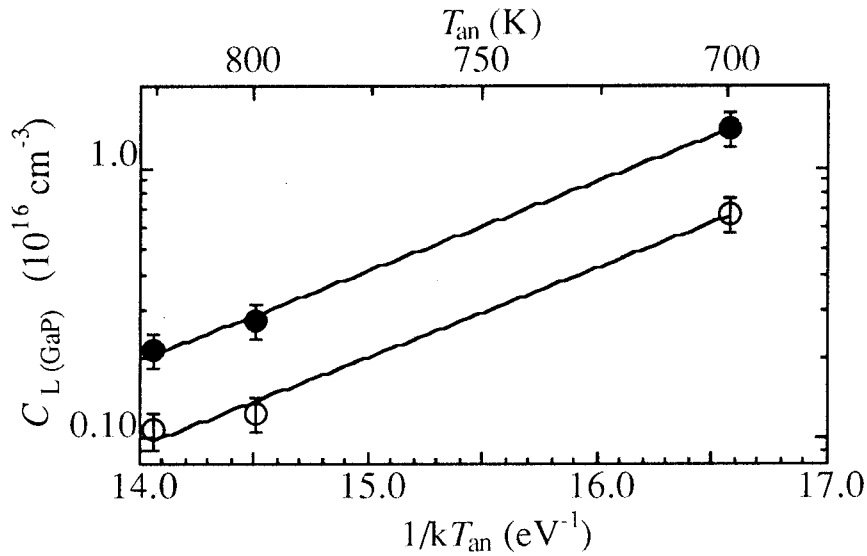

Fig. 2-4-11 The logarithms of the number densities of loops $C_{L(InP)}$ against the reciprocal of annealing temperature $1/kT_{an}$. Open and closed circles represent the densities of loops on {111} and {110} planes, respectively.

44

2-4-2-3　Radii of dislocation loops

The radii of all loops increased with τ_{an} and then reached a final value when the growth of the loops stopped. Figure 2-4-12 and 2-4-13 show the size distribution of the final radii in GaP and InP, $r_{0(GaP)}$ and $r_{0(InP)}$, respectively. The annealing temperatures T_{an} were 700 and 1000 K for GaP, and 700 and 800 K for InP. In InP, the profile of the loops on {111} planes was almost the same as one on {110} planes when T_{an} was the same. I found that the dispersion of r_0 was small; the ratio of the standard deviation of r_0 to the average of r_0 was 0.06 at T_{an}=700 K and 0.30 at T_{an}=1000 K for GaP, and was estimated as 0.14 at T_{an} = 700 K and 0.21 at T_{an} = 800 K for InP.

Figure 2-4-14 and 2-4-15 show the averaged final radius in GaP and InP, $\tilde{r}_{(GaP)}$ and $\tilde{r}_{(InP)}$ vs. T_{an}. The irradiation and annealing condition were the same as those used in Figs. 2-4-10 and 2-4-11. The marks meant the same as denoted in Figs. 2-4-10 and 2-4-11. As shown in Figs. 2-4-14 and 15, both $\tilde{r}_{(GaP)}$ and $\tilde{r}_{(InP)}$ decrease exponentially with increasing $1/kT_{an}$. The slopes of the straight lines in Fig. 2-4-14 provided the energies of -0.27 eV (open circles), -0.25 eV (squares), and -0.20 eV (closed circles), respectively. The energies in the constant temperature annealing (open circles and squares) were almost the same, while the energy in the step-annealing (closed circles) slightly differed from them. The slopes of the straight lines in Fig. 2-4-15 provided both the energies of -0.27 eV.
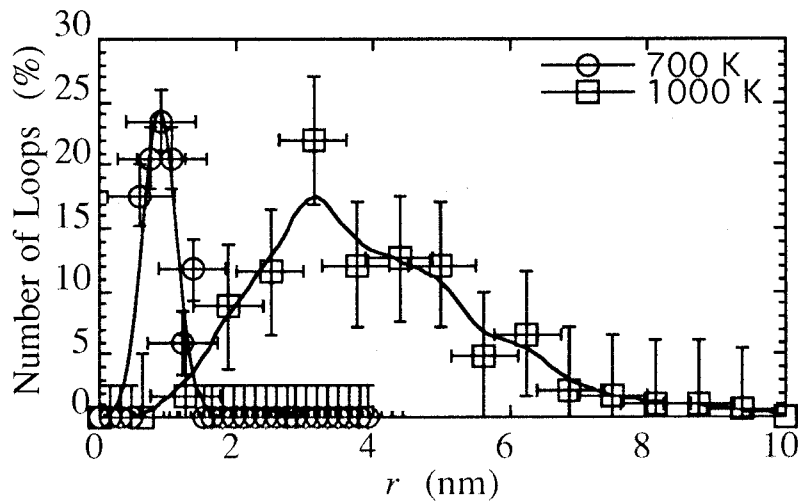

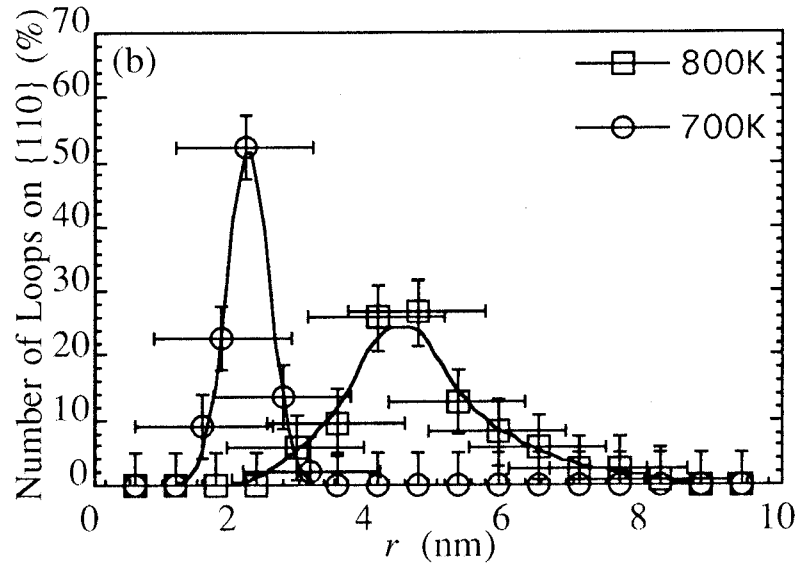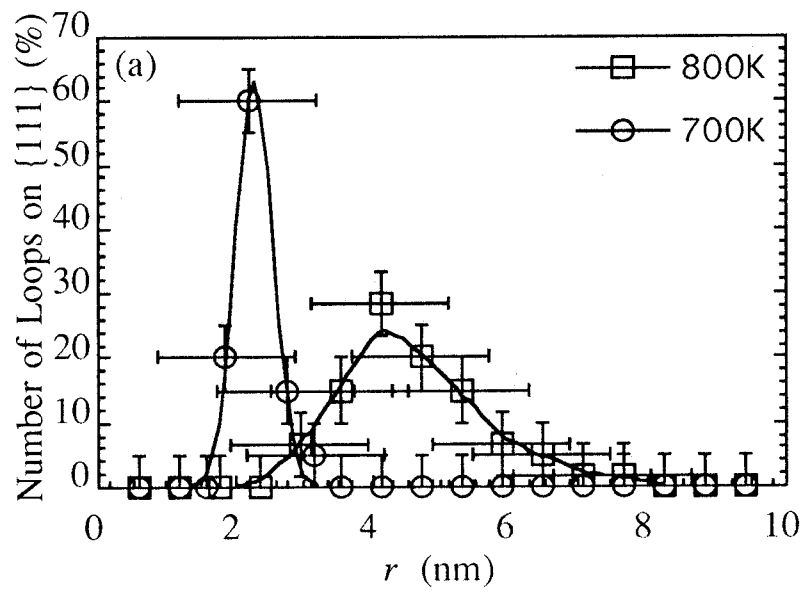Fig. 2-4-12　Size distribution of the loops in GaP at the annealing temperature of 700 and 1000 K.

Fig. 2-4-13　Size distribution of the loops in InP on (a) {111} and (b) {110} planes at the annealing temperature of 700 and 800 K.
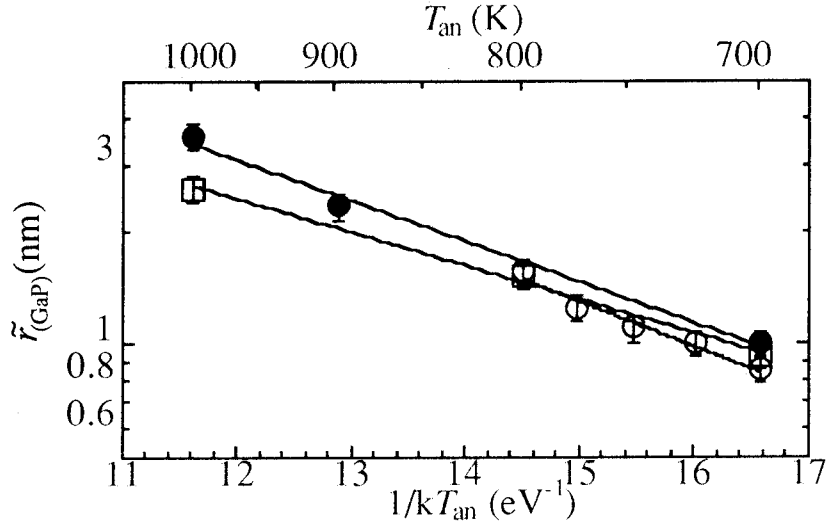
46

Fig. 2-4-14 The logarithms of the final radii of the loops in GaP $\tilde{r}_{(GaP)}$ against the reciprocal of annealing temperature $1/kT_{an}$. Irradiation period $\tau_{ir} = 3000$ s (open and closed circles) and 1500 s (open squares), respectively. The closed circles represent the results of a specimen that underwent the step annealing.
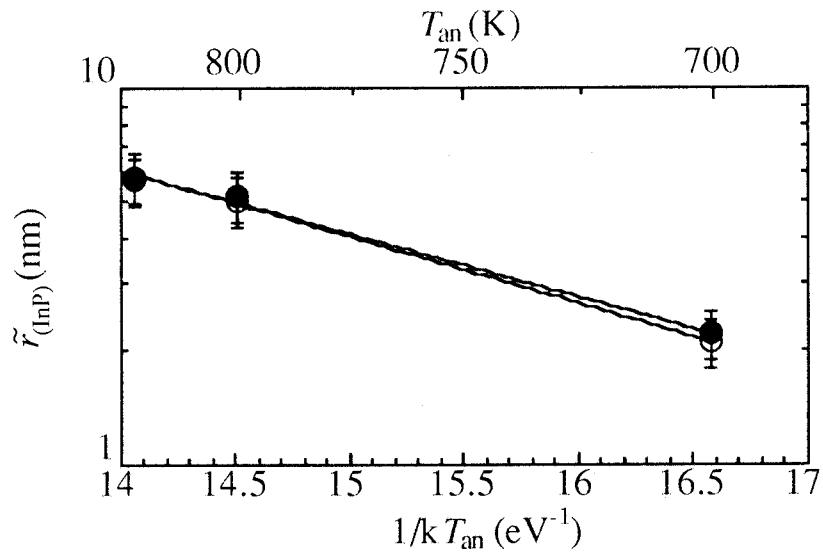

Fig. 2-4-15 The logarithms of the final radii of the loops in InP $\tilde{r}_{(InP)}$ against the reciprocal of annealing temperature $1/kT_{an}$. Open and closed circles represent the radii of loops on {111} and {110} planes, respectively.

2-4-3 Number density of aggregated interstitials in all dislocation loops

The volume number density of III_i- and V_i-interstitials aggregated in all the loops in GaP and InP, $C_{\text{IL(GaP)}}$ and $C_{\text{IL(InP)}}$, can be estimated by a simple formula,

$$C_{\text{IL(GaP)}} = \frac{2}{V} \Sigma_i \pi \cdot r_i^2 \cdot \sigma_{\text{(GaP)}}, \qquad (2\text{-}4\text{-}2)$$

$$C_{\text{IL(InP)}} = \frac{2}{V} \Sigma_i \Sigma_j \pi \cdot r_i^2 \cdot \sigma_{\text{(InP)}(j)}, \qquad (2\text{-}4\text{-}3)$$

in which V represents the specimen volume irradiated by electrons, $\sigma_{\text{(GaP)}}$ is a planar density of Ga- or P-interstitials in the loops in GaP (1.5×10^{15} cm^{-2}), and is denote individual loops. $\sigma_{\text{(InP)}(j)}$ represents a planar density of In- or P-interstitials in the loops on $\{j\}$ planes ($j = 111, 110$) in InP. Since $\sigma_{\text{(InP)}(111)} = \sigma_{\text{(InP)}(110)} \equiv \sigma_{\text{(InP)}}$ ($= 1.3 \times 10^{15}$ cm^{-2}), Eq. (2-4-3) is rewritten as,

$$C_{\text{IL(InP)}} = \frac{2}{V} \Sigma_i \pi \cdot r_i^2 \cdot \sigma_{\text{(InP)}}. \qquad (2\text{-}4\text{-}4)$$

$C_{\text{IL(GaP)}}$ and $C_{\text{IL(InP)}}$ increased with τ_{an} and reached a final value, $C_{\text{IL(GaP)}}(\infty)$ and $C_{\text{IL(InP)}}(\infty)$ when the growth of all loops stopped. Figure 2-4-16 shows $C_{\text{IL(GaP)}}(\infty)$ as a function of T_{an}. The irradiation and annealing condition was the same as those used in Fig. 2-4-10. The marks meant the same as denoted in Fig. 2-4-10. As shown in Fig. 2-4-16, $C_{\text{IL(GaP)}}(\infty)$ was independent of T_{an} on the condition of constant τ_{ir}. Moreover, $C_{\text{IL(GaP)}}(\infty)$ in the step-annealing was the same as that in the constant temperature annealing when τ_{ir} was the same. As shown in Fig. 2-4-17, the same dependence on T_{an} was also observed on $C_{\text{IL(InP)}}(\infty)$. The irradiation and annealing condition was the same as those used in Fig. 2-4-11. The marks meant the same as denoted in Fig. 2-4-11.
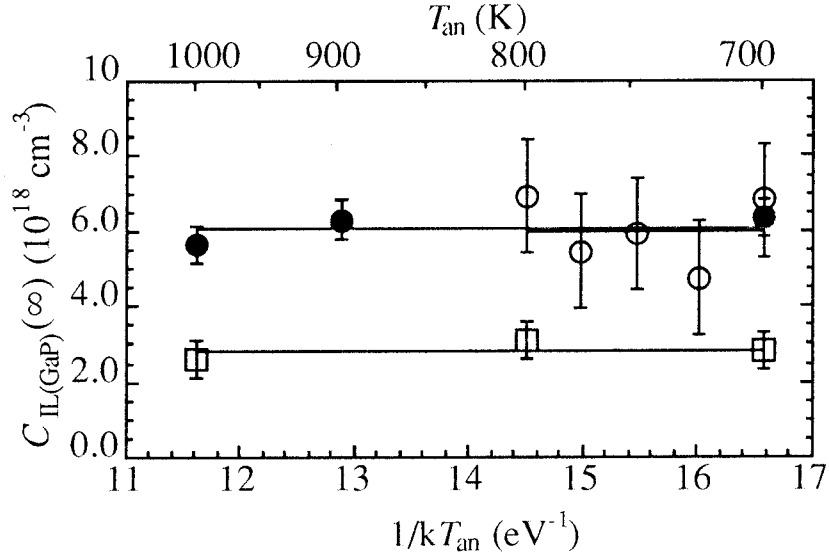
Fig. 2-4-16 Final density of aggregated interstitials $C_{IL(GaP)}(\infty)$ against the reciprocal of annealing temperatures $1/kT_{an}$. Irradiation period τ_{ir} = 3000 s (open and closed circles) and 1500 s (open squares), respectively. The closed circles represent the results of a specimen that underwent the step annealing.
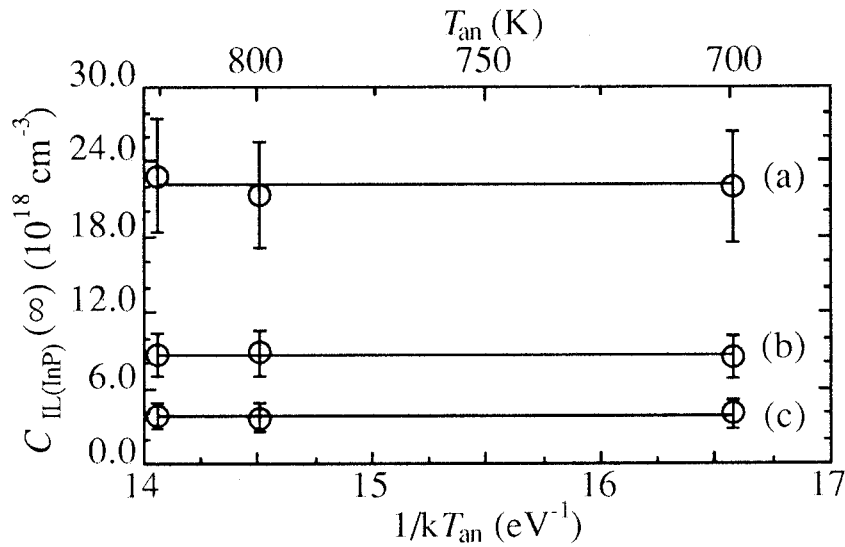

Fig. 2-4-17 Final density of aggregated interstitials $C_{IL(InP)}(\infty)$ against the reciprocal of annealing temperatures $1/kT_{an}$. Irradiation period τ_{ir} = (a) 7100, (b) 3600, and (c) 2000 s, respectively.

Figure 2-4-18 summarizes $C_{\mathrm{IL(GaP)}}(\infty)$ vs. electron dose, D; ϕ_{ir} multiplied by τ_{ir}. These results lead us to the important fact: $C_{\mathrm{IL(GaP)}}(\infty)$ is independent of ϕ_{ir}, τ_{ir} and T_{an} under the constant dose D. As seen in Fig. 2-4-18, $C_{\mathrm{IL(GaP)}}(\infty)$ increased quadratically with increasing the electron dose in the range $D \leq 2 \times 10^{22}$ cm^{-2}; $C_{\mathrm{IL(GaP)}}(\infty)$ were described by a function, $C_{\mathrm{IL(GaP)}}(\infty) = AD^2$ ($A = 1.3 \times 10^{-26}$ cm). This is a characteristic trend in a second order reaction, suggesting that the loops are formed through the migration of interstitial-pairs, that is, the pairs of Ga- and P-interstitials. Figure 2-4-19 shows the variation of $C_{\mathrm{IL(GaP)}}(\infty)$ vs. T_{ir}. Specimens were irradiated with $D = 4.0 \times 10^{22}$ cm^{-2} and subsequently annealed at $T_{\mathrm{an}} = 1000$ K. $C_{\mathrm{IL(GaP)}}(\infty)$ reached the maximum at $T_{\mathrm{ir}} = 300$ K, and it decreased rapidly with raising T_{ir}. No loops were formed when the irradiation temperature is in the temperature range $T_{\mathrm{ir}} > 700$ K.

$C_{\mathrm{IL(InP)}}(\infty)$ also showed the similar dependence on D and T_{ir}, even though the values were slightly different. Figure 2-4-20 shows $C_{\mathrm{IL(InP)}}(\infty)$ vs. D at $T_{\mathrm{ir}} = 300$ (open circles) and 110 K (closed circles). $C_{\mathrm{IL(InP)}}(\infty)$ were not fitted with a single straight line that penetrates the origin (broken line in Fig. 2-4-20). In the dose range $D \leq 2.5 \times 10^{22}$ cm^{-2}, $C_{\mathrm{IL(InP)}}(\infty)$ were well described by a function, $C_{\mathrm{IL(InP)}}(\infty) = AD^2$, where A is a constant to fit each data; $A = 2.9 \times 10^{-26}$ cm ($T_{\mathrm{ir}} = 300$ K) and 2.3×10^{-26} cm ($T_{\mathrm{ir}} = 110$ K). Figure 2-4-20 also shows $C_{\mathrm{IL(InP)}}(\infty)$ at $T_{\mathrm{ir}} = 450$ K (open squares). No loops were formed when the irradiation temperature was in the range $T_{\mathrm{ir}} \geq 400$ K.
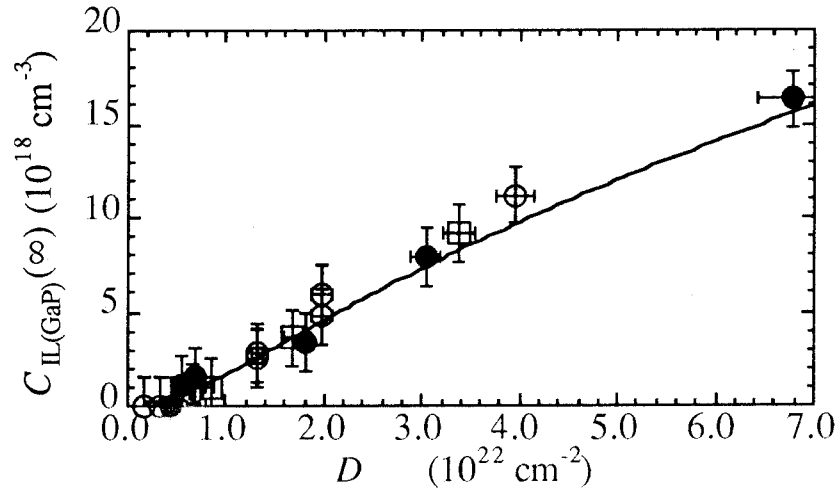
Fig. 2-4-18   Final density of aggregated interstitials $C_{IL(GaP)}(\infty)$ as a function of electron doses D.   Open marks (circles and squares); ϕ_{ir} = 5.5x10^{18} cm^{-2} s^{-1}, filled ones (circles); τ_{ir} = 1800 s.   Circles (open and filled); T_{an} = 1000 K, squares (open); T_{an} = 950 K.
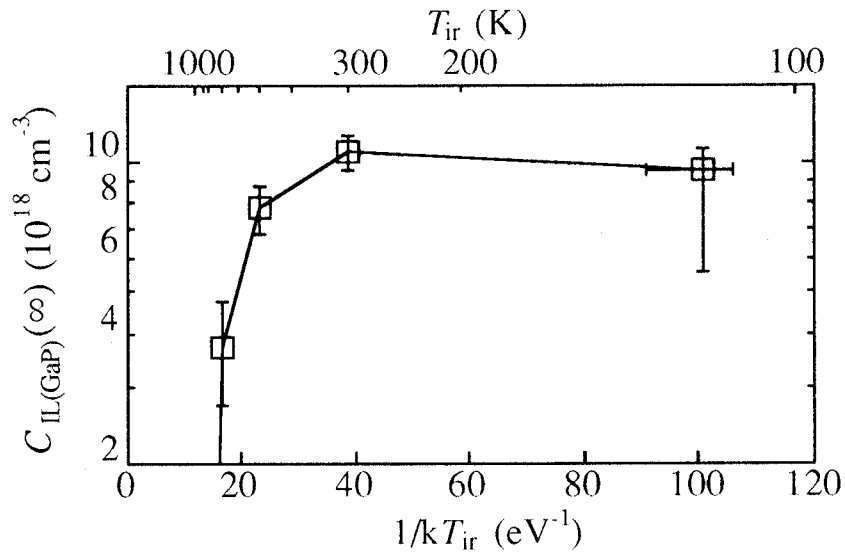
Fig. 2-4-19   Variation of the final density of aggregated interstitials $C_{IL(GaP)}(\infty)$ with several irradiation temperatures, T_{ir}.
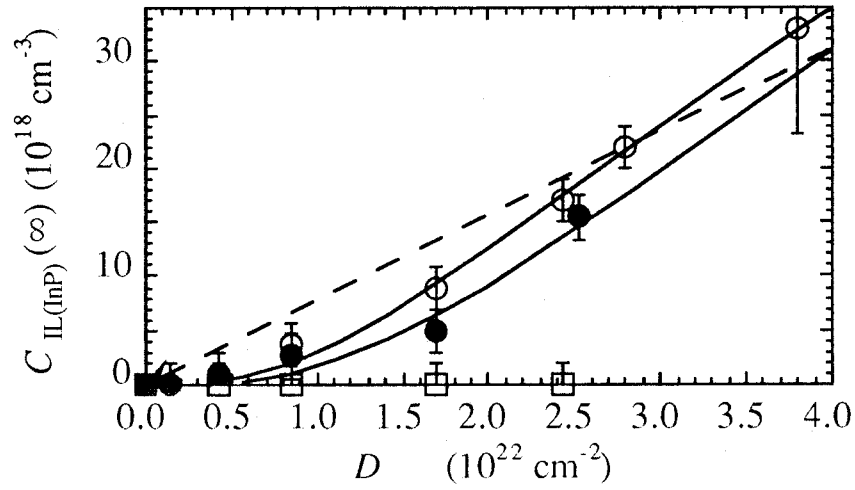
Fig. 2-4-20 Final densities of aggregated interstitials $C_{IL(InP)}(\infty)$ as a function of electron doses D. Irradiation temperatures $T_{ir} = 110$ (closed circles), 300 (open circles), and 450 (open squares) K, respectively. Solid lines represent the variation of the simulated final density based on a In_i-P_i interstitial-pairs model. Dashed line represents the theoretical density based on an isolated-interstitials model.

2-5 Discussion

2-5-1 Rate equations based on the migration of isolated interstitials

I have shown that the formation of dislocation loops is an intrinsic bulk phenomenon in GaP and InP crystals (Sec. 2-4-2). Since I confirmed that dispersion of the radii of all the loops is small (Sec. 2-4-5), I may replace r_i by the average radius $\tilde{r}$ and rewrite Eq. (2-4-2) and (2-4-4) as

$$C_{IL(GaP)} = \pi\tilde{r}_{(GaP)}^2 \cdot 2\sigma_{(GaP)} \cdot C_{L(GaP)}, \qquad (2\text{-}5\text{-}1)$$

$$C_{IL(InP)} = \pi\tilde{r}_{(InP)}^2 \cdot 2\sigma_{(InP)} \cdot \left\{ C_{L(InP)(110)} + C_{L(InP)(111)} \right\}. \qquad (2\text{-}5\text{-}2)$$

Therefore, I can apply the chemical kinetics theory, in which the homogeneous distribution of defects is usually assumed. Dislocation loops of interstitial-type are formed in various metals and alloys during an electron irradiation and the nucleation and growth of them are well understood by an interaction of point defects. Before I discuss the results in GaP and InP, let us recall the standard rate equations which applied to metals and alloys {156}. I consider the phenomena at low T_{ir}, at which only interstitials can freely migrate thermally. Point defects introduced by an irradiation annihilate when interstitials jump into the recombination volume around vacancies. Therefore the change of the concentration of interstitials C_I and vacancies C_V can be expressed as,

$$\frac{dC_I}{dt} = \frac{dC_V}{dt} = P - Z \cdot M \cdot C_I \cdot C_V, \qquad (2\text{-}5\text{-}3)$$

where P is the production rate of Frenkel-type defects, M the mobility of interstitials and Z the number of capture sites around a vacancy for interstitials. Dislocation loops of interstitial-type, of course, act as sinks for interstitials. The additional term of the variation of C_I due to dislocation loops is represented as,

$$-(2\pi \cdot \tilde{r} \cdot \alpha) \cdot M \cdot C_L \cdot C_I,$$

<div align="right">(2-5-4)</div>

where α represents the capture site number per unit length around a loop for the interstitials.

The mobility M can be estimated by measuring the variation of $\tilde{r}$ and C_L as the function of P and T_{ir}; in the model, the nucleus of dislocation loops are couples of interstitials formed by the migration of isolated interstitials, and the number density of the nuclei, C_L is proportional to $M^{-0.5}$ {156}.

2-5-2 Extended rate equations based on the migration of interstitial-pairs

The above-mentioned model is insufficient to explain the present experiments in GaP and InP. First, the onset temperature for the formation of loops (700 K) was extremely higher than that for the migration of isolated interstitials (about 100 K for Ga- and P-interstitials in GaP {30-34}, and 100-300 K for In- and P-interstitials in InP {46, 47, 60, 61}). This suggests that the loops were formed by the migration of not isolated interstitials but interstitial-related complexes. Second, the model yields the result that the final density of interstitials aggregated in all loops $C_{IL}(\infty)$ increases linearly with electron dose D, while the observed $C_{IL}(\infty)$ in GaP and InP increased quadratically as given in Fig. 2-4-23 and 2-4-25. Since the quadratic dependence of $C_{IL}(\infty)$ indicates that complexes, which are agglomerated in the loops, are formed in a second order reaction, I come to consider that the complexes are interstitial-pairs; i.e., Ga_i-P_i pairs for GaP and In_i-P_i pairs for InP, respectively. For quantitative understanding of the growth of loops, I propose an extended model. In the model, the concentration of isolated interstitials $C_I(\xi_\chi)$ and one of isolated vacancies $C_V(\xi_\chi)$ are expressed as,

$$\frac{dC_I(\xi_\chi)}{dt} = P(\xi_\chi) - Z(\xi_\chi) \cdot \left\{ M_I(\xi_\chi) + M_V(\xi_\chi) \right\} \cdot C_I(\xi_\chi) \cdot C_V(\xi_\chi)$$
$$- Z_{II} \cdot \left\{ M_I(\xi_{III}) + M_I(\xi_V) \right\} \cdot C_I(\xi_{III}) \cdot C_I(\xi_V)$$

<div align="right">(2-5-5)</div>

$$\frac{dC_V(\xi_\chi)}{dt} = P(\xi_\chi) - Z(\xi_\chi) \cdot \left\{ M_I(\xi_\chi) + M_V(\xi_\chi) \right\} \cdot C_I(\xi_\chi) \cdot C_V(\xi_\chi)$$
$$- Z_{VV} \cdot \left\{ M_V(\xi_{III}) + M_V(\xi_V) \right\} \cdot C_V(\xi_{III}) \cdot C_V(\xi_V) \qquad (2\text{-}5\text{-}6)$$

in which $P(\xi_\chi)$ is the production rate of Frenkel-type defects, and it is equal to zero during annealing. $M_I(\xi_\chi)$ and $M_V(\xi_\chi)$ are the mobilities of isolated interstitials and vacancies, respectively. ξ_χ denotes the species of atoms; ξ_{III} is Ga for GaP and In for InP, and ξ_V is P. $Z(\xi_\chi)$ represents the number of capture site of the recombination of ξ_χ-vacancy and ξ_χ -interstitials. Instead of the term (2-5-4), I add the third term in Eq. (2-5-5) which represents the rate of the disappearance of isolated interstitials by the formation of interstitial-pairs. The pair is formed when an interstitial jump into the spontaneous combination volume around an interstitial of the other kind. Z_{II} denotes the number of capture sites of the interstitial pairing. I also add the third term in Eq. (2-5-6) which represents the rate of the disappearance of isolated vacancies by the formation of vacancy-pairs. Z_{VV} denotes the number of capture sites of the vacancy pairing.

The variation of the concentration of the interstitial-pairs C_{II} and one of vacancy-pairs C_{VV} are described as,

$$\frac{dC_{II}}{dt} = Z_{II} \cdot \left\{ M_I(\xi_{III}) + M_I(\xi_V) \right\} \cdot C_I(\xi_{III}) \cdot C_I(\xi_{III})$$
$$- Z_{IIVV} \cdot M_{II} \cdot C_{II} \cdot C_{VV} \qquad (2\text{-}5\text{-}7)$$
$$- (2\pi \bar{r} \cdot \alpha) \cdot M_{II} \cdot C_L \cdot C_{II}$$

$$\frac{dC_{VV}}{dt} = Z_{VV} \cdot \left\{ M_V(\xi_{III}) + M_V(\xi_V) \right\} \cdot C_V(\xi_{III}) \cdot C_V(\xi_V)$$
$$- Z_{IIVV} \cdot M_{II} \cdot C_{II} \cdot C_{VV} \qquad (2\text{-}5\text{-}8)$$

in which M_{II} represents the mobility of interstitial-pairs. The second terms in Eq. (2-5-7) and (2-5-8) represent the rate of the recombination of interstitial-pairs and vacancy-pairs. Third term in Eq. (2-5-7) represents the rate of the disappearance of the interstitial-pairs by the formation of dislocation loops; the loops are formed by the migration of the interstitial-pairs. In the equations, I neglected the mobility of vacancy-pairs since I could not observe a

55

formation of dislocation loops of vacancy type and a shrink of dislocation loops of interstitial-type. I also assumed that a coupled Ga- and P-interstitials never combine with an isolated single Ga- or P-vacancy. This assumption means that there is no sink for interstitial-pairs except for dislocation loops; i.e., interstitial-pairs do not disappear during annealing. By this assumption, the experimental results that $C_{IL}(\infty)$ is independent of annealing temperatures (Sec. 2-4-6) can be easily explained.

The variation of the concentration of the interstitial-pairs aggregated in dislocation loops C_{IL} is explained as,

$$\frac{dC_{IL}}{dt} = (2\pi\tilde{r} \cdot \alpha) \cdot M_{II} \cdot C_L \cdot C_{II}, \qquad (2\text{-}5\text{-}9)$$

where α represents the capture site number per unit length around a loop for the interstitial-pairs.

2-5-3 Interpretation of the experimental results

2-5-3-1 Formation of Ga_i-P_i interstitial-pairs in GaP

Numerical calculations of the rate equations, (2-5-5) to (2-5-9), were performed with several sets of parameters in GaP. In the following computations, I naturally assumed that $P(\text{Ga}) = P(\text{P}) = 10^{-6}$ s^{-1} during irradiation, $P(\text{Ga}) = P(\text{P}) = 0$ s^{-1} during annealing, $Z(\text{Ga}) = Z(\text{P}) = 10^2$, and the concentrations of point defects before irradiation were zero. Since the vacancies on Ga- and P-sites are generally immobile below 700 K {9-13} and 1100 K {15-17}, I could neglect $M_V(\text{Ga})$ and $M_V(\text{P})$ (= 0) during both irradiation and annealing. I assumed that $M_I(\text{Ga}) = M_I(\text{P})$ (= $M_{I(ir)}$) and $M_{II} = 0$ during irradiation, and $M_I(\text{Ga}) = M_I(\text{P})$ (= $M_{I(an)}$) during annealing.

First, I confirmed that, in my model, C_{II} is independent of both $M_{I(an)}$ and M_{II} on the condition of constant D and $M_{I(ir)}$, since the pairs are introduced only during electron irradiation. Moreover, all interstitial-pairs agglomerate into dislocation loops after annealing. Therefore, $C_{IL(GaP)}(\infty)$ is independent of both $M_{I(an)}$ and M_{II} on the condition of constant D and M_{ir}. This reproduces the experiment shown in Fig. 2-4-21, since $M_{I(an)}$ and M_{II} are related to the annealing temperature T_{an}.

Figure 2-5-1 shows the simulated curves of $C_{IL(GaP)}(\infty)$ vs. D in which I assumed that the spontaneous recombination of Ga and P interstitials is permitted only under the condition of electron irradiation: $Z_{II} = 4$ during irradiation and $Z_{II} = 0$ during annealing. This model is interpreted as follows. There exists a potential barrier to interstitial-pairing around the spontaneous recombination volume for the pairing. Suppose the barrier is too high to cross over thermally for interstitials, interstitial pairing does not occur through the thermal migration of interstitials. This corresponds to the assumption of $Z_{II} = 0$ during annealing. During electron irradiation, the barrier lowers owing to a microscopic change of an atomic structure that should be accompanied by an ionization of atoms. This lowering results in the formation of interstitial-pairs, and thus Z_{II} has a finite value only during electron irradiation. As shown in Fig. 2-5-1, $C_{IL(GaP)}(\infty)$ increases quadratically with increasing D in the lower dose range; $C_{IL(GaP)}(\infty)$ computed with $M_{I(ir)} = 10^{-2}$ s^{-1} agrees well with the measurement shown in Fig. 2-4-23. At a certain dose, simulated $C_{IL(GaP)}(\infty)$ vary with $M_{I(ir)}$. In the range of lower mobility, the density $C_{IL(GaP)}(\infty)$ increases with increasing $M_{I(ir)}$ and in the range of higher mobility, the $C_{IL(GaP)}(\infty)$ decreases rapidly as the value $M_{I(ir)}$ increases. The variation of $M_{I(ir)}$ is related to that of T_{ir}; $M_{I(ir)}$ is small when T_{ir} is low. Therefore, the dependence of simulated $C_{IL(GaP)}(\infty)$ on T_{ir} is consistent with the experiments shown in Fig. 2-4-24. The similar results could be obtained whenever the values of Z_{II}, $Z(\xi)$ and $P(\xi)$ were in the order of 10^0, 10^2 and 10^{-6} s^{-1}, respectively. The simulated $C_{IL(GaP)}(\infty)$ with several values of Z_{II}, $Z(\xi)$ and $P(\xi)$ are summarized in the appendix.

I next considered an alternative model in which the interstitial-pairs were formed during not only irradiation but also annealing: $Z_{II} = 4$ during both irradiation and annealing. Figure 2-5-2 shows the simulated curves of $C_{IL(GaP)}(\infty)$ vs. D using the same parameters as those assumed in Fig. 2-5-1. The simulated $C_{IL(GaP)}(\infty)$ increases linearly with D. It decreases monotonously with $M_{I(ir)}$ at a certain D. Consequently the experimental data are consistently described by the former model: the Ga$_i$-P$_i$ interstitial-pairs are created only during electron irradiation.

Fig. 2-5-1　Variation of the simulated final density of aggregated interstitials in GaP $C_{IL(GaP)}(\infty)$ with several electron doses D and interstitial mobilities during irradiation $M_{I(ir)}$. $M_{I(ir)}$ in the computations are written in the figure. It is assumed that the pairs are formed only during electron irradiation.
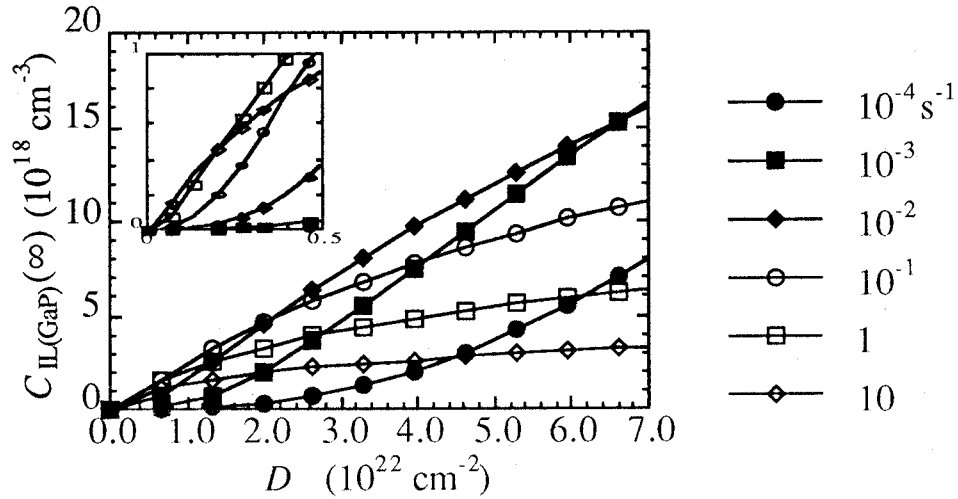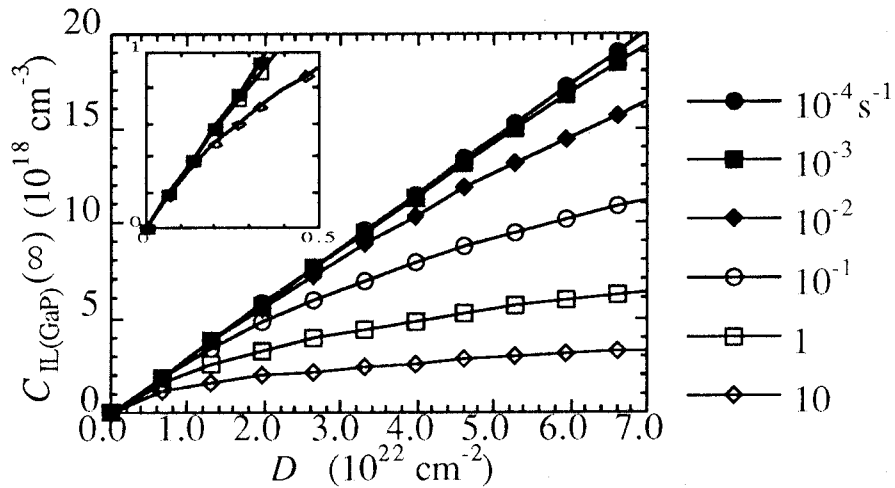

Fig. 2-5-2　Variation of the simulated final density of aggregated interstitials in GaP $C_{IL(GaP)}(\infty)$ with several electron doses D and interstitial mobilities during irradiation $M_{I(ir)}$. $M_{I(ir)}$ in the computations are written in the figure. It is assumed that the pairs are formed during both irradiation and annealing.

2-5-3-2 Formation of In_i-P_i interstitial-pairs in InP

I next performed the numerical calculations of the rate equations, (2-5-5) to (2-5-9) with several sets of parameters in InP. In the following computations, I assumed that $P(\text{In})$ = 5×10^{-6} and $P(\text{P})$ = 10^{-6} s^{-1} during irradiation, $P(\text{In})$ = $P(\text{P})$ = 0 s^{-1} during annealing, $Z(\text{In})$ = $Z(\text{P})$ = 10^2, and the concentrations of point defects before irradiation were zero. Since the P-vacancies in InP are considered to be immobile below 1023 K {39}, I assumed $M_V(\text{P})$ = 0 during both irradiation and annealing. While the In-vacancy is believed to be mobile above about 450 K {43, 60, 61}, I assumed that $M_V(\text{In})$ = 0 during irradiation and $M_V(\text{In})$ = $M_{V(\text{an})}$ during annealing. I assumed that $M_I(\text{Ga})$ = $M_I(\text{P})$ (= $M_{I(\text{ir})}$) and M_{II} = 0 during irradiation, and $M_I(\text{Ga})$ = $M_I(\text{P})$ (= $M_{I(\text{an})}$) during annealing.

First, I assumed that $M_{V(\text{an})}$ = 0. Under the assumption, $C_{IL(\text{InP})}(\infty)$ is independent of both $M_{I(\text{an})}$ and M_{II} on the condition of constant D and $M_{I(\text{ir})}$, as shown in the previous section. This reproduces the experiment shown in Fig. 2-4-22. I simulated $C_{IL(\text{InP})}(\infty)$ as a function of D in which I assumed that the pairs are created only by electron irradiation: Z_{II} = 4 during irradiation and Z_{II} = 0 during annealing. Figure 2-5-3 shows the simulated curves of $C_{IL(\text{InP})}(\infty)$ vs. D. $C_{IL(\text{InP})}(\infty)$ increases quadratically with D in the lower dose range, and $C_{IL(\text{InP})}(\infty)$ computed with $M_{I(\text{ir})}$ = 1×10^{-3} s^{-1} and 5×10^{-4} s^{-1} agreed well with the measurements at T_{ir} = 300 and 110 K, respectively (Solid lines in Fig. 2-4-25).

Figure 2-5-4 shows the simulated $C_{IL(\text{InP})}(\infty)$ at D = (a) 3.5×10^{22}, (b) 1.7×10^{22} and (c) 8.5×10^{21} cm^{-2} as a function of $M_{V(\text{an})}$. In the calculation, I assumed that $M_{I(\text{ir})}$ = 1.0×10^{-3} s^{-1} and $M_{I(\text{an})}$ = 1.5×10^{-3} s^{-1}. As shown in the figure, $C_{IL(\text{InP})}(\infty)$ is almost the same value in the mobility range $M_{V(\text{an})} \leq M_{I(\text{an})}$. It is generally believed that the mobility of isolated interstitials is much larger than one of vacancies. Therefore, the effect of $M_{V(\text{an})}$ on $C_{IL(\text{InP})}(\infty)$ is neglected; i.e., I could assume that $M_{V(\text{an})}$ is approximately zero. The experimental data are, therefore, consistently described by the model that the In_i-P_i interstitial-pairs are created only during electron irradiation.
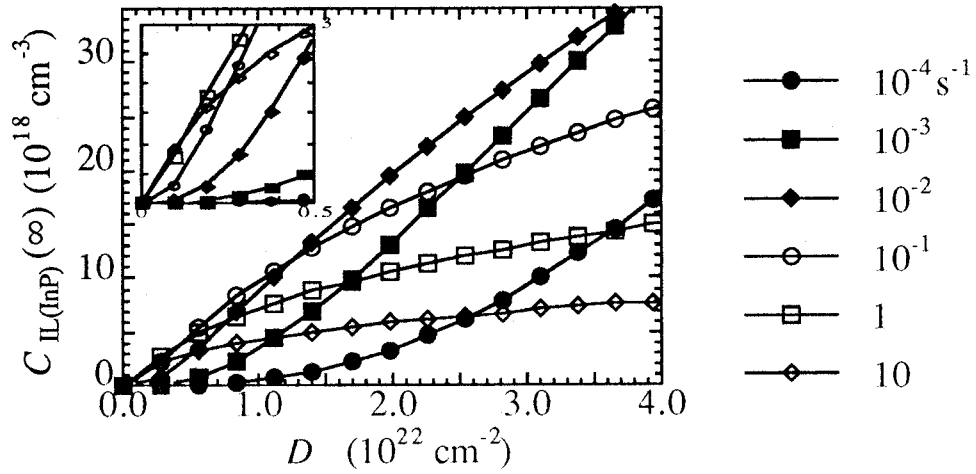
Fig. 2-5-3 Variation of the simulated final density of aggregated interstitials in InP $C_{IL(InP)}(\infty)$ with several electron doses D and interstitial mobilities during irradiation $M_{I(ir)}$. $M_{I(ir)}$ in the computations are written in the figure. It is assumed that the pairs are formed only during electron irradiation.
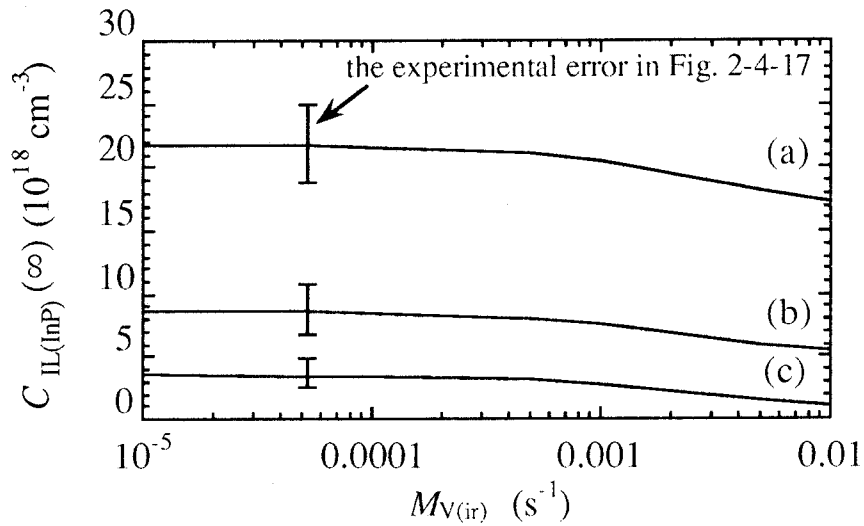

Fig. 2-5-4 Variation of the simulated final density of aggregated interstitials in InP $C_{IL(InP)}(\infty)$ with several vacancy mobilities during annealing, $M_{V(an)}$. Electron doses, D = (a) 3.5×10^{22}, (b) 1.7×10^{22} and (c) 8.5×10^{21} cm^{-2}. Interstitial mobility during irradiation and annealing, $M_{I(ir)}$ and $M_{I(an)}$ are assumed as 1.0×10^{-3} and 1.5×10^{-3} s^{-1}, respectively.

2-5-3-3 Growth of dislocation loops in GaP

I found that an interesting formula consisting of some observable parameters and the mobility M_{II} is valid during annealing. After the nucleation of all loops, the number density of loops C_L was constant during annealing (Sec. 2-4-4). From Eqs. (2-5-1) and (2-5-9), the variation of C_{IL} during an annealing is written as

$$\frac{dC_{IL}}{d\tau_{an}} = 2\pi \cdot 2\tilde{r} \frac{d\tilde{r}}{d\tau_{an}} \cdot \sigma C_L = (2\pi\tilde{r} \cdot \alpha)M_{II} \cdot C_L \cdot C_{II}. \tag{2-5-10}$$

The variation of $\tilde{r}$ during an annealing is, therefore, written as

$$\frac{d\tilde{r}}{d\tau_{an}} = \frac{\alpha M_{II}}{2\sigma} \cdot C_{II}. \tag{2-5-11}$$

The first term of Eq. (2-5-7) can be omitted because the interstitial-pairs were not formed during annealing (Sec. 2-5-3-1). Combined use of Eqs. (2-5-7) and (2-5-11), the variation of C_{II} during an annealing is written as

$$\begin{aligned}\frac{dC_{II}}{d\tau_{an}} = \frac{d}{d\tau_{an}}\left(\frac{2\sigma}{\alpha M_{II}}\frac{d\tilde{r}}{d\tau_{an}}\right) &= -(2\pi\tilde{r} \cdot \alpha)M_{II} \cdot C_L \cdot C_{II} \\ &= -(2\pi\tilde{r} \cdot \alpha)M_{II} \cdot C_L \frac{2\sigma}{\alpha M_{II}}\frac{d\tilde{r}}{d\tau_{an}}\end{aligned} \tag{2-5-12}$$

thus

$$\frac{d}{d\tau_{an}}\left(\frac{d\tilde{r}}{d\tau_{an}} + \pi\alpha M_{II} \cdot C_L \cdot \tilde{r}^2\right) = 0. \tag{2-5-13}$$

Since $C_{II} = C_{II}(\tau_{ir})$ and $\tilde{r} = 0$ at $\tau_{an} = 0$, Eq. (2-5-13) is rewritten as

$$\frac{d\tilde{r}}{d\tau_{an}} + \pi\alpha M_{II} \cdot C_L \cdot \tilde{r}^2 = \frac{\alpha M_{II}}{2\sigma} \cdot C_{II}(\tau_{ir}). \tag{2-5-14}$$

I can thus obtain the following analytical formula of $\tilde{r}$,

61

$$\tilde{r} = \left\{\frac{C_{II}(\tau_{ir})}{2\pi\sigma C_L}\right\}^{0.5} \tanh\left\{\alpha M_{II}\left(\frac{\pi C_L \cdot C_{II}(\tau_{ir})}{2\sigma}\right)^{0.5} \tau_{an}\right\}. \tag{2-5-15}$$

This result exactly corresponds to the experiments represented by Eq. (2-4-1). The product $r_0 \cdot A$ in Eq. (2-4-1) is, therefore, written as

$$r_0 \cdot A = \left\{\frac{C_{II}(\tau_{ir})}{2\pi\sigma C_L}\right\}^{0.5} \cdot \alpha M_{II}\left(\frac{\pi C_L \cdot C_{II}(\tau_{ir})}{2\sigma}\right)^{0.5} = \frac{\alpha C_{II}(\tau_{ir})}{2\sigma} M_{II}. \tag{2-5-16}$$

Since α, $C_{II}(\tau_{ir})$ and σ are independent of the annealing temperature T_{an}, the variation of $r_0 \cdot A$ with T_{an} arises from the temperature dependence of M_{II}.

2-5-4　Migration of interstitial-pairs

2-5-4-1　Migration energies for Ga_i-P_i and In_i-P_i interstitial-pairs

I estimated the migration energy for Ga_i-P_i interstitial-pairs in GaP using Eq. (2-5-16). Figure 2-5-5 shows the Arrhenius plot of the product $r_{0(GaP)} \cdot A$ with T_{an}. The slope of the straight line provides the migration energy of 0.87 eV. This value well agrees with one obtained by Hirata et al (0.9 eV) {126}, even though they claimed that the energy was related to the mobility of isolated interstitials. Using a high voltage TEM technique, they plotted $\ln(C_L)$ vs. $1/kT_{ir}$ and estimated the migration energy as the twice of the energy shown by the slope of the logarithm {126}. Suppose the loops were formed by clustering of Ga_i-P_i interstitial-pairs introduced by irradiation; the nucleus of the loops is couples of interstitial-pairs created through the thermal migration of the pairs. In this case, C_L should be proportional to $M_{II}^{-0.5}$, and the energy obtained by them is replaced with one for the interstitial-pairs. The same analysis may apply to our experimental results denoted in Fig. 2-4-15. The migration energies for the interstitial-pairs are estimated to be 0.93 eV (open circles) and 0.90 eV (open squares), which are almost the same as one estimated in Fig. 2-5-5. The estimated energy for step-annealing experiments, 1.06 eV (closed circles),

differs from one in Fig. 2-5-5. In case of step-annealing, interstitial-pairs aggregated in loops after the annealing of the first step. Some loops released the pairs during the annealing of the second step, and thus the concentration of the pairs around the loops was heightened. Since the pairs distributed inhomogeneously, the chemical kinetics theory is inapplicable to this case. Consequently, the migration energy for Ga_i-P_i interstitial-pairs is estimated as 0.9 ± 0.03 eV.

I applied the same analyses for InP. The migration energy for In_i-P_i interstitial-pairs is estimated to be 1.52 eV, as the twice the energy shown by the slope of $\ln(C_L)$ vs. $1/kT_{an}$ in Fig. 2-4-16.
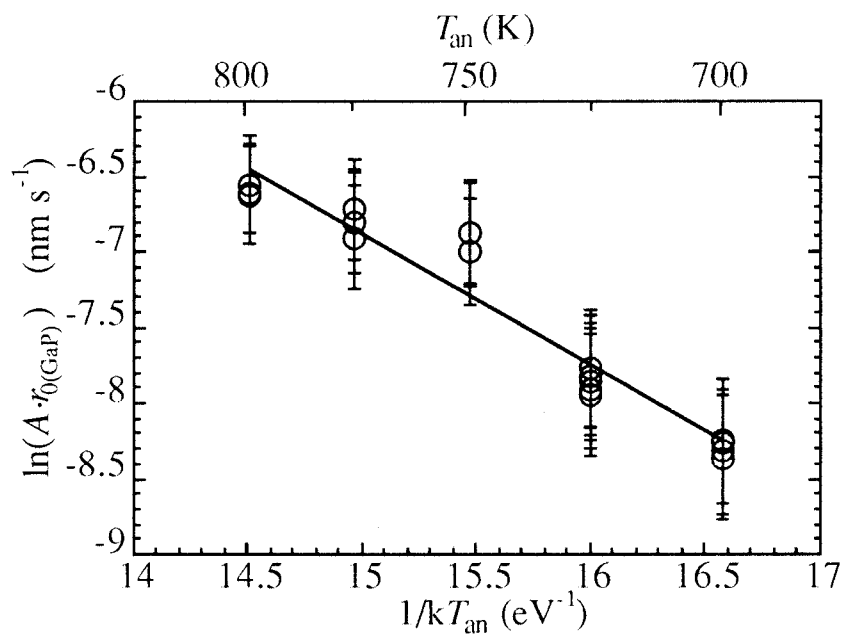

Fig. 2-5-5 Arrhenius plot of the product of the final loop-radius in GaP and growth rate $r_{0(GaP)} \cdot A$.

2-5-4-2 Onset temperature for the migration of Ga_i-P_i pairs

I observed the formation of dislocation loops at $T_{an} \geq 700$ K. Interstitial clusters whose size is less than about 1 nm may be formed by an annealing below 700 K, though they are hardly observable by TEM. Suppose the relationships between C_L and T_{an} denoted in Fig. 2-4-15 and between C_{IL} and T_{an} in Fig. 2-4-21 are held even at low T_{an}, I can estimate C_L and C_{IL} at the temperature range $T_{an} < 700$ K. At $T_{an} = 530 \sim 540$ K, C_L reaches to a quarter of C_{IL}: only two interstitial-pairs are contained in a loop. This temperature corresponds to the onset temperature for the migration of the interstitial-pairs. The estimated temperature is extremely higher than the onset temperature for the migration of isolated Ga- and P-interstitials (about 100 K {30-34}), and the fact obviously indicates that the loops are not formed by the migration of isolated interstitials. Since the estimated temperature is lower than that of isolated Ga- (700 K {9-13}) and P- (1100 K {15-17}) vacancies, formation of the loops does not relate to the migration of vacancies.

The estimated onset temperature is close to an annealing temperature of Ga(1) and B(1)-centers observed by IR in electron irradiated GaP (about 530 K) {32}. According to the work, these centers correspond to the local vibrational mode of a Ga atom on a P-site (anti-site defect) {33} and boron atom on Ga-site with P-interstitial {30}, respectively. The annealing mechanism of these defects is still uncertain. The annealing of the observed defects may be related to the migration of interstitial-pairs, though it is possible that different kinds of defects anneal at the same temperature as observed in GaAs {157}.

2-5-4-3 Onset temperature for the migration of In_i-P_i pairs

In the temperature range from 700 to 825 K, (1) C_L increased exponentially with $1/kT_{an}$ (Fig. 2-4-16) and (2) $C_{IL}(\infty)$ was independent of T_{an} on the condition of constant D and T_{ir} (Fig. 2-4-25). Suppose the relationships between C_L and T_{an} and between $C_{IL}(\infty)$ and T_{an} are held even at low T_{an}, we can estimate C_L and $C_{IL}(\infty)$ for temperatures $T_{an} < 700$ K. In the model, the temperature when C_L reaches to a quarter of $C_{IL}(\infty)$, at which only two interstitial-pairs are contained in a loop, corresponds to the onset temperature for the migration of the interstitial-

pairs.   I estimated the onset temperature to be 550 K.   The estimated temperature is extremely higher than the onset temperature for the migration of isolated In- or P-interstitials (100-300 K) {46, 47, 60, 61}, and the fact obviously indicates that dislocation loops are not formed by the migration of isolated interstitials.

The temperature is also higher than the onset temperature for the migration of isolated In vacancies (425~450 K) {43, 60, 61}.   Suppose isolated vacancies can combine with interstitial-pairs, $C_{IL}(\infty)$ should decreases with T_{an} through the thermal migration of vacancies. Since $C_{IL}(\infty)$ is independent of T_{an} (See Fig. 2-4-22), it is concluded that the interstitial-pairs do not combine with isolated vacancies; i.e., the state of coexistence of an isolated vacancy with an interstitial-pair is more stable than that of the recombination of these defects.   This experimental result is consistent with the assumption in my model.

The estimated onset temperature is close to the onset temperature of an annealing stage of anti-site defects, P_{In} {53} and In_P {57}, as similar as the case in GaP.   The estimated temperature is also close to the onset temperature of an annealing stage observed by electron conductivity measurements (543 K) {61} and PAS in electron {43} or neutron {62} irradiated InP (575 K).   The stage is believed to arise from the breaking up of vacancy clusters such as V_{In}-V_P pairs {43}.   This annealing may be simply interpreted as the recombination of a V_{In}-V_P pair and a In_i-P_i pair by the migration of interstitial-pairs.

2-6 Conclusion

I found that dislocation loops of interstitial-type are formed uniformly in GaP and InP crystal by an annealing at the temperature $T_{an} \geq 700$ K following 200 keV electron irradiation in the temperature range from 110 to 700 K for GaP and 110 to 400 K for InP. I also found that the similar types of dislocation loops are introduced in GaAs by an annealing at $T_{an} \geq 800$ K following 300 keV electron irradiation. The results of *in-situ* TEM observations showed that the loops are formed through the two processes; 1) an introduction of point defects by an electron irradiation and 2) a thermal migration of point defects by an annealing.

I pursued quantitatively the variation of the radii and number density of loops in GaP and InP by *in-situ* TEM. The loop-radius increased as a function of annealing temperatures, T_{an}. As T_{an} raised, the volume number density of loops, C_L, decreased. The final density of agglomerated interstitials in all loops, $C_{IL}(\infty)$, only depended on irradiation conditions (an electron dose, D, and an irradiation temperature, T_{ir}), and it increased quadratically with increasing D. These results were well explained by a new model that the loops are formed through the thermal migration of III_i-V_i interstitial-pairs, that is Ga_i-P_i pairs for GaP and In_i-P_i pairs for InP, introduced during electron irradiation. From the analyses, the migration energies for the interstitial-pairs were estimated as 0.9 eV for GaP and 1.5 eV for InP The threshold temperatures for the migration of the pairs were found to be about 530 K for GaP and 550 K for InP.

3 Diffusion process of interstitial atoms at low temperature

3-1 Introduction

As shown in the previous section, I found the formation of interstitial-type dislocation loops by an annealing above 700 K following 200 keV electron irradiation. From the results of TEM, I concluded that the loops are formed by a thermal migration of interstitial-pairs introduced during electron-irradiation. I confirmed that the pairs are formed even at 110 K, since the loops are formed by an electron-irradiation at 110 K and following annealing.

In addition to the interstitial-pairs, several kinds of interstitial-related complexes are formed even at a temperature of about 100 K. For examples, B(1)- and C(1)-center observed by IR spectroscopy, i.e. boron and carbon atom on Ga-site with P interstitials, are formed at 100 K in GaP {30-32} and GaAs {89, 90}. A defect of a Ga atom on P-site, Ga(1)-center, is also introduced in GaP by an electron irradiation at 100 K {32, 24}. It is generally believed that these defects are formed by the migration of isolated interstitials, even though there is no reliable information on the kinetics of the defects at low temperature to our knowledge. More detailed investigation is necessary for a general understanding of diffusion process of point defects in III-V compound semiconductors.

In order to understand the kinetics of interstitial atoms at low temperature in detail, I performed *in-situ* optical spectroscopy (PL and CL) in a transmission electron microscope in the temperature range from 20 to 130 K. The new experimental method, *in-situ* TEM-PL/CL spectroscopy, is extremely useful for microscopic characterization of electronic and dynamical properties, as mentioned in the following section. Using the method, I found a decrease of luminescence intensities due to non-radiative recombination centers that are formed by electron-irradiation-induced defects. From the analyses of the decrease-rate of the intensity, I concluded that Frenkel-type defects and interstitial-pairs are formed during electron-irradiation through the migration of interstitial atoms.

3-2 Experimental setup for in-situ TEM-PL spectroscopy [158-160]

3-2-1 Introduction

TEM has been extensively applied to understanding structural properties of extended defects in semiconducting materials; this method is usually applied to analyzing nature, distribution, chemical compositions and atomic structures of rather extended defects. Point defects and their complexes, which are hardly observable by TEM, have been investigated by ESR, DLTS, PAS, etc. Optical spectroscopy, such as CL [161-165] and PL [166-168] methods, has been most extensively utilized for characterizing the complexes.

For the purpose of characterizing electronic property in the same microscopical area, TEM-mode CL method, whose spatial resolution is less than 1 μm, has been used [162-165]. However, in certain cases electron-irradiation may create lattice defects and then alters electronic properties of materials temporarily or permanently during an observation. Moreover, electron-excitation causes not only radiative electronic transitions but also many non-radiative recombination events, and some emissions are therefore suppressed in CL.

PL method can supplement the weak points in CL. By choosing a suitable excitation wavelength, intense PL emission due to a lattice defect is observed. TEM method and PL spectroscopy have so far been performed by utilizing independent instruments, and therefore the same microscopic area has not usually been studied (*Ex-situ* TEM/PL observation). In this section, I recommend a new apparatus which enables us to obtain simultaneously the complemental data of the same microscopical area, i.e. structural data in higher spatial resolution by TEM and optical data by PL (*In-situ* TEM/PL observation). The apparatus is extremely useful for microscopic characterization of structural and electronic properties in an inhomogeneous material. The apparatus will be further applied to study optical properties of ionized materials under electron-irradiation. Of course, CL spectra are observable without any modifications of the apparatus, as previous studies [162-165]. Combined use of PL and CL allows me to obtain proper optical data due to lattice defects in a microscopic area.

3-2-2　Outline of in-situ TEM-PL spectroscopy

I have accomplished the *in-situ* TEM/PL observation apparatus, which is installed in a JEOL 2000EX transmission electron microscope of side-entry type (Fig. 3-2-1).　For optical excitation, a top surface of a specimen is illuminated by a laser-beam as shown in Fig. 3-2-2. The laser-beam is introduced into the microscope through an optical window of 40 mm in diameter which is attached on the side of the microscope column.　The laser-beam is then reflected to the specimen by a reflection mirror in the column, which is located above the objective lens and on the axis of an electron-beam.　The electron-beam passes through an opening of 5 mm in diameter in the middle of the reflection-mirror.　The opening is large enough to tilt the electron-beam by 2.5° with regard to the optical axis of the objective lens for dark field imaging.　Thus the specimen is illuminated simultaneously by both electron- and laser-beams.　The small opening in the mirror does not decrease the reflection efficiency of laser light significantly.
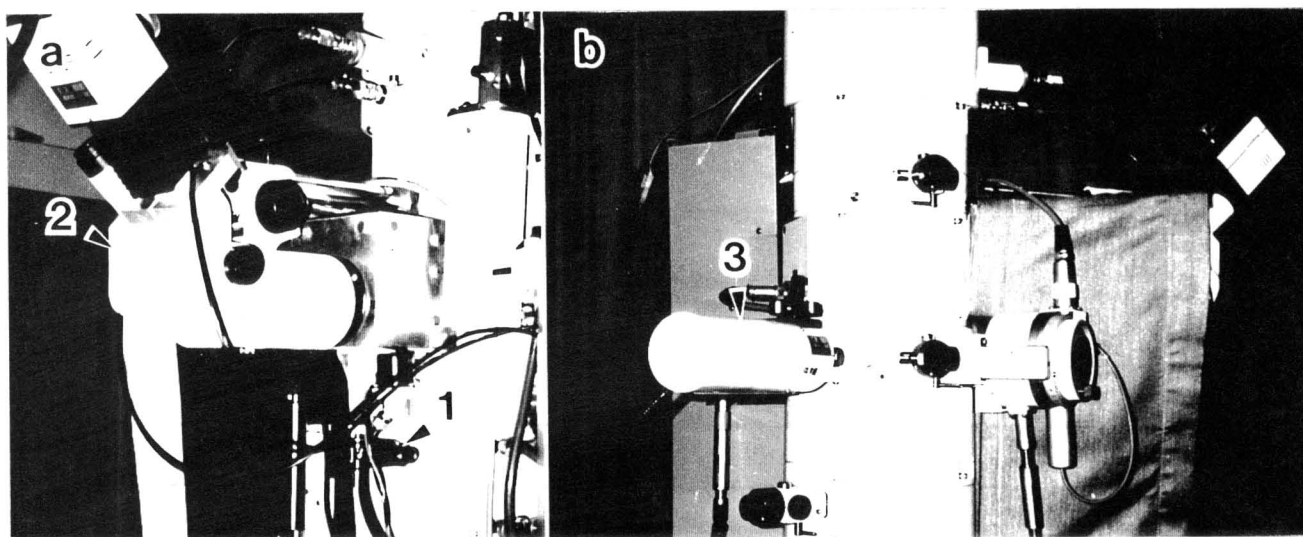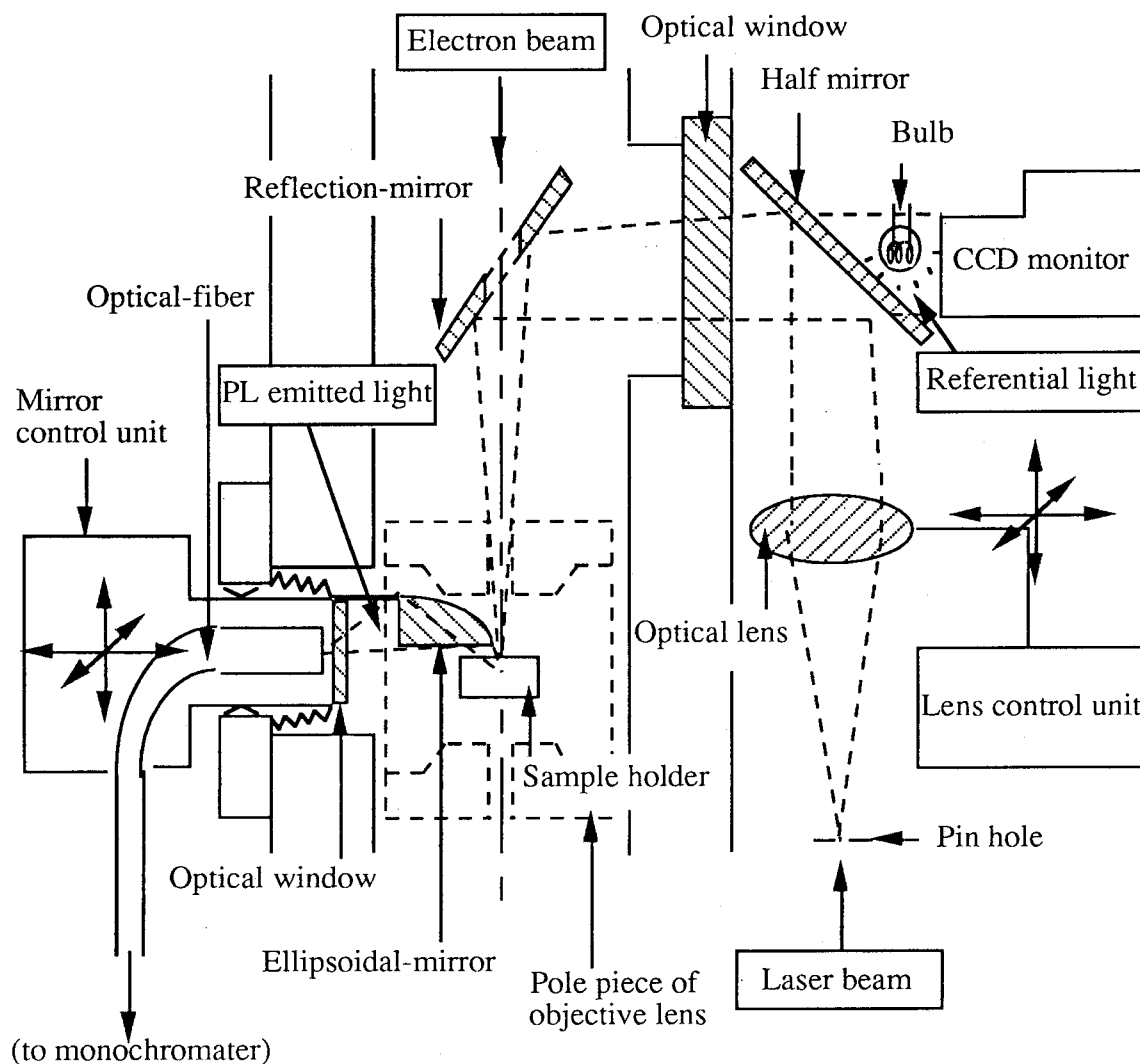

Fig. 3-2-1　External appearance of the *in-situ* TEM-PL observation apparatus.　(a) An apparatus for optical excitation of a specimen in a TEM; 1) an optical lens for focusing a laser-beam, and 2) a telescope equipped with a CCD camera for optical observation of a specimen in a TEM.　(b) An apparatus for collecting luminescent light.

69

Introduction of a laser-beam into a TEM	Collection of PL	Optical monitoring of a specimen in a TEM
Spot size : 20 μm	Collection rate : 10 %	Magnification : x150
Position control : 1 μm	Polarization : observable	

Fig. 3-2-2 Outline of the *in-situ* TEM-PL observation apparatus. TEM images and PL spectra are observable simultaneously under the same experimental condition.

In detail, the laser-beam is first converged outside the microscope and passes through a pin-hole of 10 μm in diameter for making a virtual point source. The divergent beam from the pin-hole is then focused on a specimen surface by an optical convex lens (focal distance; 300 mm) outside the microscope, which attaches to a computer-aided lens-position control unit (designated by 1 in Fig. 3-2-1(a)). The position of the laser-spot on the surface can be shifted by displacement of the lens horizontally.

A specimen generally exhibits CL emission during TEM observation, and CL spectra are also observable without any modifications of the apparatus (Fig. 3-2-3). In order to distinguish PL emission from CL, PL spectra are observed when the illumination of an electron-beam is suspended. For collecting luminescent light from the specimen, I use an ellipsoidal mirror, which is inserted inside the gap of the pole pieces of the objective lens and is located above the specimen. The long and short radii of the ellipse are, respectively, 19.8 mm and 7.0 mm, the two foci being 37 mm apart. The mirror is truncated in part so that an electron-beam illuminates the specimen during collecting luminescent light. In order to collect luminescent light efficiently, the mirror is movable along the three orthogonal axes in accuracy of a few μm; a focal point can be precisely adjusted to coincide the luminescent point. A similar mirror has commonly been used for collecting CL emission in a transmission electron microscope {162-165}.

Collected light is guided to the outside of the evacuated column through an optical window of 4 mm in diameter, and is then focused on the end of an optical fiber which is located at the other focal point of the ellipsoidal mirror. Focused light is introduced in a monochromator through the optical fiber (designated by 3 in Fig. 3-2-1(b)).

I have attached an optical-monitoring system for observing a specimen inside the microscope. This system is a requisite in order that the locations of electron- and laser-beams coincide on a top surface of the specimen. The optical path of the monitoring system is partly in common with that of the laser-beam (Fig. 3-2-2). Emitted light from a bulb passes through a half mirror, reflects at the reflection-mirror, and illuminates the specimen. Optical images of the specimen are magnified by a telescope equipped with a CCD camera (designated by 2 in Fig. 3-2-1(a)), the final magnifications on a CCD monitor being 150 times.
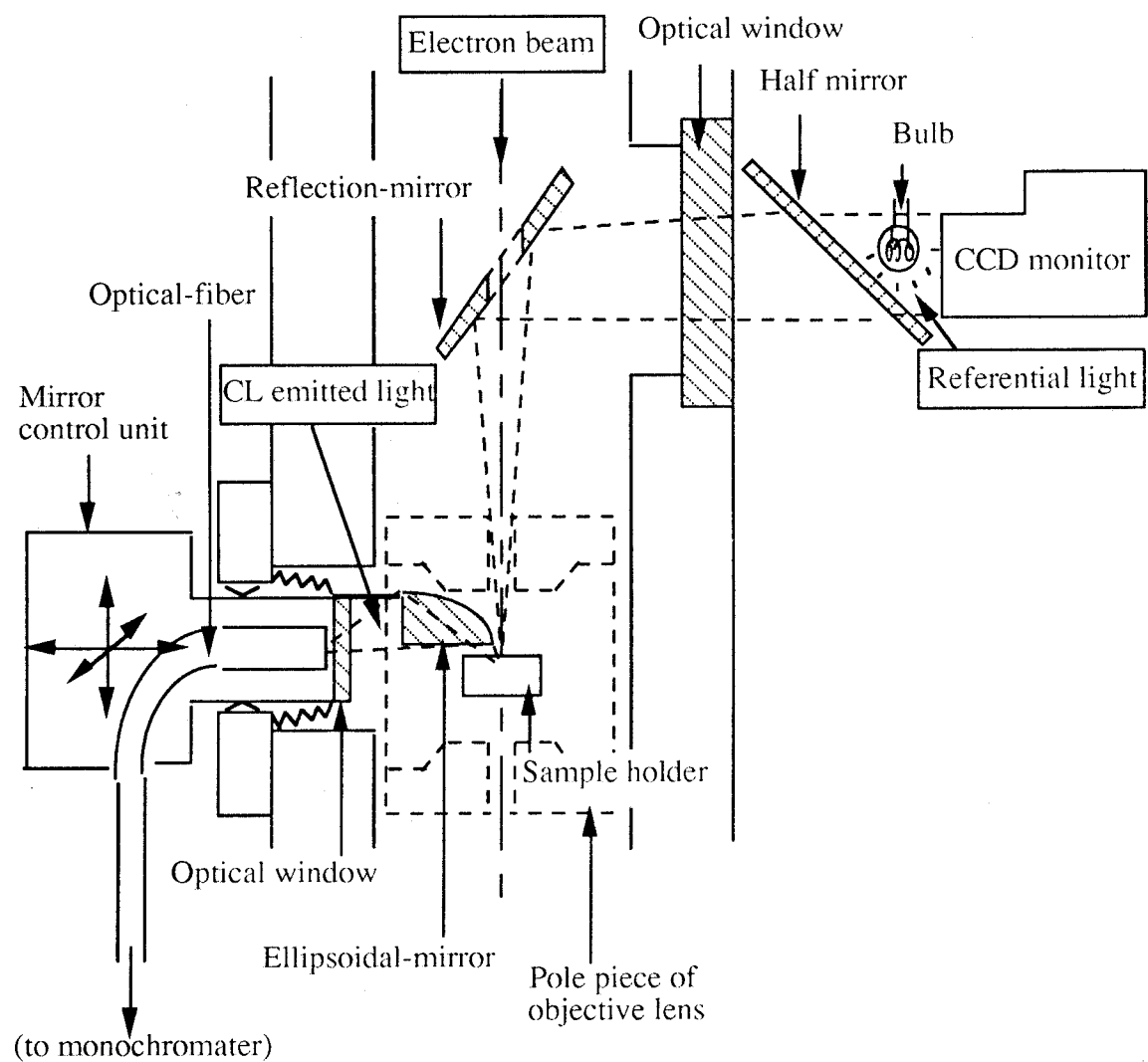
Fig. 3-2-3　Schematic representation of an *in-situ* TEM-CL observation.　TEM images and

CL spectra are observable simultaneously under the same experimental condition.

3-2-3 TEM observation during in-situ TEM-PL spectroscopy

It is emphasized that the attached apparatus does not interrupt any electron imaging and diffraction experiments. A specimen is mounted on a conventional specimen-container of side-entry type, and is placed at the standard specimen-position inside the microscope. The tilt angle of the specimen is limited to $\pm 25°$ on the container for room-temperature observation, $\pm 5°$ for high (~ 1100 K) or low (~ 20 K) temperature observation, since an ellipsoidal mirror for collecting luminescent light is also inserted inside the gap (20 mm) of the magnetic pole pieces of the objective lens. The spatial resolution of TEM observation is estimated to be 0.5 nm.

3-2-4 PL spectroscopy during in-situ TEM-PL spectroscopy

For PL excitation, a laser-beam is focused on a top surface of a specimen in the microscope. The laser power transmitted to the specimen is estimated to be about 1 % of the primary laser output. The laser-spot on the specimen can be laterally shifted in the accuracy of 1 μm. At the present time, the focused laser spot of 20 μm in diameter is obtained on the specimen surface. The spatial resolution of my PL measurements is therefore rather poor in comparison with CL, whose spatial resolution is similar to the size of an electron-beam, i.e. far smaller than 1 μm. The size of the spot is limited, in my experiment, by the long focal distance of a focusing lens outside of the microscope. It is necessary to attach another focusing lens near the specimen in order to obtain a better spatial resolution of PL.

Luminescent light is introduced in a monochromator through an optical window and optical fiber. Considering the reflection at the window and the end of the optical fiber, I expect that about 10 % of luminescent light is collected. It is possible to measure polarization of PL by placing a polarizing plate on the end of the optical fiber.

3-2-5 Coincidence of the area of TEM and PL measurements

Figure 3-2-2 shows the optical and TEM images of a Cu grid under both electron and laser illumination. In the optical image with illumination by a bulb (Fig. 3-2-3 (a)), the laser spot is clearly visible as well as the Cu-grid. By inspecting a characteristic shape of the specimen observed in both optical (as seen in Fig. 3-2-3 (a)) and TEM (as seen in Fig. 3-2-3 (b)) images, it is possible to converge the electron-beam in the area under laser illumination. This method is generally applied to any specimens, even though the accuracy of the coincidence is rather poor at the present time; the accuracy is roughly estimated to be less than a few tenth μm.

In another method that the two kinds of beams coincide more accurately, I observe CL emission from a specimen directly by the optical-monitoring system. The method is demonstrated in Fig. 3-2-4, in which the observed specimen is diamond. The optical images in this figure were observed without illumination of a bulb. In Fig. 3-2-4 (a), a focused laser-beam on the specimen (~20 μm in diameter) is designated by 1, while the spot designated by 2 is due to CL; in other words, the area was illuminated by a focused electron-beam. By adjusting precisely the location of the optical lens outside the microscope, the two bright spots coincide as shown in Fig. 3-2-4 (b). Thus the method is applied to any specimens that show CL emission, and the accuracy of the coincidence is estimated to be less than 10 μm. In general, specimens show strong CL emission only at a low temperature. Therefore, I normally perform a TEM-PL/CL experiment at a temperature below 110 K.
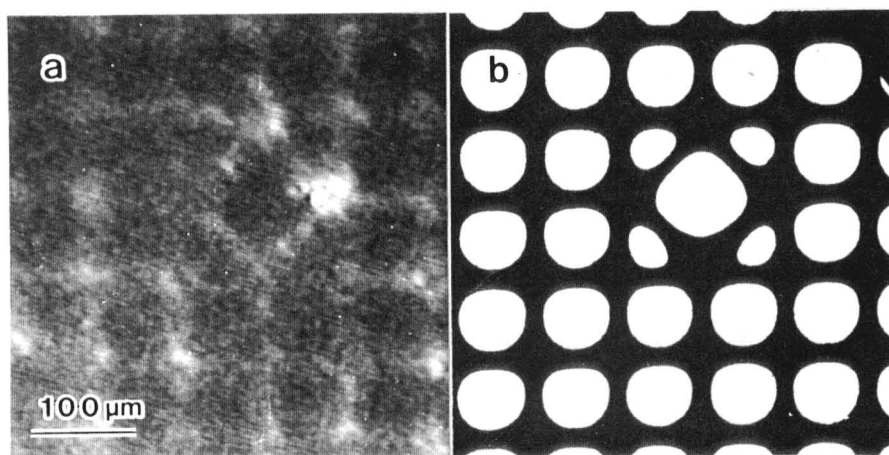
Fig. 3-2-4   (a) Optical image of a laser-beam on a specimen with light from a bulb.   The size of the laser-spot is about 20 μm in diameter.   (b) TEM image of the specimen.   These two images are obtained simultaneously.
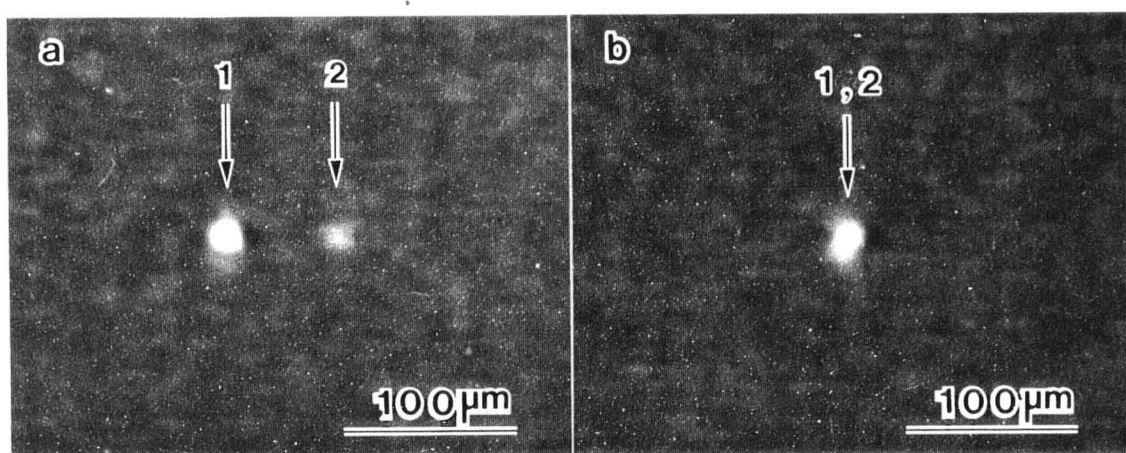

Fig. 3-2-5   (a) A laser spot (1) and CL (2) on a specimen in a microscope are observed on a CCD monitor at the temperature of 110 K.   (b) Both laser- and electron-beams illuminate the same microscopic area after adjusting the position of the optical lens.

3-3 Theoretical basis of PL in semiconductors

PL provides a non-destructive technique to find certain impurities or radiation-induced point defects in semiconductors. It is particularly suitable to the detection and identification of impurities, but can also be applied to certain lattice defects.

Photons are emitted in radiative recombination processes. In non-radiative recombination mechanism, no photons are emitted any more. PL method can detect, therefore, only impurities or lattice defects that produce radiative recombination processes. In this section, I summarize the details of PL in semiconductores.

3-3-1 Formation of energy-levels in the midgap due to lattice defects

Impurities that contribute electrons to the conduction band, i.e. donors, have a higher valence than the atoms of the host; thus an electron is donated to the conduction band, which leads to an excess of mobile electrons. Impurities that supply holes to the valence band, i.e. acceptors, have a lower valence than the host, which leads to incomplete atomic bonding in the lattice; thus they capture electrons. The binding energy E_D of the electron to the donor impurity can be estimated by considering an extra electron in the donor atom as a particle with an effective mass m^* moving in the presence of a positive net charge; i.e., the situation is analogous to a hydrogen atom embedded in the dielectric medium of the crystal. The binding energy is measured relative to the conduction-band level; thus, in terms of the energy-band diagram, donor impurities introduce levels E_d below the bottom of the conduction band E_C so $E_D = E_C - E_d$. Similar considerations can be applied to acceptor impurities. In the band structure diagram the acceptor impurities introduce levels at energies E_a lying above the top of the valence band. In addition to the impurity-induced levels, a wide variety of lattice defects may also give rise to bound states (donor or acceptor levels) in the forbidden gap.

3-3-2 Electronic transition process in semiconductors

Figure 3-3-1 shows electronic transition processes in semiconductors due to optical excitation that are discussed in detail by Pankove {169}, Bergh and Dean {170}, and Dean {171}. Samples are excited by an optical source, typically a laser with a photon energy above the band-gap energy, to generate electron-hole pairs (Process 0). Process 1 is an intraband transition: an electron excited well above the conduction-band edge dribbles down and reaches thermal equilibrium with the lattice. Processes 2 and 3 are a band-to-band recombination and excitonic recombination, respectively. For GaP, the probabilities of these transitions are usually small, since GaP is a indirect-gap semiconductor. Processes 4~8 are concerned with a localized energy-level due to lattice defects. Processes 4 and 5 are the trapping of free electron on a localized donor level and one of free hole on an acceptor level, respectively. Process 6 is a combination of a free hole with a neutral donor and forms a positively charged excitonic ion or a bound exciton (BE). Similarly, electrons combining with neutral acceptors also form BEs (process 7). An electron which escaped from a neutral donor can recombine with a hole in a neutral acceptor (process 8): the well-known donor-acceptor recombination.
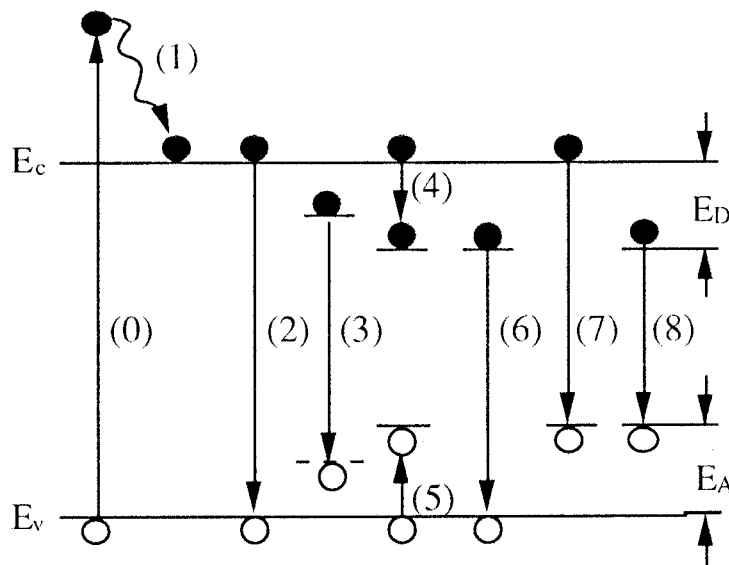

Fig. 3-3-1   Schematic representation of electronic transition processes in semiconductors.

3-3-3 Radiative recombination process in semiconductors

The carriers generated in semiconductors by optical excitation will undergo diffusion, followed by recombination that gives rise to the emission of photons. These three processes, generation, diffusion, and recombination, are of interest in describing the luminescence phenomena. The diffusion process may be treated in terms of the differential equation of continuity for the diffusion of the excess minority carriers:

$$D\nabla^2(\Delta n) - (\Delta n/\tau) + g(r) = 0, \qquad (3\text{-}3\text{-}1)$$

in which D is the diffusion coefficient, Δn the excess minority-carrier density per unit volume, τ the minority-carrier lifetime, and $g(r)$ the generation rate of excess carriers per unit volume {172}. This equation is valid under the conditions that τ is independent of Δn and that the motion of excess carriers is purely diffusive. The former condition is satisfied if Δn is small compared with the majority carrier density; this condition can usually be satisfied by using an excitation-beam with low power. The latter one is valid for sample regions without depletion zones or applied fields.

Recombination centers with energy levels in the gap of a semiconductor can be either radiative or non-radiative depending on whether they lead to the emission of a photon or not. These centers are characterized by a probability of recombination P, that is inversely proportional to a recombination lifetime. In general, when both radiative and non-radiative centers are present, the observable lifetime τ_{obs} is

$$\tau_{\text{obs}} = \frac{\tau_r \tau_{\text{nr}}}{\tau_r + \tau_{\text{nr}}} \qquad (3\text{-}3\text{-}2)$$

where τ_r and τ_{nr} are the radiative and non-radiative recombination lifetimes, respectively. Here τ_{nr} is the result of different non-radiative recombination processes ($\tau_{\text{nr}}^{-1} = \sum \tau_{\text{nr}}(i)^{-1}$). The radiative recombination efficiency η, which is defined as the ratio of the radiative

78

recombination probability P_r to the total recombination probability P, is

$$\eta = \frac{P_r}{P} = \frac{\tau}{\tau_r}$$

$$= \frac{1}{1+\left(\tau_r / \tau_{nr}\right)} \quad . \qquad (3\text{-}3\text{-}3)$$

The rate of PL emission L_{PL} is proportional to η and the generation rate of electron-hole pairs $g(r)$. L_{PL} also contain factors which account for the fact that not all photons generated in the semiconductor are able to leave through its surface. The loss mechanisms include (1) an absorption, characterized by a decrease in intensity of the form $\exp(-\alpha d)$, where α is the absorption coefficient and d the length of the photon path in the interior of the material; and (2) reflection processes at the semiconductor/vacuum interfaces, characterized by the total reflection of a portion of photons R {172, 173}. Thus the observed PL emission rate is written as

$$L_{PL} = g(r)\eta F(\alpha, R), \qquad (3\text{-}3\text{-}4)$$

where $F(\alpha, R)$ is a function that accounts for losses due to the absorption and reflection processes.

For a material that contains only one type of radiative and one type of non-radiative recombination center, one can write L_{PL} using $\tau = 1/(N\sigma v)$,

$$L_{PL} = \frac{g(r)\eta F(\alpha, R)}{1+\left(\dfrac{N_{nr}\sigma_{nr}}{N_r \sigma_r}\right)}, \qquad (3\text{-}3\text{-}5)$$

where N_r and N_{nr} are the densities of the radiative and non-radiative recombination centers, respectively; σ_r and σ_{nr} are the radiative and non-radiative capture cross sections, and v is the carrier velocity.

3-4 Experimental conditions

The TEM-PL/CL observation apparatus is attached with a microscope operated with 200 keV. Since point defects in GaAs are introduced by an electron irradiation with an electron energy above 270 keV, I could not observe an irradiation effect on PL/CL spectra in my experiments. Moreover, I observed no PL/CL spectra in InP in my observed spectral range. In order to obtain an irradiation effect due to the displacement of Ga, In, and P atoms in semiconductors, I performed an optical spectroscopy in GaP and GaInP crystals under electron irradiation.

GaP sample was the same as in Sec. 2-2, and specimens for TEM observation were prepared in the same way mentioned in Sec. 2-2. GaInP of 0.55 μm thick, provided by Mitsubishi Chemical Co., was grown at the temperature about 700 °C on a GaAs substrate by metal-organic vapor-phase epitaxy. The substrate was 2° off from (001) towards [110]. The cross sections of GaInP sample for TEM were prepared as follows. Growth surfaces of two wafers were glued together, the composite was sliced up a small piece along [110]. The strips of the composite were dimpled and then perforated with Ar^+ ions accelerated with an acceleration voltage of 2 kV. The irradiation for introducing point defect was performed at 20, 90~110, and 300 K with the flux range from 2.0×10^{16} to 3.1×10^{19} electrons $cm^{-2}s^{-1}$.

PL spectra were measured at 20, 90 and 300 K in the spectral range from 550 to 900 nm. PL emission was excited by an Ar-ion laser, 514.5 nm of the wavelength, and the laser power reached on the specimen was estimated to be 2-3 mW. The probe size of the laser-beam on a specimen surface was measured directly using the optical monitoring system. The smallest probe size was estimated to be 20 μm in diameter. The specimen thickness of the probed-area was about 1 μm. The wavelength resolution was about 1 nm, and the spectral response characteristic of a photomultiplier (HAMAMATU R636-10) was not calibrated. CL were measured at the same temperature, and with the same spectral range and wavelength resolution as the PL measurements.

3-5 Results of in-situ TEM-PL/CL spectroscopy in GaP {174}

3-5-1 TEM observation of an electron-irradiated area

Figure 3-5-1 shows weak-beam images of an electron-irradiated area of GaP, taken with a 220 reflection. The area was irradiated earlier with $f = 4.7 \times 10^{18}$ electrons $cm^{-2}s^{-1}$ for $\tau_{ir} = 1800$ s at $T_{ir} = 90$ K. No distinct image contrast due to defects can be observed (Fig. 3-5-1(a)). After the specimen was annealed at $T_{an} = 900$ K for $\tau_{an} = 1800$ s without electron-irradiation, I found that numerous dislocation loops of interstitial-type were formed uniformly only in the irradiated area (Fig. 3-5-1(b)). As shown in the previous section, the result demonstrated in Fig. 3-5-1 clarifies that the loops are formed by thermal migration of point defects, i.e. Ga_i-P_i interstitial pair, that are introduced by an electron-irradiation at $T_{ir} = 90$ K. In order to investigate the kinetics of the defects, which are hardly observable by TEM (Fig. 3-5-1(a)), I next performed the *in-situ* PL and CL spectroscopy in a transmission electron microscope by utilizing the *in-situ* TEM-PL/CL apparatus.
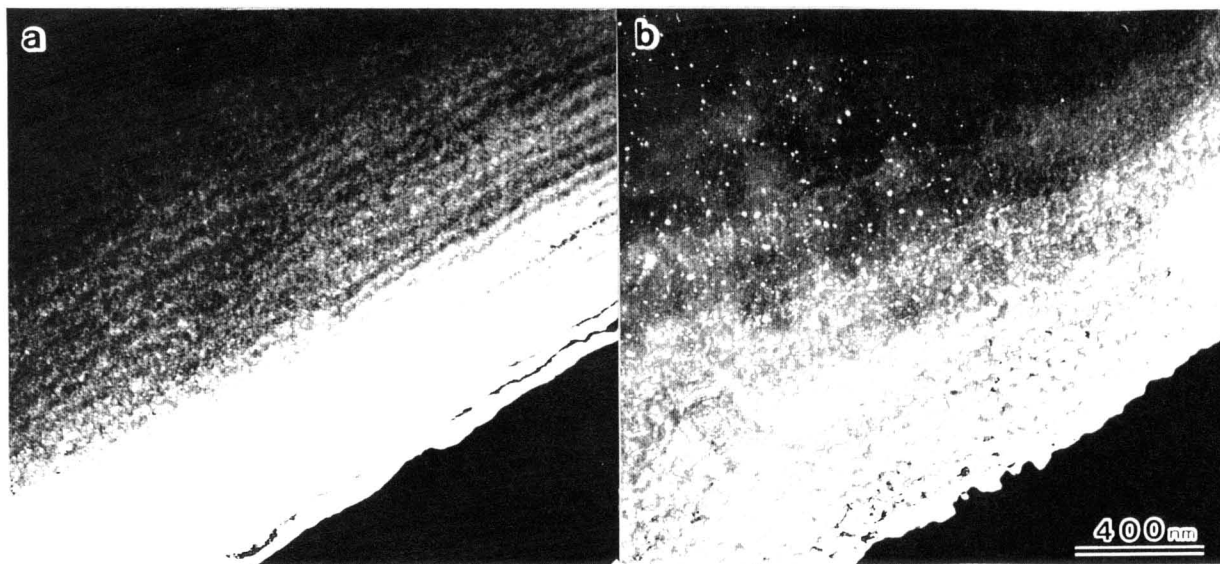

Fig. 3-5-1 Weak-beam images of GaP before (a) and after (b) annealing at 900 K for 1800 s, taken with a 113 reflection. Specimen was irradiated earlier with a flux of 4.7×10^{18} electrons $cm^{-2}s^{-1}$ for 1800 s at 90 K.

81

3-5-2 General trends of luminescence spectra

Figure 3-5-2 depicts PL spectrum of a GaP crystal that were obtained at 20, 90 and 300 K. The area examined by the spectroscopy was irradiated earlier with the same irradiation condition as in Fig. 3-5-1, i.e. $f = 4.7 \times 10^{18}$ electrons cm^{-2} s^{-1} for $\tau_{ir} = 1800$ s. The PL emission, scarcely observed at 300 K, was more enhanced in the lower temperatures. Spectra were clearly observed below 90 K. In the observed spectral range, the three spectra appeared; the stronger ones peaking at 565 nm and 850 nm, and the weaker and broader one peaking around 725 nm. The emission around 565 nm was observed with its phonon sidebands. The weak 725 nm peak can be found clearly in the spectrum inserted in Fig. 3-5-2, which is a magnified one, by ten times in the vertical axis, of the PL spectra at 20 K and is fitted by two spectra; 725 and 850 nm (dotted lines in Fig. 3-5-2). At a lower temperature, the spectra were slightly sharper with their peak positions almost unchanged. The emission peaking at 565 nm is attributed to intrinsic defects associated with sulfur impurities {175}, and the broad emission around 725 nm is due to the hole trap; the complex of sulfur donors with native defects {176}. Since PL emission peaking around 860 nm is observed only in as-grown GaP doped with oxygen atoms {177}, the emission is considered to be attributed to intrinsic defects associated with oxygen impurities. Irradiation-effects were the decrease of luminescence intensities with irradiation-time as shown in the next section.

Figure 3-5-3 shows the PL and CL spectrum obtained at 20 K from the same area observed in Fig 3-5-2. The figure obviously indicates that there is no significant difference in shape between the PL and CL spectra.
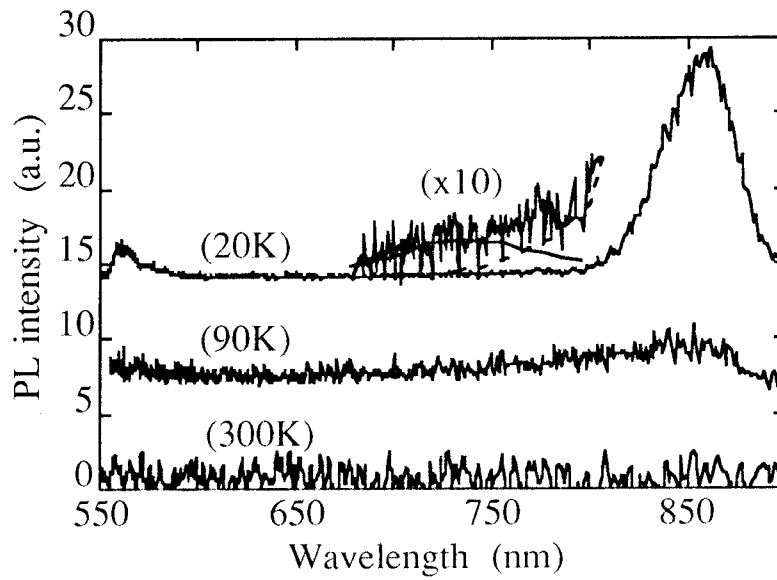
Fig. 3-5-2 PL spectra of GaP observed at 20, 90, and 300 K. Specimen is irradiated earlier with a flux of 4.7×10^{18} electrons cm^{-2} s^{-1} for 1800 s. Three peaks are observable at 565, 725 (weak), and 850 nm.
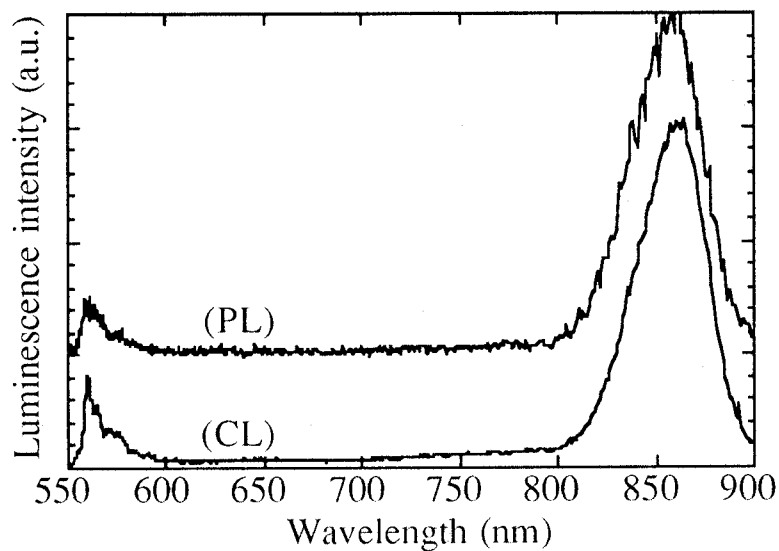

Fig. 3-5-3 PL and CL spectra obtained from the same area in a GaP at 20 K. Specimen was irradiated earlier with a flux of 4.7×10^{18} electrons $cm^{-2} s^{-1}$ for 1800 s.

3-5-3 Irradiation effects on luminescence spectra at 90 K

The luminescence intensities decreased rapidly under electron-irradiation in the temperature range above 90 K. Decrease of the CL intensity during a measurement could not be ignored, since it takes about 5-10 minutes to obtain a spectrum. In order to obtain an irradiation effect on luminescence intensities at several wavelengths quantitatively, I performed in-situ PL spectroscopy during electron-irradiation. Since a laser-beam for PL excitation may not form any additional lattice-defects in GaP, I could obtain the relative decrease-rate of luminescence intensities at several wavelengths quantitatively by the PL method. Figure 3-5-4 shows the decreases of the PL intensities measured at the three peak positions; triangles, circles, and squares represent 565, 725, and 850 nm, respectively. Irradiation and spectroscopy were performed at T_{ir} = 90 K, and f = 4.0×10^{18} cm^{-2} s^{-1}. The luminescence intensity is normalized as in the formula $100 \cdot I(\tau_{ir})/I_0$, in which I_0 and $I(\tau_{ir})$ represent, respectively, the observed luminescence intensity before electron-irradiation and after electron-irradiation for τ_{ir} s. As shown in Fig. 3-5-4, luminescence intensity decreased rapidly during electron-irradiation, and the rates of these decreases depended on luminescence centers.

The variation of the luminescence intensity at a specific wavelength with electron-irradiation is directly observable by CL measurement. Figure 3-5-5 shows the CL intensities at 725 nm as a function of irradiation-time, normalized by the same way as in PL. The electron-irradiation at 90 K performed with the three different fluxes (f = 4.7×10^{18}, 1.7×10^{19} and 3.1×10^{19} electrons cm^{-2} s^{-1}) yielded the decreases of the normalized CL intensities, $I_{nom}(\tau_{ir})$. I found that all intensities were well fitted with the same function,

$$I_{nom}(\tau_{ir}) = \frac{100}{1 + A\tau_{ir} + (B\tau_{ir})^2},$$
(3-5-1)

where A and B are constants to fit for each spectrum. The normalized PL intensities were also well fitted with the equation; A = 1.0×10^{-6} s^{-1} (565 nm), 0.0 s^{-1} (725 nm), 1.7×10^{-5} s^{-1} (850

nm), and B = 3.6x10^{-5} s^{-1} (565 nm), 1.8x10^{-3} s^{-1} (725 nm), 5.4x10^{-5} s^{-1} (850 nm), respectively. The fittings are shown by the solid lines in Fig. 3-5-4.

Figure 3-5-6 summarizes the fitting parameters A (squares) and B (circles) for the peak at 725 nm as a function of f. The open and closed marks represent the result of CL and PL, respectively. It is found that the parameter A and B are in proportion to f. Thus, I_{nom} is rewritten as the following equation,

$$I_{nom} = \frac{100}{1 + \sigma_1 D + (\sigma_2 D)^2} \, ,$$

(3-5-2)

in which D represents the electron dose, σ_1 and σ_2 the fitting parameters. With Fig. 3-5-6, σ_1 and σ_2 are estimated as 2.4x10^{-24} and 3.1x10^{-22} cm^2.
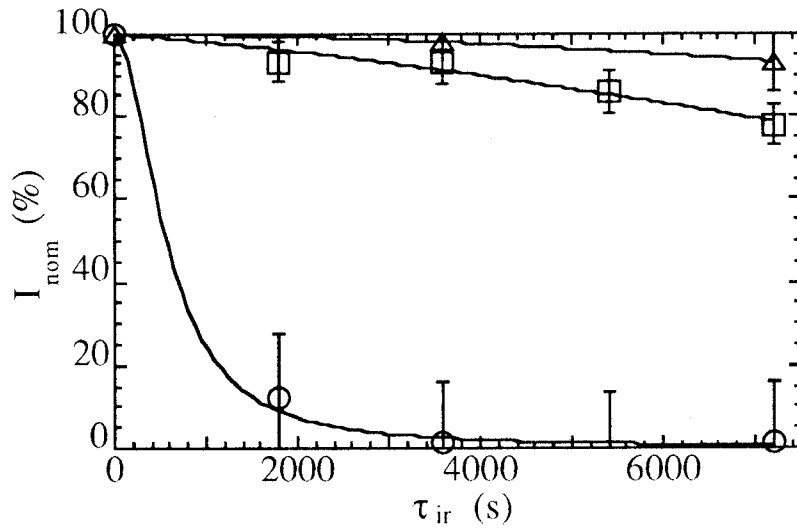
Fig. 3-5-4   Decrease of PL intensities I_{nom} at the wavelength of 565 (triangles), 725 (circles), and 820 nm (squares) vs. electron irradiation time τ_{ir}. The irradiation temperature is 90 K, and electron fluence f is 4.0x10^{18} cm^{-2} s^{-1}.
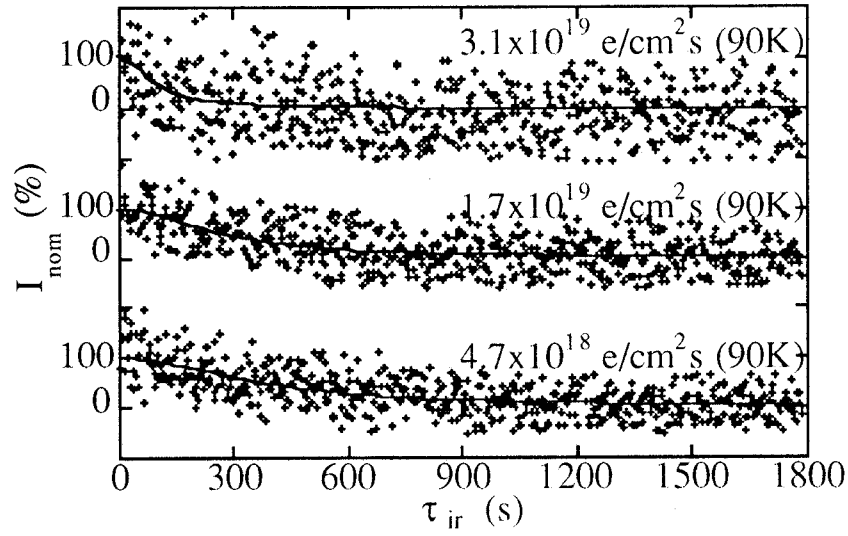
Fig. 3-5-5　Decrease of CL intensities I_{nom} at 725 nm at several electron fluences f as a function of irradiation time τ_{ir}.　Irradiation and observation temperatures are 90 K.
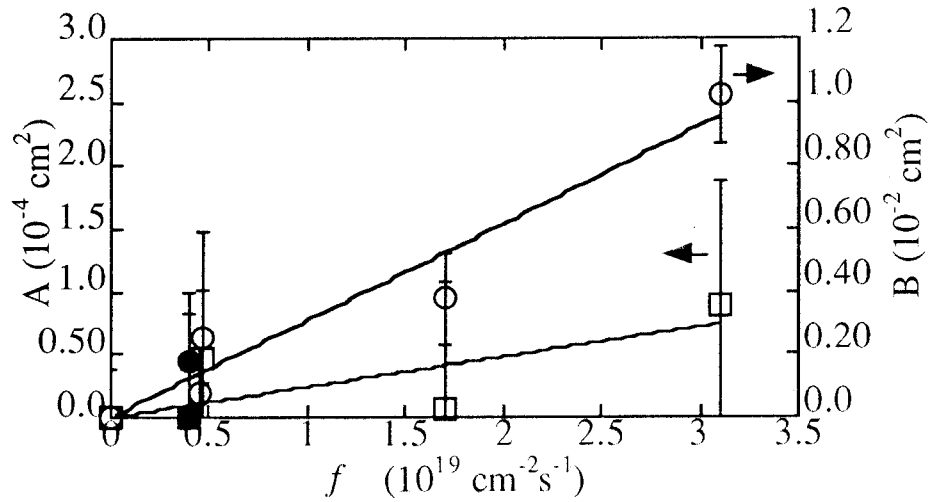

Fig. 3-5-6　Fitting parameters A (squares) and B (circles) for the emission at 725 nm vs. electron fluence f.　Irradiation and observation temperatures are 90 K.　The open and closed marks represent the result of CL and PL, respectively.

3-5-4 Irradiation effects on luminescence spectra at 20 K

Figure 3-5-7 shows the CL intensities at 725 nm as a function of τ_{ir}, normalized by the same way as in PL. Irradiation and spectroscopy were performed at 20 K with the three different fluxes $f = 4.7 \times 10^{18}$, 1.7×10^{19} and 3.1×10^{19} electrons cm^{-2} s^{-1}. I found that the CL intensity during irradiation at $\tau_{ir} = 20$ K almost remains the same, whereas, during irradiation at $T_{ir} = 90$ K, it decreases rapidly with irradiation time (Fig. 3-5-5). I also confirmed that the PL intensity at 20 K after irradiation is almost the same as one before irradiation.

Solid lines in Fig. 3-5-7 show the result for the fitting with Eq. 3-5-1. Figure 3-5-8 summarizes the fitting parameter A as a function of f. The value of the fitting parameter B was ignored within the experimental error. I found that the parameter A was in proportion to the flux, as similar as in Fig. 3-5-6. This indicates that $I_{nom}(t)$ observed at 20 K was also fitted with Eq. 3-5-2, and σ_1 and σ_2 were estimated as 2.9×10^{-24} and 0.0 cm^2, respectively.

The result shown in Fig. 3-5-8 obviously indicates that isolated interstitial atoms and isolated vacancies are introduced in a GaP specimen by an electron irradiation even at 20 K. Comparison of the results shown in Fig. 3-5-6 and 3-5-8 suggests that 1) complexes of point defects that cause the quadratic decrease of luminescence intensity with D are formed by an electron-irradiation at $T_{ir} = 90$ K, and 2) isolated interstitials and vacancies affect on the luminescence intensity even though the effect is much smaller than one for complexes.
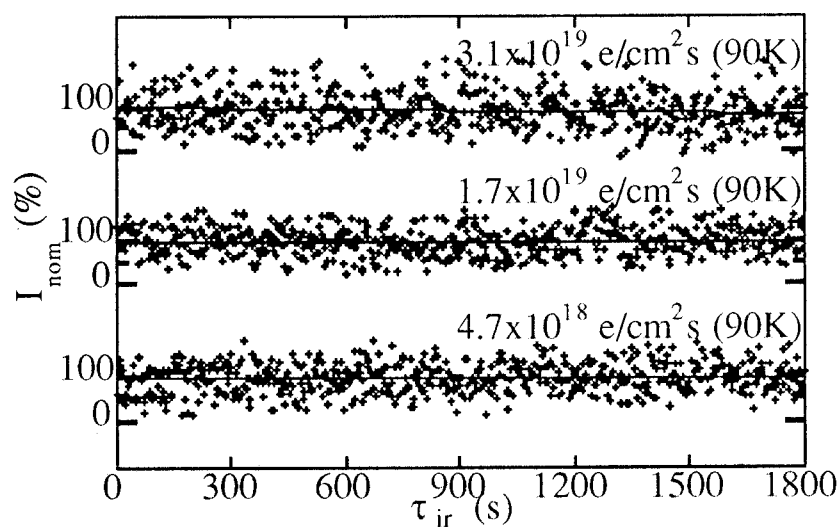
Fig. 3-5-7   Decrease of CL intensities I_{nom} at 725 nm at several electron fluences f as a function of irradiation time τ_{ir}.   Irradiation and observation temperatures are 20 K.
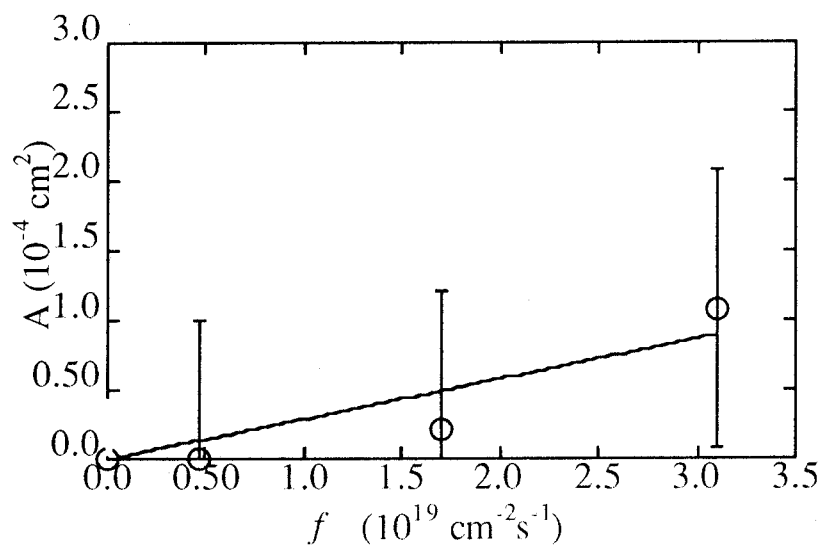

Fig. 3-5-8   Fitting parameters A for the emission at 725 nm vs. the flux of electron-beam f. Irradiation and observation temperatures are 20 K.

3-5-5 Annealing effects on luminescence spectra

I performed the next experiment in order to understand the phenomena and the nature of the complexes. 1) The specimen was irradiated at 20 K with $f = 4.7 \times 10^{18}$ electrons $cm^{-2}s^{-1}$ for 300 s. 2) CL was measured at 20 K immediately after irradiation. 3) It was then annealed at 90 K for 1800 s without electron-irradiation. 4) CL from the irradiated and subsequently annealed area was then measured at 20 K. The CL spectroscopy at 20 K does not affect luminescence intensity as I confirmed (Fig. 5). I found that the intensity at 725 nm after an annealing at 90 K decreases by 23 ± 5 %, compared with that before the annealing.

I next performed the other experiment. The specimen was annealed at 90 K under irradiation with the same flux and irradiation-time as above. I then measured the CL intensity at 725 nm immediately after the irradiation and annealing. I found that the intensity was weaker than that after only annealing at 90 K by 14 ± 5 %; the decrease rate of the CL intensity by the irradiation at 90 K is larger than one by the annealing at 90 K following an irradiation at 20 K, when the electron doses for an irradiation are the same.

3-6 Results of in-situ TEM-CL spectroscopy in GaInP

3-6-1 Irradiation effects on TEM data at 110 K

Figure 3-6-1(a) shows the TED pattern of GaInP taken with $E = 140$ kV; $f = 7.8 \times 10^{18}$ cm^{-2} s^{-1}. Ordered spot appeared from the two orientation variants of the CuPt-type ordered structure with ordered planes normal to [$\bar{1}11$] and [$1\bar{1}1$]. Figure 3-6-2(b) shows the intensities of the ordered spot as a function of D. The intensity remained constant during an electron irradiation with $E \leq 140$ keV; a result with $E = 140$ keV is shown in the figure. Noda and Takeda reported that the electron diffraction intensity of ordered spot decreases with electron irradiation when $E \geq 150$ keV {145}; the results with $E = 150$, 160, and 170 keV are also shown in Fig. 3-6-2(b). The decrease is explained as the disordering of the CuPt-type ordered structure in GaInP due to an atomic displacement at both the Ga- and In-sites {145}. The threshold electron energies for displacement of both Ga and In atoms are roughly estimated to be 150 kV {145}.

I performed TEM observation of an electron irradiated and annealed GaInP; a specimen was irradiated earlier with 200 keV electrons with $f = 4.7 \times 10^{18}$ electrons cm^{-2}s^{-1} for $\tau_{ir} = 5400$ s at $T_{ir} = 300$ K. I performed an annealing following the irradiation in the temperature range from 700 to 900 K, and found no defect contrast in the irradiated area. As shown in Sec. 2, dislocation loops in III-V compounds are formed by a thermal migration of III$_i$-V$_i$ interstitial pairs that are introduced by an electron irradiation. It is expected that Frenkel-type defects on Ga-, In- and P-site are introduced by the irradiation. Thus the result suggests that a) the interstitial pairs are not introduced by an electron irradiation in an ordered GaInP or b) the interstitial-pairs could not migrate in an ordered GaInP even though the pairs are introduced in the crystal.
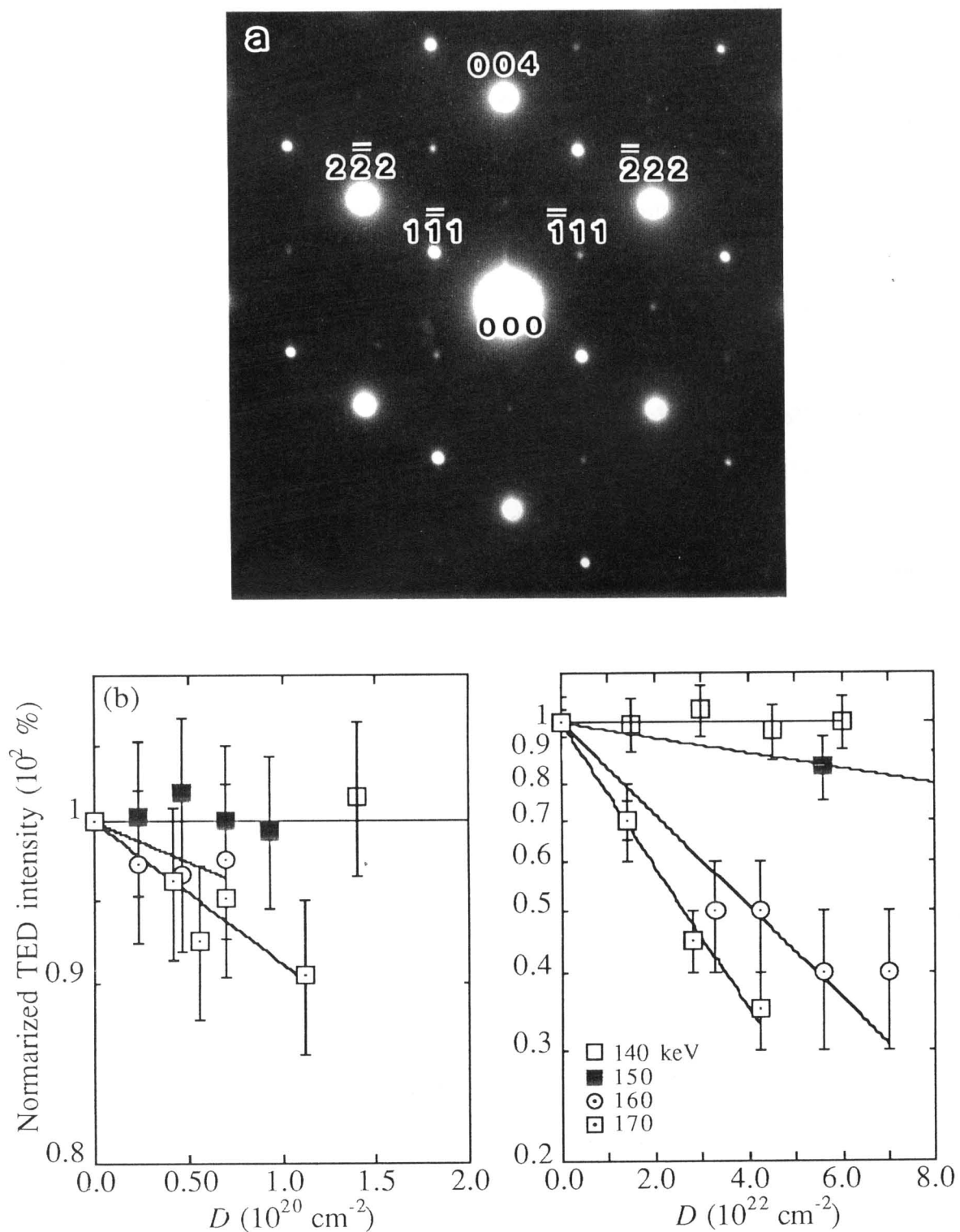
Fig. 3-6-2 (a) TED pattern taken with an electron energy $E = 140$ kV. (b) The electron diffraction intensity of an ordered spot vs. electron dose D. E for an irradiation are shown in the figure.

91

3-6-2 Irradiation effects on luminescence spectra at 110 K

Figure 3-6-2 depicts the change of CL spectra with an electron irradiation with $E = 130$ (a) and 170 keV (b), respectively. $f = 7.8 \times 10^{16}$ cm^{-2} s^{-1}, and τ_{ir} are depicted in the figure. In the observed spectral range, only one spectrum peaking at the wavelength near 650 nm was observed; recombination of electrons from the conduction band and holes in the valence band in GaInP with the Cu-Pt type ordered structure {178-180}. No new peaks were obtained after the irradiation. I found that the CL spectra do not change with an electron irradiation when $E \leq 120$ keV. I thus obtained all CL spectra with an electron beam with $E = 100$ keV to avoid irradiation effects. An effect of electron-irradiation with $E > 120$ keV was the decrease of the peak intensity, as similar as in GaP (see Sec. 3-5). Moreover, as shown in Fig. 3-6-3(b), the shape of CL spectra changed with an electron irradiation when $E \geq 150$ keV.
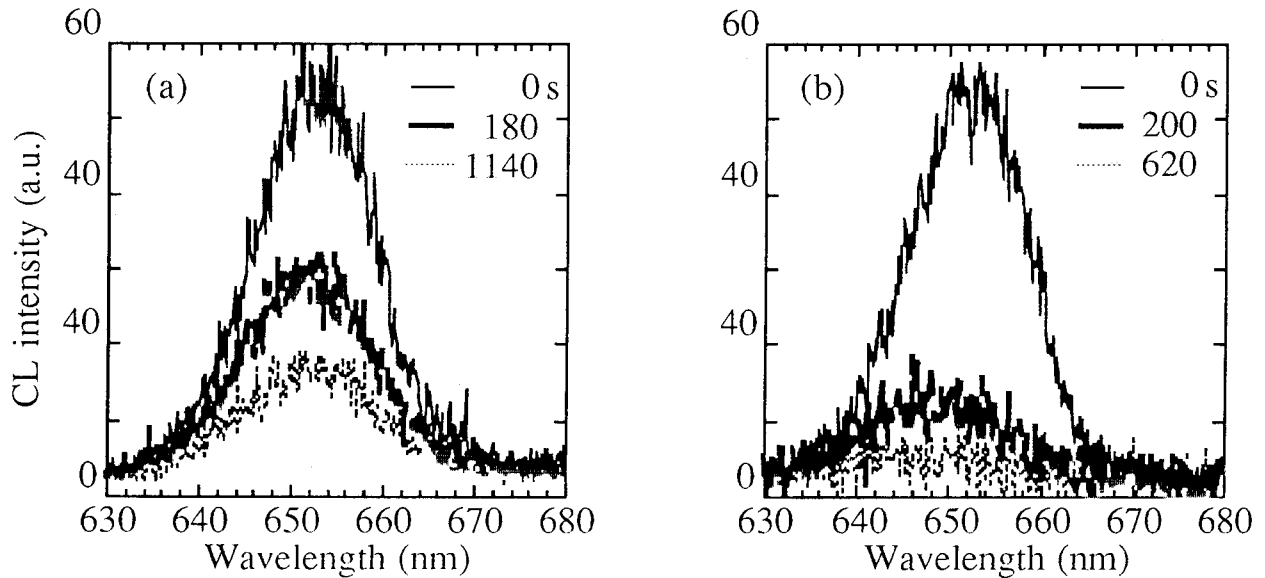
Fig. 3-6-2   CL spectra of electron-irradiated GaInP with the CuPt-type ordered structure. Specimens are irradiated with a flux of 7.8×10^{16} electrons cm^{-2} s^{-1} at 110 K for a period represented in the figure. The electron energies are (a) 130, (b) 170 keV, respectively.

3-6-2-1 Irradiation effects on CL intensities

Figure 3-6-3 shows the variation of the peak intensities of CL spectra with several τ_{ir} and E. $f = 1.96 \times 10^{16}$ (open triangles), 4.7×10^{16} (open squares), and 7.8×10^{16} (open circles) $cm^{-2} s^{-1}$. The intensity, I_{nom} was normalized with Eq. 3-5-1. As shown in the figure, I_{nom} remained constant with D when $E = 120$ keV. Above 130 keV electron irradiation, I_{nom} decreased with D, and the rate of the decrease was fast when E is a large value. Since the intensity decreased rapidly, I could not observe the change of the CL intensity quantitatively when $E > 170$ keV. I found that CL intensities with $E > 120$ keV are well fitted with the same function,

$$I_{nom} = \frac{100}{1 + \sigma_1 D},$$
(3-6-1)

where σ_1 is a constant to fit for each spectrum. The fittings are shown by the solid lines in Fig. 3-6-3. The changes of the value σ_1 with E are summarized in Fig. 3-6-4. $\sigma_1 = 0$ when $E \leq 120$ keV, and it increased with an electron energy when $E > 120$ keV.

3-6-2-2 Irradiation effects on peak energies

Figure 3-6-5 shows the shifts of the CL peak energy ΔE_{peak} with D in the energy range of E from 120 to 170 keV. ΔE_{peak} were estimated with the following function,

$$\Delta E_{peak} = E_{peak}(D) - E_{peak}(0),$$
(3-6-2)

where $E_{peak}(D)$ represents the peak energy of the CL spectra after an electron irradiation with D. When E was below 150 keV, the value of ΔE_{peak} unchanged with D. ΔE_{peak} increased with D when $E \geq 150$ keV. The rate of the increase depended on E; when an electron energy was high, the rate was fast.
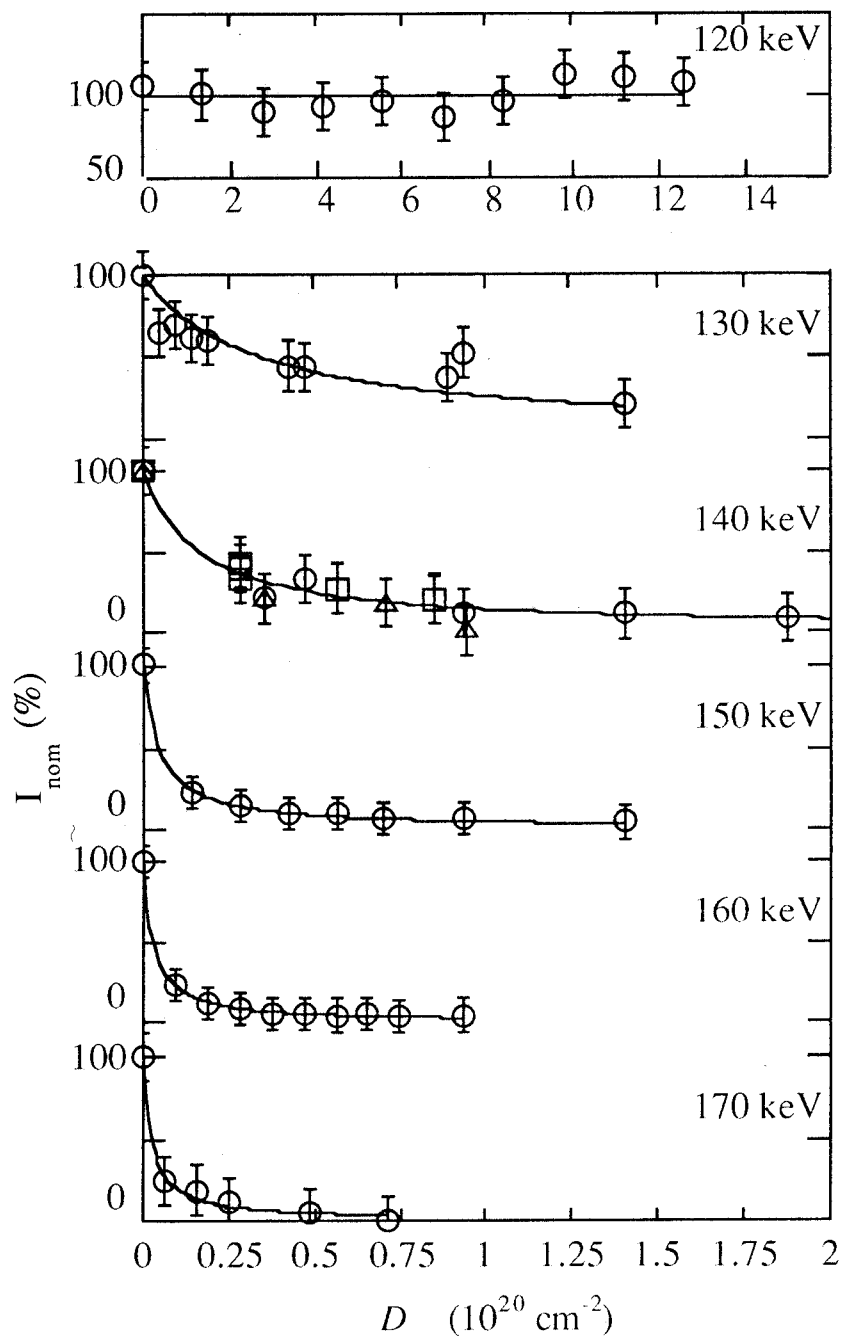
Fig. 3-6-3 Decrease of CL peak intensities I_{nom} by electron irradiation with several electron energies E vs. electron dose D. Irradiation temperature is 110 K.
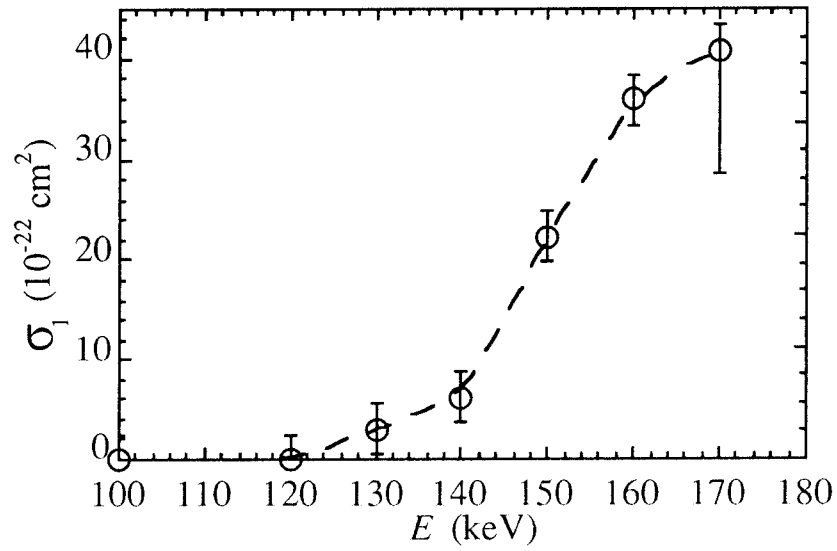
Fig. 3-6-4   Fitting parameter σ_1 vs. electron energies E.   Irradiation temperature T_{ir} is 110 K.
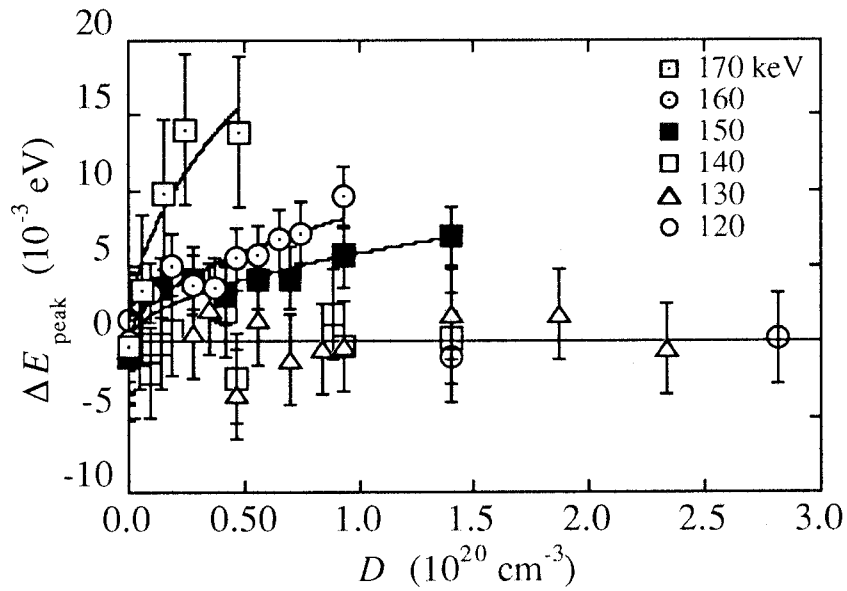

Fig. 3-6-5   Shift of the peak energies of CL spectra ΔE_{peak} with electron doses D.   The electron energies E for an irradiation are shown in the figure.

3-7 Discussion

3-7-1 Recombination model based on defect-induced energy levels

The normalized luminescence intensities in GaP and GaInP decreased with electron-irradiation. I found that the decreases of luminescence intensities for GaP and GaInP are well described in Eqs. 3-5-2 and 3-6-2, respectively. For understanding these phenomena quantitatively, I consider an energy-levels system; co-existence of intrinsic luminescence centers and non-radiative recombination centers that are introduced during electron irradiation. Some of carriers, i.e. electrons and holes exited by a laser- or an electron-beam, are trapped into the i-th luminescence centers in the probabilities $P_r(i)$, whose transitions are accompanied by emission of light. The other carriers are trapped into the j-th non-radiative recombination centers in the probability $P_D(j)$, which does not emit light. The probabilities, $P_r(i)$ and $P_D(j)$, are expressed as {159}

$$P_r(i) = \sigma_r(i)N_r(i)v, \tag{3-7-1}$$

$$P_D(j) = \sigma_D(j)N_D(j)v, \tag{3-7-2}$$

where $\sigma_r(i)$ denotes the transition coefficient for carriers becoming trapped in the i-th luminescence centers, $N_r(i)$ the concentration of the centers and v the carrier velocity. $\sigma_D(j)$ and $N_D(j)$ represent the transition coefficient for carriers becoming trapped in the j-th non-radiative recombination centers and the concentration of the centers, respectively.

In GaP, $\sigma_D(j)$ is usually much larger than $\sigma_r(i)$ {161}. Suppose $P_D(j) \gg P_r(i)$, i.e. $N_D(j) \geq N_r(i)$. This is a realistic assumption under an electron irradiation, since the concentration of existing point defects (about 10^{19} cm^{-3}) is larger than that of intrinsic impurities (about 10^{18} cm^{-3}). Accordingly, the luminescence center traps the carriers that are excited

near it. Most of carriers are trapped into the non-radiative recombination centers. Therefore the luminescence efficiency of the i-th luminescence center, $\eta(i)$, is independent of the trap-probabilities of the other luminescence centers. In GaInP, I found only one luminescence center in the observed spectral range. Therefore, $\eta(i)$ is written as

$$
\eta(i) = \frac{P_{\mathrm{r}}(i)}{P_{\mathrm{r}}(i) + \sum_j P_{\mathrm{D}}(j) + P_{\mathrm{nr}}}
$$

$$
= \frac{1}{1 + \dfrac{\sum_j \sigma_{\mathrm{D}}(j) N_{\mathrm{D}}(j) + P_{\mathrm{nr}}}{\sigma_{\mathrm{r}}(i) N_{\mathrm{r}}(i)}} \quad , \tag{3-7-3}
$$

where P_{nr} represents the probability of non-radiative recombination due to electron-phonon interactions. i represents luminescence centers peaking at 565, 725 and 850 nm for GaP, and about 650 nm for GaInP, respectively. Since the temperature was kept at a low constant (less than 110 K) during PL and CL measurements, P_{nr} remained a small constant. The concentration of non-radiative recombination centers, $N_{\mathrm{D}}(j)$ increases with an electron-irradiation. The observable intensity of PL and CL emission is proportional to $\eta(i)$. The normalized luminescence intensity is, therefore, rewritten as the following equation,

$$
I(i) = \frac{100 \cdot \eta(i)}{\eta_0}
$$

$$
= \frac{100}{1 + \dfrac{\sum_j \sigma_{\mathrm{D}}(j) N_{\mathrm{D}}(j)}{\{\sigma_{\mathrm{r}}(i) N_{\mathrm{r}}(i) + P_{\mathrm{nr}}\}}} \quad , \tag{3-7-4}
$$

where η_0 represents the luminescence efficiency without non-radiative recombination centers; i.e., luminescence efficiency before an electron-irradiation.

3-7-2 Interpretation of the experimental results

3-7-2-1 Onset temperature for the migration of interstitials in GaP

The decrease of PL and CL intensity in the irradiated area was quite small after an electron-irradiation at $T_{ir} = 20$ K; the intensity almost remained the same during an irradiation (Fig. 3-5-7). Even at this temperature, Frenkel-type defects are introduced in a specimen, and the concentration of the defects is expected to more than 10^{18} cm^{-3}. These results indicate that the effect of Frenkel-type defects on the optical properties in GaP is quite small; the transition coefficient σ_D for Frenkel-type defects is small.

The luminescence intensity, however, decreased by the subsequent annealing at $T_{an} = 90$ K without electron-irradiation following an electron-irradiation at $T_{ir} = 20$ K. In the temperature range from 20 to 90 K, no extended defects like a dislocation loop were created by electron irradiation. The experimental evidence implies that complexes were formed at $T_{an} = 90$ K due to a thermal migration of point defects, which are introduced by an electron-irradiation at $T_{ir} = 20$ K. So far, there is no direct information on kinetics of point defects in GaP at the temperature below 100 K. Some data are available in InP and GaAs, which are also the III-V compound semiconductors. A Huang x-ray diffuse scattering (HDS) experiment of InP and GaAs, irradiated by electrons at 4.7 K, shows that Frenkel defects are stable up to 120 K in InP and 200 K in GaAs {60}. The temperatures are the onset of interstitial migration, since it is generally accepted that vacancies in the compounds are immovable below room temperature {60}. The studies by ESR {9}, DLTS {10}, and PAS {11-13, 15-17} of GaP show that vacancies at Ga or P sites are immobile below 600-900 K, similar to InP and GaAs. The general behaviors of point defects upon annealing are thought to be similar in III-V compound semiconductors. With the data in hand, I explained my results as follows. 1) Frenkel-type defects, introduced in GaP by electron-irradiation at $T_{ir} = 20$ K, are no longer frozen in the temperature range between 20 K and 90 K. 2) Thermal migration of isolated interstitials results in a formation of complexes.

3-7-2-2 Formation of interstitial-related complexes in GaP

As shown in Sec. 3-5, I_{nom} in GaP was well fitted with Eq. 3-5-2. Since σ_1 is much smaller than σ_2 at 90 K, I_{nom} is approximately rewritten as,

$$I_{nom} = \frac{100}{1 + (\sigma_2 D)^2} \quad .$$

(3-7-5)

Based on the model of Eq. 3-7-4, either the increase of $N_D(j)$ or the decrease of $N_r(i)$ causes the decreases of the luminescence intensities. Suppose $N_D(j)$ remains constant. All the $N_r(i)$s must be inversely proportional to the square of D, since I observed that the three kinds of the luminescence intensities decrease in the same manner as described in Eq. (3-5-2). This is very rarely expected. The observed decrease is more simply accounted for if $N_D(j)$ increases with τ_{ir} under the condition that all the $N_r(i)$s kept constant; i.e. complexes that cause the decrease of luminescence intensities are formed in a second order reaction. The different rates of the decreases are due to the different $\sigma_r(i)N_r(i)$ values.

According to the analysis above, the fact that the migration of interstitial atoms at 90 K gives rise to a non-radiative recombination center formed in a second order reaction, indicating that the center should be associated with anti-site defects (P_{Ga} and Ga_P), interstitial pairs (Ga_i-P_i), or interstitial-vacancy pairs (V_{Ga}-Ga and V_P-P_i). In the present study, a specimen was irradiated with $D \gg 10^{19}$ cm^{-2}. It is known that the concentrations of P_{Ga} and Ga_P introduced by electron irradiation approach to a maximum value of about 10^{17} cm^{-3} when $D \geq 10^{18}$ {32, 181} and 4×10^{18} {31} cm^{-2}, respectively. Thus the change of the concentration of anti-site defects with D is approximately ignored.

The decrease of luminescence intensity was also observed in a specimen that was annealed at T_{an} = 90 K without electron irradiation following electron irradiation at T_{ir} = 20 K. As shown in Sec. 2, Ga_i-P_i interstitial-pairs were introduced only during electron irradiation,

99

and they did not introduced during electron irradiation at T_{ir} = 20 K since σ_2=0 at 20 K.

From the result, it is considered that the decrease of luminescence intensity after T_{an} = 90 K

annealing following an electron-irradiation at T_{ir} = 20 K caused by complexes associated with

interstitial-vacancy pairs, that are formed by thermal migration of Ga_i and/or P_i introduced by

electron irradiation. An introduction of such defects was observed by DLTS {20, 21}; the E

centers in an electron irradiated GaP are proposed to associate P_i interstitials located at

different distances from V_p.

As shown in Sec. 3-5-5, when D was the same, the decrease of luminescence intensity

after an electron-irradiation at T_{an} = 90 K was larger than that after annealing at T_{an} = 90 K

following an electron-irradiation at T_{ir} = 20 K. Since D in the two kinds of experiments were

set at the same value, the same numbers of displacement events must occurred. As I showed,

Ga_i-P_i interstitial-pairs were introduced only during electron-irradiation at above 90 K. The

concentration of the pairs increased with electron doses even when D was more than 10^{23}

cm^{-2}, and the concentration (about 10^{19} cm^{-3}) was much higher than that of anti-site defects

(about 10^{17} cm^{-3}). The onset temperature for the migration of the pairs was estimated to be

about 530 K, and the temperature was the same as one of an annealing stage in electron-irradiated

GaP. Hence the results suggest that Ga_i-P_i interstitial-pairs, that are introduced in a second

order reaction only during electron-irradiation, might cause the decrease of luminescence

intensities. Another possibility for the decrease during an irradiation at T_{ir} = 90 K is due to

the electron-irradiation enhanced defect-migration: the migration of point defects, probably

giving rise to the formation of complexes, is more promoted under electron-irradiation than

annealing without electron-irradiation. Such an effect was suggested by Corbett and Bourgoin

{182} and Afanas'ev et al {183}, and was observed in GaAs {184-186} and GaP {187}.

3-7-2-3   Formation of Frenkel-type defects in GaInP

As shown in Sec. 3-6, $I_{nom}(t)$ in GaInP was written as,

$$I_{nom}(t) = \frac{100}{1 + \sigma_1 D} .$$

$\qquad\qquad$ (3-7-6)

Based on the model of Eq. 3-7-4, either the increase of $N_D(j)$ or the decrease of $N_r(i)$ causes the decreases of the luminescence intensities. Since $N_r(i) \gg N_D(j)$ for GaInP, the change of N_r during irradiation can be ignored. We thus concluded that the observed decrease of the CL intensity is due to the formation of non-radiative recombination centers formed in a first order reaction; i.e., the formation of Frenkel-type defects. The formation of the defects is suggested with DLTS results in 1 MeV-electron irradiated GaInP {188, 189}.

When the value of an electron dose D is small, the concentration of Frenkel-type defects is approximately in proportion to D. Suppose all the Frenkel-type defects on j-th atomic site introduced by an irradiation behave as a non-radiative recombination center. The concentration of the non-radiative center $N_D(j)$ is written as,

$$N_D(j) = \alpha_{FP}(j) \cdot D,$$

$\qquad\qquad$ (3-7-7)

where $\alpha_{FP}(j)$ represents the introduction rate of Frenkel-type defects on j-th atomic site ($j =$ Ga, In, P). Thus Eq. 3-7-4 is rewritten as,

$$I(i) = \frac{100}{1 + \dfrac{\sum_j \sigma_D(j) \cdot \alpha_{FP}(j)}{\{\sigma_r(i)N_r(i) + P_{nr}\}} D}$$
$$\equiv \frac{100}{1 + \sum_j \gamma(j) \cdot \alpha_{FP}(j) \cdot D}$$

$\qquad\qquad$ (3-7-8)

Solid lines in Fig. 3-7-1 represent the best fitting with the equation; in the fitting, I assume that the threshold electron energies for the displacement of Ga, In, and P atoms are 140, 120,

and 100 keV, respectively. The values of $\alpha_{FP}(j)$ s are estimated with Eqs. 2-5-5 and 2-5-6 (broken and dotted lines in the figure). $\gamma(j)$ for Ga, In, and P sites are roughly estimated to be 3.0×10^{-19}, 5.6×10^{-20}, and 0.0×10^{-20} cm^3, respectively.

I could not obtain the evidence for the formation of defect complexes formed by second- or higher-order reactions. As shown in Sec. 3-6-1, I could not observe the formation of interstitial agglomerates in the electron-irradiated and annealed GaInP. According to my model shown in Sec. 2, interstitial agglomerates are formed through the migration of III_i-V_i interstitial-pairs. Thus the CL result is consistent of the TEM results; in GaInP with the Cu-Pt ordered structure, interstitial-pairs are scarcely introduced by electron irradiation.
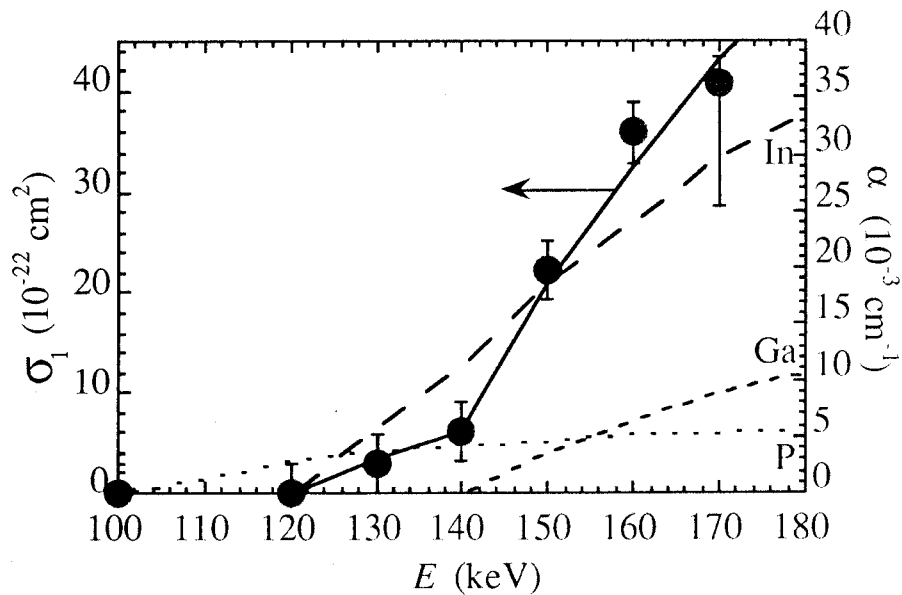
Fig. 3-7-1 Fitting parameter σ_1 vs. electron energy E. Solid line represents the variation of the simulated parameter σ_1. The threshold electron energies for the displacement of Ga, In, and P atoms in the simulation are 140, 120, and 100 keV, respectively. The estimated introduction rates α for Frenkel-type defects on Ga, In, and P sites are also shown in the figure (broken and dotted lines).

3-7-2-4 *Phase transformation due to electron irradiation in GaInP*

I observed the peak-shift of the CL spectra to a higher value with an electron irradiation with $E \geq 150$ keV, and the shift was not explained by the model of Eq. 3-7-4. The TED measurements with several E indicate that the electron irradiation with $E \geq 150$ keV causes the disordering of the Cu-Pt type ordered structure in GaInP {145}. The peak energy of the CL spectra in GaInP is approximately the same as the band-gap energy, since the luminescence causes by the recombination of electrons from the conduction band and holes in the valence band. From a theoretical result {190}, it is expected that the energy gap between the conduction and valence bands in an ordered GaInP changes to a wider value with increasing the degree of disordering. In *Ex-situ* PL measurements, the shift of the PL peak energy in GaInP/AlGaInP heterostructures by annealing at the temperature above 800 °C was reported {191}, and the peak shift was explained as the disordering of ordered structure due to an atomic displacement at both the Ga and In sites; self diffusion of both Ga and In atoms {192}. The change of PL peak energy in GaInP depending on a growth temperature and substrates is also explained as the effect of the formation of the CuPt-type ordered structure in the crystal {193-198}. The peak shift observed by *in-situ* CL measurements is, therefore, due to the change of atomic structure through a disordering; the change of the electronic structure due to the phase transformation from the CuPt-type ordered structure to a disordered one through a migration of both Ga- and In-atoms under an electron irradiation.

3-7 Conclusion

I have investigated electron-irradiation-effects in GaP and GaInP. In GaP, the CL and PL intensities measured at the wavelength of 565, 725 and 850 nm almost remained the same during electron-irradiation at 20 K. However, I found that these intensities decrease by the subsequent annealing at 90 K. I also found that the luminescence intensity measured at 90 K under electron-irradiation decreases with electron-doses. From the results, I concluded as follows; 1) Frenkel-type defects, introduced in GaP crystal by an electron-irradiation at 20 K, are no longer frozen in the temperature range between 20 K and 90 K. 2) Above 90 K, interstitial atoms can migrate and form the complexes associated with non-radiative recombination center in a second order reaction. 3) The complexes should be interstitial-vacancy pairs (Ga_i-V_{Ga} and P_i-V_P) and Ga_i-P_i interstitial-pairs introduced by electron-irradiation.

The decrease of CL intensities was also observed in GaInP with the CuPt-type ordered structure, and the decrease was well explained as the introduction of non-radiative recombination centers due to the formation of Frenkel-type defects. In GaInP, Frenkel-type defects strongly affect on the optical properties in the crystal, and I could not confirm the formation of defect complexes. When an electron energy was above 140 keV, I also found a shift of the peak energy of CL spectra with electron irradiation; the shift was due to the disordering of the CuPt-type ordered structure in GaInP through the migration of both Ga and In atoms. From the analyses of the decrease-rate, I estimated the threshold electron energies for the displacement of Ga and In atoms to be 140 and 120 keV, respectively.

4 Conclusion and summary

I found that dislocation loops of interstitial-type are introduced in GaP, InP, and GaAs by an annealing following an electron irradiation; the loops are formed by thermal migration of interstitial atoms introduced by electron irradiation. In order to understand the kinetics of the defect, I have systematically examined the growth of the loops by *in-situ* transmission electron microscopy (TEM). The loops were formed by an annealing at the temperature above 700 K for GaP and InP, and above 800 K for GaAs following an electron irradiation. When the irradiation conditions (an electron dose and an irradiation temperature) were fixed, the number density of the loops depended on annealing temperatures; the logarithms of the densities were in proportion to the reciprocal of annealing temperature. The size of the loops increased with annealing time and then reached a final value when the growth of the loops stopped. The number density of interstitial atoms aggregated in the loops, therefore, reached a maximum value after stopping the growth. The maximum density depended on not annealing temperature but irradiation condition, and it increased quadratically with electron doses. The experimental results were well explained with a new model that the loops were formed through the thermal migration of III_i-V_i interstitial-pairs that were introduced during electron irradiation. From the analysis, I estimated the migration energies for Ga_i-P_i pairs in GaP and In_i-P_i pairs in InP to be 0.9 and 1.5 eV, respectively. The onset temperatures for the migration of Ga_i-P_i pairs in GaP and In_i-P_i pairs in InP are about 530 and 550 K.

I also investigated electron-irradiation-induced defects in GaP and GaInP introduced during an electron irradiation at low temperatures, which are hardly observable by TEM. In order to investigate the defects, I accomplished the *in-situ* TEM-PL/CL observation apparatus, which enables me to obtain simultaneously TEM images and photoluminescence (PL) / cathodoluminescence (CL) spectra. With the apparatus, I found that the luminescence

4 Conclusion and summary

I found that dislocation loops of interstitial-type are introduced in GaP, InP, and GaAs by an annealing following an electron irradiation; the loops are formed by thermal migration of interstitial atoms introduced by electron irradiation. In order to understand the kinetics of the defect, I have systematically examined the growth of the loops by *in-situ* transmission electron microscopy (TEM). The loops were formed by an annealing at the temperature above 700 K for GaP and InP, and above 800 K for GaAs following an electron irradiation. When the irradiation conditions (an electron dose and an irradiation temperature) were fixed, the number density of the loops depended on annealing temperatures; the logarithms of the densities were in proportion to the reciprocal of annealing temperature. The size of the loops increased with annealing time and then reached a final value when the growth of the loops stopped. The number density of interstitial atoms aggregated in the loops, therefore, reached a maximum value after stopping the growth. The maximum density depended on not annealing temperature but irradiation condition, and it increased quadratically with electron doses. The experimental results were well explained with a new model that the loops were formed through the thermal migration of III_i-V_i interstitial-pairs that were introduced during electron irradiation. From the analysis, I estimated the migration energies for Ga_i-P_i pairs in GaP and In_i-P_i pairs in InP to be 0.9 and 1.5 eV, respectively. The onset temperatures for the migration of Ga_i-P_i pairs in GaP and In_i-P_i pairs in InP are about 530 and 550 K.

I also investigated electron-irradiation-induced defects in GaP and GaInP introduced during an electron irradiation at low temperatures, which are hardly observable by TEM. In order to investigate the defects, I accomplished the *in-situ* TEM-PL/CL observation apparatus, which enables me to obtain simultaneously TEM images and photoluminescence (PL) / cathodoluminescence (CL) spectra. With the apparatus, I found that the luminescence

5 Acknowledgments

5 Acknowledgments

Fig. 6-1-a   Variation of the simulated final density $C_{IL}(\infty)$ with several electron doses D and production rate of Frenkel defects P. $P(Ga) = P(P)$ is assumed, and $P(P)$ in the computations are written in the figure.

Fig. 6-1-b   Variation of the simulated final density $C_{IL}(\infty)$ with several electron doses D and production rate of Frenkel defects P. $P(Ga) = 10^6 \ s^{-1}$ is assumed, and $P(P)$ in the computations are written in the figure.
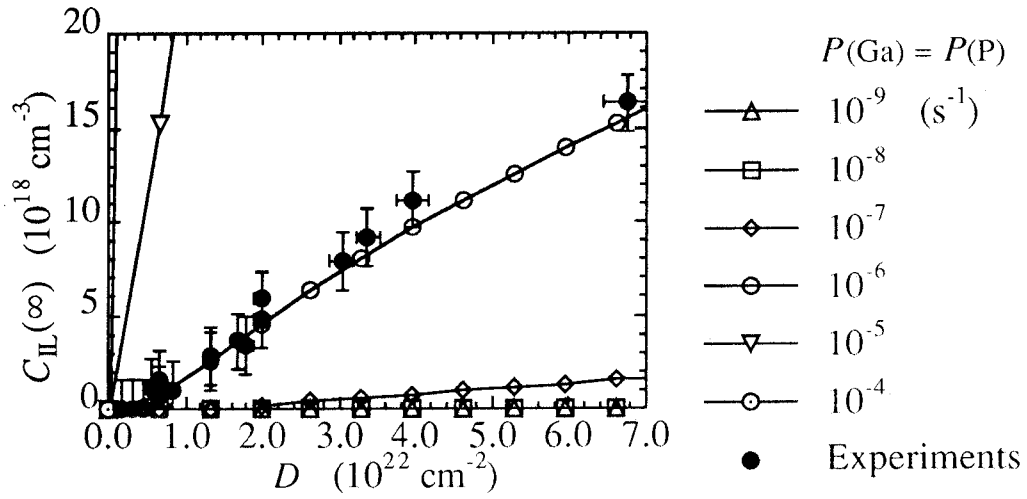
Fig. 6-1-a Variation of the simulated final density $C_{IL}(\infty)$ with several electron doses D and production rate of Frenkel defects P. $P(Ga) = P(P)$ is assumed, and $P(P)$ in the computations are written in the figure.
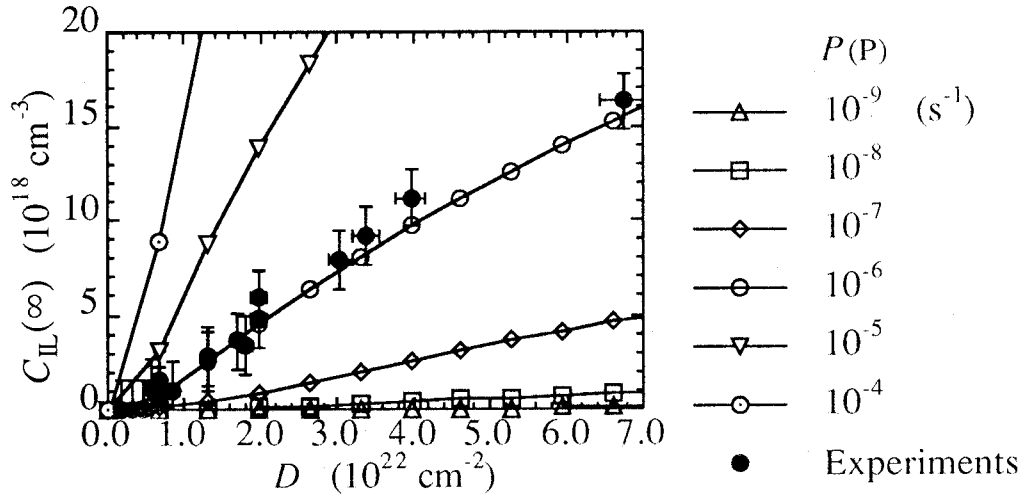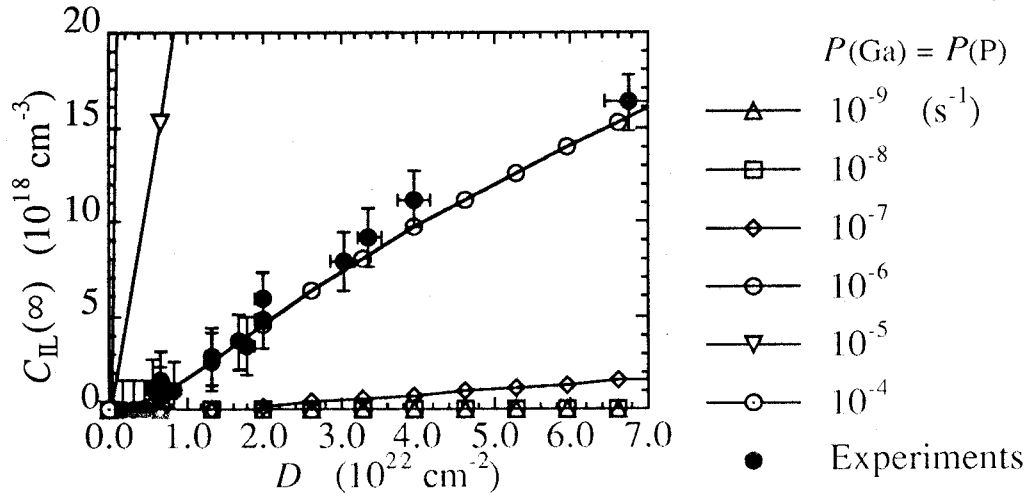

Fig. 6-1-b Variation of the simulated final density $C_{IL}(\infty)$ with several electron doses D and production rate of Frenkel defects P. $P(Ga) = 10^6$ s^{-1} is assumed, and $P(P)$ in the computations are written in the figure.

Fig. 6-3-a Variation of the simulated final density $C_{IL}(\infty)$ with several electron doses D and capture-site number for recombination-annihiration of interstitials Z. $Z(Ga) = Z(P)$ is assumed, and $Z(P)$ in the computations are written in the figure.

Fig. 6-3-b Variation of the simulated final density $C_{IL}(\infty)$ with several electron doses D and capture-site number for recombination-annihiration of interstitials Z. $Z(Ga) = 10^2$ is assumed, and $Z(P)$ in the computations are written in the figure.

Fig. 6-3-a Variation of the simulated final density $C_{IL}(\infty)$ with several electron doses D and capture-site number for recombination-annihiration of interstitials Z. $Z(Ga) = Z(P)$ is assumed, and $Z(P)$ in the computations are written in the figure.
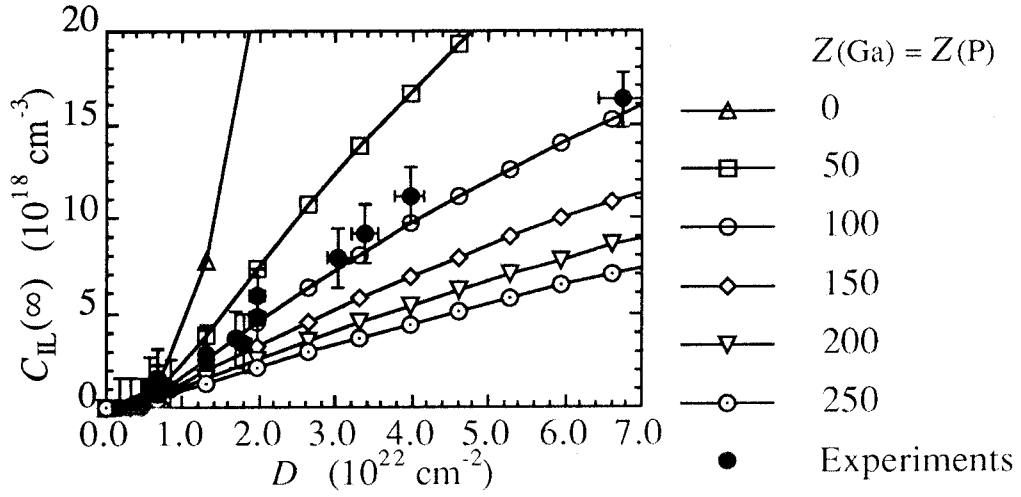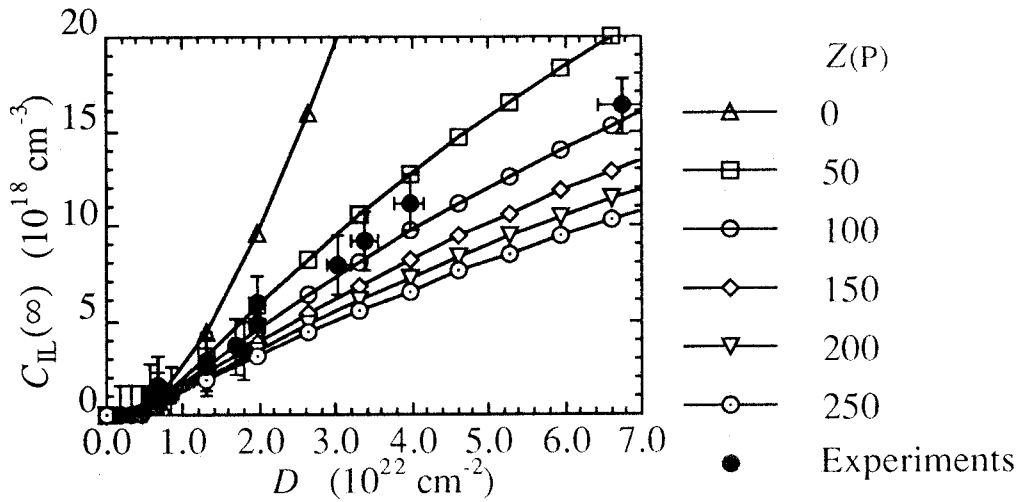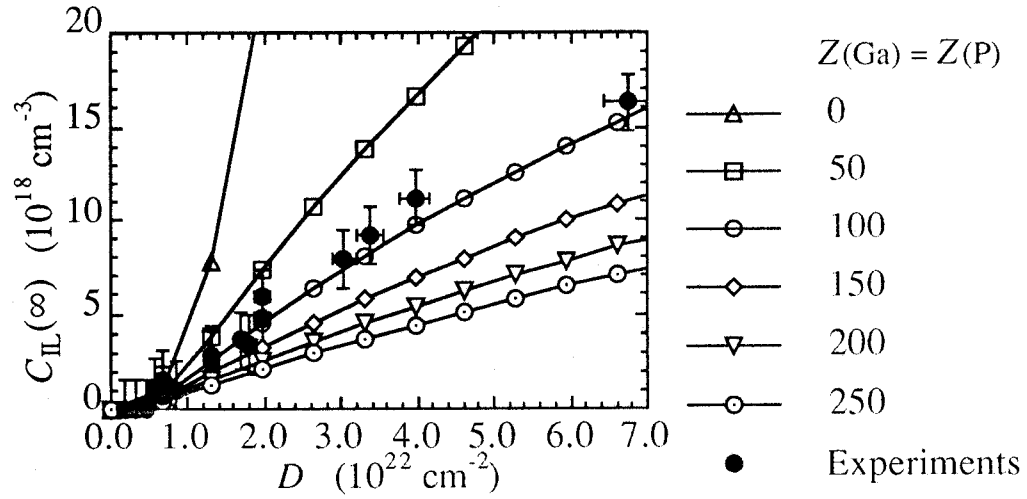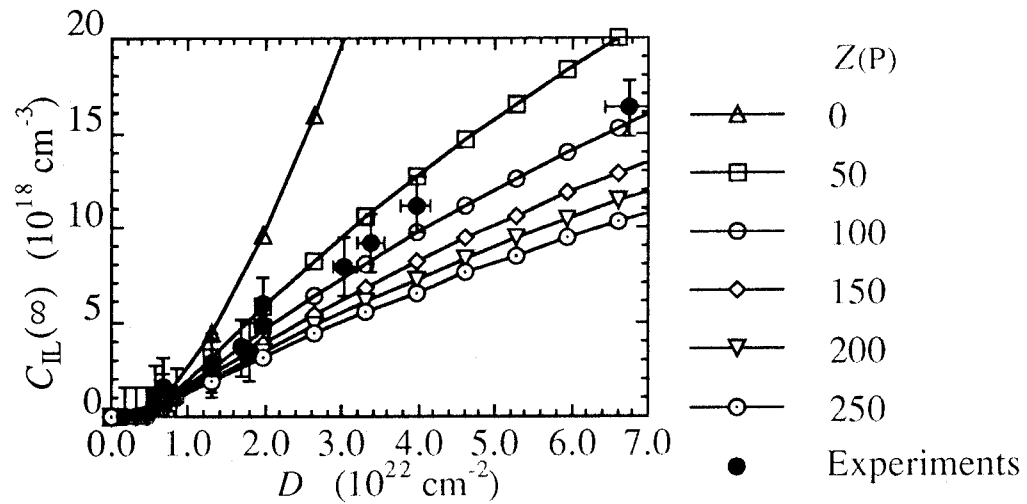

Fig. 6-3-b Variation of the simulated final density $C_{IL}(\infty)$ with several electron doses D and capture-site number for recombination-annihiration of interstitials Z. $Z(Ga) = 10^2$ is assumed, and $Z(P)$ in the computations are written in the figure.

7 References

{1}   For a review, D. V. Lang, Inst. Phys. Conf. Ser. **31**, 70 (1977)

{2}   J. W. Corbett and J. C. Bourgoin, in *Point Defect in Solids 2*, ed. J. H. Crawford Jr and L. M. Slifkin (Plenum, New York, 1975), p. 1

{3}   L. W. Aukerman, in *Semiconductors and Semimetals 4*, ed. K. Willardson and A. C. Beer (Academic Press, New York, 1968), p. 343

{4}   F. H. Eisen, in *Radiation Effects in Semiconductors* (Gordon and Breach, New York, 1971)

{5}   T. A. Kennedy and N. D. Wilsey, Phys. Rev. Lett. **41**, 977 (1978)

{6}   T. A. Kennedy and N. D. Wilsey, Phys. Rev. **B23**, 6585 (1981)

{7}   T. A. Kennedy, N. D. Wilsey, J. J. Krebs, and G. H. Stauss, Phys. Rev. Lett. **50**, 1281 (1978)

{8}   M. Scheffler, J. Bernholc, N. O. Lipari, and S. T. Pantelides, Phys. Rev. **B29**, 3269 (1983)

{9}   P. M. Moony, T. A. Kennedy, and M. B. Small, Physica **116B**, 431 (1983)

{10}   P. M. Moony and T. A. Kennedy, J. Phys. C: Solid State Phys. **17**, 6277 (1984)

{11}   V. N. Brudnyi, S. A. Vorobiev, A. A. Tsoi, and V. I. Shahovtsov, Radiation Effects **79**, 123 (1983)

{12}   F. Dominguez-Adame, J. Piqueras, N. de Diego and P. Moser, Solid State Commun. **67**, 665 (1988)

{13}   R. Sommerfeldt, L. Holtmann, E. Krätzig, and B. C. Grabmaier, Phys. Stat. Sol. **A106**, 89 (1988)

{14}   P. Hautojärvi, P. Moser, M. Stucky, C. Corbel, and F. Plazaola, Appl. Phys. Lett. **48**, 809 (1986)

{15}   G. Dlubek, O. Brümmer and A. Polity, Appl. Phys. Lett. **49**, 385 (1986)

{16}   A. Polity, Th. Abgarjan, and R. Krause-Rehberg, Appl. Phys. **A60**, 541 (1995)

{17}   S. Dannefaer and D. Kerr, Phys. Rev. **B50**, 14096 (1994)

{18}   J. A. Van Vechten, J. Electron. Mat. **4**, 1159 (1975)

{19}   M. J. Puska, J. Phys.: Condens. Matter **1**, 7347 (1989)

7 References

{1}   For a review, D. V. Lang, Inst. Phys. Conf. Ser. **31**, 70 (1977)

{2}   J. W. Corbett and J. C. Bourgoin, in *Point Defect in Solids 2*, ed. J. H. Crawford Jr and L. M. Slifkin (Plenum, New York, 1975), p. 1

{3}   L. W. Aukerman, in *Semiconductors and Semimetals 4*, ed. K. Willardson and A. C. Beer (Academic Press, New York, 1968), p. 343

{4}   F. H. Eisen, in *Radiation Effects in Semiconductors* (Gordon and Breach, New York, 1971)

{5}   T. A. Kennedy and N. D. Wilsey, Phys. Rev. Lett. **41**, 977 (1978)

{6}   T. A. Kennedy and N. D. Wilsey, Phys. Rev. **B23**, 6585 (1981)

{7}   T. A. Kennedy, N. D. Wilsey, J. J. Krebs, and G. H. Stauss, Phys. Rev. Lett. **50**, 1281 (1978)

{8}   M. Scheffler, J. Bernholc, N. O. Lipari, and S. T. Pantelides, Phys. Rev. **B29**, 3269 (1983)

{9}   P. M. Moony, T. A. Kennedy, and M. B. Small, Physica **116B**, 431 (1983)

{10}   P. M. Moony and T. A. Kennedy, J. Phys. C: Solid State Phys. **17**, 6277 (1984)

{11}   V. N. Brudnyi, S. A. Vorobiev, A. A. Tsoi, and V. I. Shahovtsov, Radiation Effects **79**, 123 (1983)

{12}   F. Dominguez-Adame, J. Piqueras, N. de Diego and P. Moser, Solid State Commun. **67**, 665 (1988)

{13}   R. Sommerfeldt, L. Holtmann, E. Krätzig, and B. C. Grabmaier, Phys. Stat. Sol. **A106**, 89 (1988)

{14}   P. Hautojärvi, P. Moser, M. Stucky, C. Corbel, and F. Plazaola, Appl. Phys. Lett. **48**, 809 (1986)

{15}   G. Dlubek, O. Brümmer and A. Polity, Appl. Phys. Lett. **49**, 385 (1986)

{16}   A. Polity, Th. Abgarjan, and R. Krause-Rehberg, Appl. Phys. **A60**, 541 (1995)

{17}   S. Dannefaer and D. Kerr, Phys. Rev. **B50**, 14096 (1994)

{18}   J. A. Van Vechten, J. Electron. Mat. **4**, 1159 (1975)

{19}   M. J. Puska, J. Phys.: Condens. Matter **1**, 7347 (1989)

{40}   Y. Yamazoe, Y. Sasai, T. Nishino, and Y. Hamakawa, Jpn. J. Appl. Phys. **20**, 347 (1981)

{41}   M. Deiri, A. Kana-ah, B. C. Cavenett, T. A. Kennedy, and N. D. Wilsey, Semicond. Sci. Technol. **3**, 706 (1988)

{42}   M. Törnqvist, J. Nissilä, F. Kiessling, C. Corbel, K. Saarinen, A. P. Seitsonen, and P. Hautojärvi, Mater. Sci. Forum **143/147**, 347 (1994)

{43}   V. N. Brudnyi, S. A. Vorobiev, and A. A. Tsoi, Appl. Phys. **A29**, 219 (1982)

{44}   A. P. Seitsonen, R. Virkkunen, M. J. Puska, and R. M. Nieminen, Indium and phosphorous vacancies and antisites in InP, unpublished

{45}   A. Sibille, J. Suski, and M. Gilleron, J. Appl. Phys. **60**, 595 (1986)

{46}   J. Suski, A. Sibille, and J. Bourgoin, Solid State Commun. **49**, 875 (1984)

{47}   A. Sibille and J. Suski, Phys. Rev. **B31**, 5551 (1985)

{48}   T. A. Kennedy and N. D. Wilsey, J. Cryst. Growth **83**, 198 (1987)

{49}   T. A. Kennedy and N. D. Wilsey, Appl. Phys. Lett. **44**, 1089 (1984)

{50}   M. Deiri, A. Kana-ah, B. C. Cavenett, T. A. Kennedy, and N. D. Wilsey, J. Phys. C: Solid State Phys. **17**, L793 (1984)

{51}   D. Y. Jeon, H. P. Gislason, J. F. Donegan, and G. D. Watkins, Phys. Rev. **B36**, 1324 (1987)

{52}   H. J. Sun, H. P. Gislason, C. F. Rong, and G. D. Watkins, Phys. Rev. **B48**, 17092 (1993)

{53}   H. Hausmann and P. Ehrhart, Phys. Rev. **B51**, 17542 (1995)

{54}   K. Ando, A. Katsui, D. Y. Jeon, G. D. Watkins, and H. P. Gislason, Mater. Sci. Forum **38/41**, 761 (1989)

{55}   S. I. Radautsan, I. M. Tiginyanu, V. V. Ursaki, F. P. Korshunov, N. A. Sobolev, and E. A. Kudryavtseva, Solid State Commun. **85**, 525 (1993)

{56}   F. P. Korshunov, S. I. Radautsan, N. A. Sobolev, I. M. Tiginyanu, V. V. Ursaki, and E. A. Kudryavtseva, Sov. Phys. Semicond. **23**, 980 (1989)

{57}   K. Kuriyama, K. Sakai, M. Okada, and K. Yokoyama, Phys. Rev. **B52**, 14578 (1995)

{58}   J. A. Van Vechten and J. F. Wagner, J. Appl. Phys. **57**, 1966 (1985)

{40} Y. Yamazoe, Y. Sasai, T. Nishino, and Y. Hamakawa, Jpn. J. Appl. Phys. **20**, 347 (1981)

{41} M. Deiri, A. Kana-ah, B. C. Cavenett, T. A. Kennedy, and N. D. Wilsey, Semicond. Sci. Technol. **3**, 706 (1988)

{42} M. Törnqvist, J. Nissilä, F. Kiessling, C. Corbel, K. Saarinen, A. P. Seitsonen, and P. Hautojärvi, Mater. Sci. Forum **143/147**, 347 (1994)

{43} V. N. Brudnyi, S. A. Vorobiev, and A. A. Tsoi, Appl. Phys. **A29**, 219 (1982)

{44} A. P. Seitsonen, R. Virkkunen, M. J. Puska, and R. M. Nieminen, Indium and phosphorous vacancies and antisites in InP, unpublished

{45} A. Sibille, J. Suski, and M. Gilleron, J. Appl. Phys. **60**, 595 (1986)

{46} J. Suski, A. Sibille, and J. Bourgoin, Solid State Commun. **49**, 875 (1984)

{47} A. Sibille and J. Suski, Phys. Rev. **B31**, 5551 (1985)

{48} T. A. Kennedy and N. D. Wilsey, J. Cryst. Growth **83**, 198 (1987)

{49} T. A. Kennedy and N. D. Wilsey, Appl. Phys. Lett. **44**, 1089 (1984)

{50} M. Deiri, A. Kana-ah, B. C. Cavenett, T. A. Kennedy, and N. D. Wilsey, J. Phys. C: Solid State Phys. **17**, L793 (1984)

{51} D. Y. Jeon, H. P. Gislason, J. F. Donegan, and G. D. Watkins, Phys. Rev. **B36**, 1324 (1987)

{52} H. J. Sun, H. P. Gislason, C. F. Rong, and G. D. Watkins, Phys. Rev. **B48**, 17092 (1993)

{53} H. Hausmann and P. Ehrhart, Phys. Rev. **B51**, 17542 (1995)

{54} K. Ando, A. Katsui, D. Y. Jeon, G. D. Watkins, and H. P. Gislason, Mater. Sci. Forum **38/41**, 761 (1989)

{55} S. I. Radautsan, I. M. Tiginyanu, V. V. Ursaki, F. P. Korshunov, N. A. Sobolev, and E. A. Kudryavtseva, Solid State Commun. **85**, 525 (1993)

{56} F. P. Korshunov, S. I. Radautsan, N. A. Sobolev, I. M. Tiginyanu, V. V. Ursaki, and E. A. Kudryavtseva, Sov. Phys. Semicond. **23**, 980 (1989)

{57} K. Kuriyama, K. Sakai, M. Okada, and K. Yokoyama, Phys. Rev. **B52**, 14578 (1995)

{58} J. A. Van Vechten and J. F. Wagner, J. Appl. Phys. **57**, 1966 (1985)

(1992)

{79}   K. Krambrock and J. M. Spaeth, Mater. Sci. Forum **83/87**, 887 (1992)

{80}   A. Pillukat and P. Ehrhart, Mater. Sci. Forum **83/87**, 947 (1992)

{81}   H. Hausmann, A. Pillukat and P. Ehrhart, Phys. Rev. **B54**, 8527 (1996)

{82}   A. Pillukat and P. Ehrhart, Phys. Rev. **B45**, 8815 (1992)

{83}   C. Bourgoin, H. J. von Bardeleben, and D. Stiévenard, J. Appl. Phys. **64**, R65 (1988)

{84}   A. Goltzené, B. Meyer, and C. Schwab, J. Appl. Phys. **57**, 1332 (1985)

{85}   D. Stiévenard, X. Boddaert, and C. Bourgoin, Phys. Rev. **B34**, 4048 (1986)

{86}   M. R. Brozel and R. C. Newman, J. Phys. C: Solid State Phys. **11**, 3135 (1978)

{87}   J. D. Collins, G. A. Gledhill, R. Murray, P. S. Nandhra, and R. C. Newman, Phys. Stat. Solidi **B151**, 469 (1989)

{88}   G. A. Gledhill, S. B. Upadhyay, M. R. Brozel and R. C. Newman, J. Molecular Structure **247**, 313 (1991)

{89}   B. Özbay, R. C. Newman, J. Woodhead, J. Phys. C: Solid State Phys. **15**, 581 (1982)

{90}   F. Thompson, S. R. Morrison, and R. C. Newman, J. Phys. C: Solid State Phys. **15**, L1045 (1982)

{91}   R. J. Wagner, J. J. Krebs, G. H. Stavss, and A. M. White, Solid State Commun. **40**, 473 (1981)

{92}   T. L. Reinecke and P. J. Lin-Chung, Solid State Commun. **40**, 285 (1981)

{93}   R. C. Newman, J. Phys. C: Solid State Phys. **17**, 2653 (1984)

{94}   K. Krambrock and J. M. Spaeth, Phys. Rev. **B47**, 3987 (1993)

{95}   P. W. Yu, W. C. Mitchel, M. G. Mier, S. S. Li, and W. L. Wang, Appl. Phys. Lett. **41**, 532 (1982)

{96}   K. R. Elliott, D. E. Holmes, R. T. Chen, and C. G. Kirkpatrich, Appl. Phys. Lett. **40**, 898 (1982)

{97}   K. Krambrock, B. K. Heyer, and J. M. Spaeth, Phys. Rev. **B39**, 1973 (1989)

{98}   A. Mircea and A. Mitonneau, Appl. Phys. **8**, 15 (1975)

{99}   E. R. Weber and J. Schneider, Physica **116B**, 398 (1983)

{100}   T. Wosinski, Appl. Phys. **A36**, 213 (1985)

(1992)

{79}   K. Krambrock and J. M. Spaeth, Mater. Sci. Forum **83/87**, 887 (1992)

{80}   A. Pillukat and P. Ehrhart, Mater. Sci. Forum **83/87**, 947 (1992)

{81}   H. Hausmann, A. Pillukat and P. Ehrhart, Phys. Rev. **B54**, 8527 (1996)

{82}   A. Pillukat and P. Ehrhart, Phys. Rev. **B45**, 8815 (1992)

{83}   C. Bourgoin, H. J. von Bardeleben, and D. Stiévenard, J. Appl. Phys. **64**, R65 (1988)

{84}   A. Goltzené, B. Meyer, and C. Schwab, J. Appl. Phys. **57**, 1332 (1985)

{85}   D. Stiévenard, X. Boddaert, and C. Bourgoin, Phys. Rev. **B34**, 4048 (1986)

{86}   M. R. Brozel and R. C. Newman, J. Phys. C: Solid State Phys. **11**, 3135 (1978)

{87}   J. D. Collins, G. A. Gledhill, R. Murray, P. S. Nandhra, and R. C. Newman, Phys. Stat. Solidi **B151**, 469 (1989)

{88}   G. A. Gledhill, S. B. Upadhyay, M. R. Brozel and R. C. Newman, J. Molecular Structure **247**, 313 (1991)

{89}   B. Özbay, R. C. Newman, J. Woodhead, J. Phys. C: Solid State Phys. **15**, 581 (1982)

{90}   F. Thompson, S. R. Morrison, and R. C. Newman, J. Phys. C: Solid State Phys. **15**, L1045 (1982)

{91}   R. J. Wagner, J. J. Krebs, G. H. Stavss, and A. M. White, Solid State Commun. **40**, 473 (1981)

{92}   T. L. Reinecke and P. J. Lin-Chung, Solid State Commun. **40**, 285 (1981)

{93}   R. C. Newman, J. Phys. C: Solid State Phys. **17**, 2653 (1984)

{94}   K. Krambrock and J. M. Spaeth, Phys. Rev. **B47**, 3987 (1993)

{95}   P. W. Yu, W. C. Mitchel, M. G. Mier, S. S. Li, and W. L. Wang, Appl. Phys. Lett. **41**, 532 (1982)

{96}   K. R. Elliott, D. E. Holmes, R. T. Chen, and C. G. Kirkpatrich, Appl. Phys. Lett. **40**, 898 (1982)

{97}   K. Krambrock, B. K. Heyer, and J. M. Spaeth, Phys. Rev. **B39**, 1973 (1989)

{98}   A. Mircea and A. Mitonneau, Appl. Phys. **8**, 15 (1975)

{99}   E. R. Weber and J. Schneider, Physica **116B**, 398 (1983)

{100}   T. Wosinski, Appl. Phys. **A36**, 213 (1985)

{118} S. Kuisma, K. Saarinen, P. Hautojärvi, and C. Corbel, Phys. Rev. B53, R7588 (1996)

{119} J. Dabrowski and M. Scheffler, Phys. Rev. B40, 10391 (1989)

{120} K. Thommen, Rad. Effects 2, 201 (1970)

{121} Y. Itoh and H. Murakami, Appl. Phys. A58, 59 (1994)

{122} V. N. Brudnyi, A. D. Pogrebnyak, Yu. P. Surov, and A. S. Rudnev, Phys. Stat. Sol. A114, 481 (1989)

{123} G. Dlubek, A. Dlubek, R. Krause, and O. Brümmer, Phys. Stat. Sol. A107, 111 (1988)

{124} E. Yu. Brailovskii and V. N. Brudnyi, Sov. Phys. Semicond. 5, 1101 (1971)

{125} E. Yu. Brailovskii and V. N. Brudnyi, Sov. Phys. Semicond. 8, 619 (1974)

{126} M. Hirata, S. Takeda, M. Hirata, and M. Kiritani, in *Proc. 13th Int. Conf. on Defects in Semicond.*, ed. L. C. Kimerling (Colonado, California, 1984), p. 359

{127} M. Hirata, M. Hirata and M. Kiritani, in *Proc.of Int. Symp. on "Behavior of Lattice Imperfections in Materials - In situ Experiments with HVEM"*, ed. H. Fujita (Osaka, 1985), p. 199

{128} M. Hirata, M. Hirata, S. Takeda, and M. Kiritani, Mat. Sci. Forum 38-41, 1181 (1989)

{129} M. Hirata, M. Hirata, S. Takeda, and M. Kiritani, Diffusion and Defect Data-Solid State Data A62-63, 69 (1989)

{130} F. Reynaud and B. Legros-de Mauduit, Rad. Effects 88, 1 (1986)

{131} D. Loretto and M. H. Loretto, Philos. Mag. A60, 597 (1989)

{132} S. Ishino, Oyo Buturi 46, 458 (1977) <in Japanese>

{133} P. B. Hirsch, A. Howie, and M. J. Whelan, Philos. Trans. R. Soc. London S A252, 499 (1960)

{134} N. F. Mott, Proc. Roy. Soc. A124, 426 (1929)

{135} N. F. Mott, Proc. Roy. Soc. A135, 429 (1932)

{136} W. A. MacKinley and H. Feshbach, Phys. Rev. 74, 1759 (1948)

{137} D. Pons, P. M. Mooney, and J. C. Bourgoin, J. Appl. Phys. 51, 2038 (1980)

{138} A. H. Kalma, R. A. Berger, C. J. Fischer, and B. A. Green, IEEE. Trans. Nucl. Sci. NS-22, 2277 (1975)

{139} A. Mevlenberg, C. M. Dozier, W. T. Anderson, S. D. Mittleman, M. H. Zugieh, and

{118} S. Kuisma, K. Saarinen, P. Hautojärvi, and C. Corbel, Phys. Rev. **B53**, R7588 (1996)

{119} J. Dabrowski and M. Scheffler, Phys. Rev. **B40**, 10391 (1989)

{120} K. Thommen, Rad. Effects **2**, 201 (1970)

{121} Y. Itoh and H. Murakami, Appl. Phys. **A58**, 59 (1994)

{122} V. N. Brudnyi, A. D. Pogrebnyak, Yu. P. Surov, and A. S. Rudnev, Phys. Stat. Sol. **A114**, 481 (1989)

{123} G. Dlubek, A. Dlubek, R. Krause, and O. Brümmer, Phys. Stat. Sol. **A107**, 111 (1988)

{124} E. Yu. Brailovskii and V. N. Brudnyi, Sov. Phys. Semicond. **5**, 1101 (1971)

{125} E. Yu. Brailovskii and V. N. Brudnyi, Sov. Phys. Semicond. **8**, 619 (1974)

{126} M. Hirata, S. Takeda, M. Hirata, and M. Kiritani, in *Proc. 13th Int. Conf. on Defects in Semicond.*, ed. L. C. Kimerling (Colonado, California, 1984), p. 359

{127} M. Hirata, M. Hirata and M. Kiritani, in *Proc.of Int. Symp. on "Behavior of Lattice Imperfections in Materials - In situ Experiments with HVEM"*, ed. H. Fujita (Osaka, 1985), p. 199

{128} M. Hirata, M. Hirata, S. Takeda, and M. Kiritani, Mat. Sci. Forum **38-41**, 1181 (1989)

{129} M. Hirata, M. Hirata, S. Takeda, and M. Kiritani, Diffusion and Defect Data-Solid State Data **A62-63**, 69 (1989)

{130} F. Reynaud and B. Legros-de Mauduit, Rad. Effects **88**, 1 (1986)

{131} D. Loretto and M. H. Loretto, Philos. Mag. **A60**, 597 (1989)

{132} S. Ishino, Oyo Buturi **46**, 458 (1977) <in Japanese>

{133} P. B. Hirsch, A. Howie, and M. J. Whelan, Philos. Trans. R. Soc. London S **A252**, 499 (1960)

{134} N. F. Mott, Proc. Roy. Soc. **A124**, 426 (1929)

{135} N. F. Mott, Proc. Roy. Soc. **A135**, 429 (1932)

{136} W. A. MacKinley and H. Feshbach, Phys. Rev. **74**, 1759 (1948)

{137} D. Pons, P. M. Mooney, and J. C. Bourgoin, J. Appl. Phys. **51**, 2038 (1980)

{138} A. H. Kalma, R. A. Berger, C. J. Fischer, and B. A. Green, IEEE. Trans. Nucl. Sci. **NS-22**, 2277 (1975)

{139} A. Mevlenberg, C. M. Dozier, W. T. Anderson, S. D. Mittleman, M. H. Zugieh, and

{162} P. M. Petroff, D. V. Lang, R. A. Logan and J. L. Strudel, Scanning Electron Microscopy **1**, 325 (1978).

{163} R. J. Graham, J. C. H. Spence and H. Alexander, Proc. Charact. Defects in Mater. Symp., p235 (1986).

{164} N. Yamamoto, Mat. Trans. JIM **31**, 659 (1990).

{165} R. J. Graham and K. V. Ravi, Appl. Phys. Lett. **60**, 1310 (1992).

{166} M. D. Lumb, *Luminescence Spectroscopy* (Academic Press, London, 1978)

{167} B. Henderson and G. F. Imbusch, *Optical Spectroscopy of Inorganic Solids* (Clarendon Press, Oxford, 1989)

{168} B. Di Bartolo, *Optical Properties of Excited States in Solids* (Plenum Press, 1992)

{169} J. I. Pankove, *Optical Processes in Semiconductors* (Prentice-Hall, Englewood Cliffs, NJ, 1971)

{170} A. A. Bergh and P. J. Dean, *Light Emitting Diodes* (Clarendon, Oxford, 1976)

{171} P. J. Dean, "Photoluminescence as a diagnostic for semiconductors", Cryst. Growth Characterization **5**, 89 (1982)

{172} D. B. Holt, *"Quantitative SEM Studies of CL in Adamantane Semiconductors"*, in Quantitative Scannimg Electron Microscopy, edited by D. B. Holt, M. D. Muir, P. R. Grant, and I. M. Boswarva (Academic, London, 1974), p.335

{173} G. Pfefferkorn, W. Brocker, and M. Hastenrath, *"The Catodoluminescence Method in the Scanning Electron Microscope"*, in Scanning Electron Microscopy/1980, edited by O. Johari (SEM Inc., Chicago, IL, 1980), p. 251

{174} Y. Ohno and S. Takeda, J. Electron Microsc. **45**, 73 (1996)

{175} P. J. Dean, C. J. Frosch and C. H. Henry, J. Appl. Phys. **39**, 5631 (1968)

{176} M. Tajima, Y. Okada and Y. Tokumaru, Jp. J. Appl. Phys. **17**, 93 (1978)

{177} J. M. Dishman, D. F. Daly, and W. P. Knox, J. Appl. Phys. **43**, 4693 (1972)

{178} A. Gomyo, T. Suzuki, and S. Iijima, Phys. Rev. Lett. **60**, 2645 (1988)

{179} O. Ueda, M. Takikawa, J. Komeno, and J. Umebu, Jpn. J. Appl. Phys. **26**, L1824 (1987)

{180} A. Gomyo, T. Suzuki, K. Kobayashi, S. Kawata, I. Hino, and T. Yuasa, Appl. Phys.

{162} P. M. Petroff, D. V. Lang, R. A. Logan and J. L. Strudel, Scanning Electron Microscopy **1**, 325 (1978).

{163} R. J. Graham, J. C. H. Spence and H. Alexander, Proc. Charact. Defects in Mater. Symp., p235 (1986).

{164} N. Yamamoto, Mat. Trans. JIM **31**, 659 (1990).

{165} R. J. Graham and K. V. Ravi, Appl. Phys. Lett. **60**, 1310 (1992).

{166} M. D. Lumb, *Luminescence Spectroscopy* (Academic Press, London, 1978)

{167} B. Henderson and G. F. Imbusch, *Optical Spectroscopy of Inorganic Solids* (Clarendon Press, Oxford, 1989)

{168} B. Di Bartolo, *Optical Properties of Excited States in Solids* (Plenum Press, 1992)

{169} J. I. Pankove, *Optical Processes in Semiconductors* (Prentice-Hall, Englewood Cliffs, NJ, 1971)

{170} A. A. Bergh and P. J. Dean, *Light Emitting Diodes* (Clarendon, Oxford, 1976)

{171} P. J. Dean, "Photoluminescence as a diagnostic for semiconductors", Cryst. Growth Characterization **5**, 89 (1982)

{172} D. B. Holt, *"Quantitative SEM Studies of CL in Adamantane Semiconductors"*, in Quantitative Scannimg Electron Microscopy, edited by D. B. Holt, M. D. Muir, P. R. Grant, and I. M. Boswarva (Academic, London, 1974), p.335

{173} G. Pfefferkorn, W. Brocker, and M. Hastenrath, *"The Catodoluminescence Method in the Scanning Electron Microscope"*, in Scanning Electron Microscopy/1980, edited by O. Johari (SEM Inc., Chicago, IL, 1980), p. 251

{174} Y. Ohno and S. Takeda, J. Electron Microsc. **45**, 73 (1996)

{175} P. J. Dean, C. J. Frosch and C. H. Henry, J. Appl. Phys. **39**, 5631 (1968)

{176} M. Tajima, Y. Okada and Y. Tokumaru, Jp. J. Appl. Phys. **17**, 93 (1978)

{177} J. M. Dishman, D. F. Daly, and W. P. Knox, J. Appl. Phys. **43**, 4693 (1972)

{178} A. Gomyo, T. Suzuki, and S. Iijima, Phys. Rev. Lett. **60**, 2645 (1988)

{179} O. Ueda, M. Takikawa, J. Komeno, and J. Umebu, Jpn. J. Appl. Phys. **26**, L1824 (1987)

{180} A. Gomyo, T. Suzuki, K. Kobayashi, S. Kawata, I. Hino, and T. Yuasa, Appl. Phys.

Published Papers

<Chapter 2>

Y. Ohno, S. Takeda, and M. Hirata, Mat. Sci. Forum **196-201**, 1279-1284 (1995), "Clustering process of point defects in GaP studied by transmission electron microscopy"

Y. Ohno, S. Takeda, and M. Hirata, Phys. Rev. B **54**, 4642-4649 (1996), "Clustering process of interstitial atoms in gallium phosphide studied by transmission electron microscopy"

Y. Ohno, S. Takeda, and M. Hirata, Mat. Res. Soc. Symp. Proc. **442**, 435-439 (1997), "Diffusion process of interstitial atoms in InP studied by transmission electron microscopy"

Y. Ohno, N. Saitoh, S. Takeda, and M. Hirata, Jpn. J. Appl. Phys. **36**, 5628-5632 (1997), "Diffusion process of interstitial atoms in an electron irradiated InP studied by transmission electron microscopy"

<Chapter 3>

Y. Ohno, S. Takeda, and M. Hirata, in *Proceedings of the 13th International Congress on Electron Microscopy*, edited by B. Jouffrey and C. Colliex (Les Editions de Phisique, Paris, 1994), 829-830, "*In-situ* TEM-PL study of lattice defects in CVD-diamond"

Y. Ohno and S. Takeda, Rev. Sci. Instrum. **66** (1995) 4866-4869, "A new apparatus for *in-situ* photoluminescence spectroscopy in a transmission electron microscope"

Y. Ohno and S. Takeda, J. Electron Microsc. **45** (1996) 73-78, "Study of electron-irradiation-induced defects in GaP by *in-situ* optical spectroscopy in a transmossion electron microscope"

S. Takeda and Y. Ohno, Denshi-kenbikyo **32** (1997) 107-109, "Toka denshi-kenbikyo nai sono-ba kashibunko sochi no kaihatsu to sono oyo" <in Japanese>

Published Papers

<Chapter 2>

Y. Ohno, S. Takeda, and M. Hirata, Mat. Sci. Forum **196-201**, 1279-1284 (1995), "Clustering process of point defects in GaP studied by transmission electron microscopy"

Y. Ohno, S. Takeda, and M. Hirata, Phys. Rev. B **54**, 4642-4649 (1996), "Clustering process of interstitial atoms in gallium phosphide studied by transmission electron microscopy"

Y. Ohno, S. Takeda, and M. Hirata, Mat. Res. Soc. Symp. Proc. **442**, 435-439 (1997), "Diffusion process of interstitial atoms in InP studied by transmission electron microscopy"

Y. Ohno, N. Saitoh, S. Takeda, and M. Hirata, Jpn. J. Appl. Phys. **36**, 5628-5632 (1997), "Diffusion process of interstitial atoms in an electron irradiated InP studied by transmission electron microscopy"

<Chapter 3>

Y. Ohno, S. Takeda, and M. Hirata, in *Proceedings of the 13th International Congress on Electron Microscopy*, edited by B. Jouffrey and C. Colliex (Les Editions de Phisique, Paris, 1994), 829-830, "*In-situ* TEM-PL study of lattice defects in CVD-diamond"

Y. Ohno and S. Takeda, Rev. Sci. Instrum. **66** (1995) 4866-4869, "A new apparatus for *in-situ* photoluminescence spectroscopy in a transmission electron microscope"

Y. Ohno and S. Takeda, J. Electron Microsc. **45** (1996) 73-78, "Study of electron-irradiation-induced defects in GaP by *in-situ* optical spectroscopy in a transmossion electron microscope"

S. Takeda and Y. Ohno, Denshi-kenbikyo **32** (1997) 107-109, "Toka denshi-kenbikyo nai sono-ba kashibunko sochi no kaihatsu to sono oyo" <in Japanese>